In the large field of nanotechnology, polymer matrix based nanocomposites have become a prominent area of current research and development. This book deal with the fabrication of nanocomposite (PANI_CNTs nanofiber) by electrochemical method for NH3, HCl, and H2 sensors with described the mechanism of its interactions. The effect of weight proportion of CNTs to polyaniline to making nanofiber composite on sensitivity and response time and recovery time are described.

Asst. Prof. Ph.D. Nanotechnology/materials/Physics Department/University of Baghdad. Now he placed President of Al-Karkh University of science / Ministry of Higher Education and Scientific Research. U.S.Excellence Award(2014). Member of the Technical Committee, ISS, ASME and Association of Scientists.

978-3-659-80558-5

Nanocomposite Fabrication of PANI-CNTs

A. A. Hassan

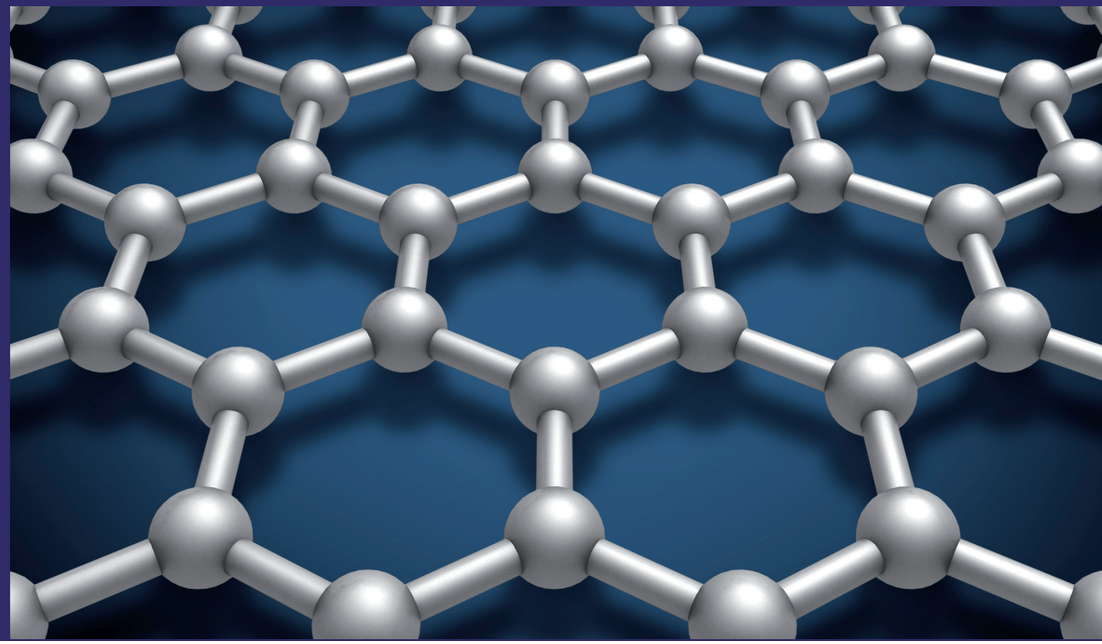

Thamir A. A. Hassan

Nanocomposite Fabrication of PANI-CNTs Nanofiber for Chemical Sensing

LAP LAMBERT Academic Publishing

Thamir A. A. Hassan

Nanocomposite Fabrication of PANI-CNTs Nanofiber for Chemical Sensing

Thamir A. A. Hassan

Nanocomposite Fabrication of PANI-CNTs Nanofiber for Chemical Sensing

LAP LAMBERT Academic Publishing

Impressum / Imprint
Bibliografische Information der Deutschen Nationalbibliothek: Die Deutsche Nationalbibliothek verzeichnet diese Publikation in der Deutschen Nationalbibliografie; detaillierte bibliografische Daten sind im Internet über http://dnb.d-nb.de abrufbar.

Bibliographic information published by the Deutsche Nationalbibliothek: The Deutsche Nationalbibliothek lists this publication in the Deutsche Nationalbibliografie; detailed bibliographic data are available in the Internet at http://dnb.d-nb.de.

Coverbild / Cover image: www.ingimage.com

Verlag / Publisher:
LAP LAMBERT Academic Publishing
ist ein Imprint der / is a trademark of
OmniScriptum GmbH & Co. KG
Heinrich-Böcking-Str. 6-8, 66121 Saarbrücken, Deutschland / Germany
Email: info@lap-publishing.com

Herstellung: siehe letzte Seite /
Printed at: see last page
ISBN: 978-3-659-80558-5

Nanocomposite Fabrication of PANI-CNTs Nanofiber for Chemical Sensing

Editor

Asst. Prof.
Dr. Thamir Abdul Ameer Hassan
President of Al-Karkh University of Science

Dedicated to

The pure spirit of my father and my mother

Love and loyalty

To

My wife: Dr. Eftechar

My children: Sara, Ali and Mustafa

Love and respect

Thamir A.A. Hassan

Acknowledgments

First, the author thanks deeply Allah for supporting him to achieve this work. I wishes to express my great thanks and the sincerest gratitude to Prof. Dr. Ezzat M. Al-Essa & Prof. Dr. Ekram A. Al-Ajaj for their valuable guidance and useful suggestions.

My greatest thanks and sincerest gratitude to my colleagues especially: Dr. Abdul Kareem M. Ali from (Chemical Dept) and Dr. Abdul Redha Hassani for help me and to the committee for monitoring preparation.

I do not forget to thank Prof. Dr. Bahaa T. Chid (As sistant Baghdad University President), and Physics Department staf f for their support, specially the head of the department, Prof. Dr. Raad Al-Hadad for their support and encouragement.

Also, I would like to thank all, Prof. Dr. Harit Ib rahim (Materials unit Chairman), Assist. Prof Dr. Mahdy Hassan Suheel, Dr. Raid Nofi Hassaan, and Dr. Loay Kadhum for their supports and encouragements.

Finally, I express my deep gratefulness to my Family for their patience and encouragement throughout this work. And I have to say thank you for everything.

Thamir Abdul Ameer Hassan

Abstract

In the present chemical sensing experiments polyaniline (PANI) and carbon nanopowder (CNpowder) have been fabricated. The PANI was prepared by electrochemical method using a number of solutions containing either HCl or H_2SO_4 with aniline .The first set of solutions contained of 0.1 M distilled aniline with 0.1 M, 0.2 M ,and 0.3M HCl while the second set contained 0.1 M distilled aniline with 0.1 M, 0.2 M, and 0.3M H_2SO_4. A cyclic potential ranged from -100 mV to 1500 mV was applied on working electrodes (SUS 304 stainless steel) which were dipped in these solutions at scan rate of 30mV s^{-1} at room temperature. Scanning Electron Microscope (SEM)images showed that the PANI nanofibers structure with diameters range (60nm-100nm) were formed by 0.1 M aniline with 0.1 M HCl and(50nm-70 nm) were formed by 0.1 M aniline with 0.3 M H_2SO_4. The resulted PANI had better homogeneity with no formation of aggregates when the aniline and 0.3 M H_2SO_4 were taken as an effective solutions.

CNpowder was also fabricated by arc discharge technique at a pressure of 10^{-6} mbar. After being purified by nitric acid, the CNpowder of 0.25wt %, 0.5wt % and 1wt% was added to 0.1 M distilled aniline under reflex procedure with 0.3 H_2SO_4 for mixing purposes to form analyte as prerequisite for fabricating PANI/CNpowder composite. Analyses of current –voltage (I-V) curves exhibited a reduction in electrical conductivity with increasing proportion of CNpowder.

To establish higher electrical conductivity CNpowder were replaced by similar proportions of Multi Wall Carbon Nanotubes (MWNTs) (purity 95% were produced via the chemical vapor deposition method(CVD) , average outer diameter 20-30 nm and the length of 10-30 μm (purchased from Cheap Tubes Inc) subjected to the same above procedure. Results of I-V curves showed increase in electrical conductivity with increasing proportion of (CNTs).Therefore, these structures were used as a fundamental material of sensors.

In the liquid type sensing, it was found that with the increase of HCl concentrations, the value of current density (J) could be raised and found pronounced at 3000 ppm and 4000ppm concentration along with PANI/0.5 wt %CNTs and PANI/1 wt% CNTs sensors out of the four corresponding four solutions and for sensors. The reason behind that may be the enhancement of more efficient transfer of charges.

On the other hand a reduction in current density (J) was obtained with increasing concentration of NH_3 and clearly observed at 1000 ppm and 2000 ppm for PANI/0.5 wt %CNTs and PANI/1 wt% CNTs sensors.

For H_2 gas sensing, PANI and PAN I/ CNTS were deposited onto interd igitated electrode IDE(Au electrode) by spin coating .These sensors were inspected with 1%, 2%, 3% ,and 4% H_2:air mixing at 298K temperature and 333K. Under 1wt%CNTS and 333K conditions, the PANI/CNTS composite sensor was found as the best in terms of sensitivity and both response and recovery times.

Table Contents

Abbreviation and Acronyms

γ_0	C-C tight binding overlap energy
(m, n)	Possible chiral vector in terms of the integers
=NH-	Imine
Δx	Distance between two fringes and is the
0D	Zero Dimension
2D	Two Dimensions system
3 D	Three Dimension system
A.C.	Alternating current
A_{c-c}	Nearest neighbor C-C distance
AFM	Atomic Force microscope
CNS	Coexisting carbon
CS	Chemical synthesized
CSA	Camphorsulfonic Acid
CT	Charge transfer polymer
CVD	Chemical Vapor deposition
d	Diameter of a nanotube
D	Crystallite size
D.C.	Direct current
DMF	Dimethyl formamide
DMSO	Dimethylsulfoxide
DOS	Density of state
EB	Emeraldine Base
ECS	Electrochemical Synthesized
E_g	Energy Gap
ES	Emeraldine salt
G	Conductance
G_0	Quantum unit of the conductance
GCE	Glassy Carbon Electrode
ICDD	International centered diffraction data
ICPs	Intrinsically conducting polymers
IDE	Interdigitated Electrode
ipa	Maximum anodic current
ipc	Maximum cathodic current
ITO	Indium-Doped tin oxide
J	Current density
JCPDS	Join committee on powder diffraction stds
K'	Constant 0.9
LE	leucomeraldine
m	Mass
m.wt	Molecular weight

MFC	Mass Flow controllers
MWNTS	Multi Wall carbon Nanotubes(CNTs)
n	Concentration
-NH-	Amine
NMP	Methyl Pyrrolidinone
PANI	Polyanilie
PN	Pernigraniline
PP	Polyphenylene
PPV	Polyphenylene
PPY	polypyrrol
PS	Polyasolfone
PTh	polythiophene
R_{air}	Sensor resistance in air
R_g	Sensor resistance at gas exposure
S	Sensitivity
S/cm	Conductivity unit $(\Omega.cm)^{-1}$
SCE	Saturated Calmole electrode
SDS	Sodium dodecyl sulfate
SEM	Scan Electron Microscope
SWNTs	Single Wall carbon Nanotubes
t	Thickness
THT	Tetrahydrofuran
wt%	weight Percentage
x	Fringe width
β'	Angular line width at half maximum
θ	Bragg's diffraction angle
λ	wavelength
σ	Overall conductivity
σ_c	Intermolecular conductivity
σ_h	Intermolecular hopping conductivity
σ_i	Ionic conductivity

Chapter One

Nanocomposite Concepts and Literature Review

1.1 Introduction

One goal of today's technology is the miniaturization of the electronic, actuating, sensing, and optical devices and their components; hence, nanotechnology is an advanced technology that has received a lot of attention from the worlds of the science and industry for its ability to make use of the unique properties of nanosized materials. Nanotechnology is capable of manipulating and controlling material structures at the nano level (a nanometer is equal to one millionth of a millimeter) and offering unprecedented functions and excellent material properties. [1].

Nanotechnology can be defined as the ability to work near the molecular level, atom by atom, to create large structures with fundamentally new properties and functions. Nanotechnology can be described as the precision-creation and precision control of atomic-scale matter [2] .It offers new design, characterization, production, and application of systems, devices and materials at the nanometer scale. It is an interesting and vibrant field of research. Their roots can be traced back to Feynman's famous lecture in 1959, in which he suggested that for entities with nanoscopic dimensions new physical phenomena should arise [3].

The nanoscale dimension is important because quantum mechanical properties of electronics, photons, and atoms are evident at this scale. Its structures permit the control of fundamental properties of materials without changing the materials' chemical status. Nanostructures, such as nanophotonic devices, nanowires, carbon nanotubes, plasmonic devices, among others, are planned to be more powerful communication systems and quantum computers [4].

Nanoscale structures are used to study a range of interesting effects that occur when electrons are confined to very small geometries. For example, the quantized electron wave states in a nanostructure are reflected in measurements of electron transport through the structure. Electron transport experiments have been used to investigate many different nanostructures. As the scale of materials reduces to nanometers, the tendency of surfaces to minimize their free energy may drive structural changes [5].

This book give a general information to nanotechnolgy as well as a discussion on the various ways to synthesize polyaniline and carbon nanotubes and their structure, followed by considerations about conducting polymers the physical properties of nanotubes and application of carbon nanotube and also include of

describing the device characterizations before turning to the experimental methods employed during this project. Finally, the results obtained are presented and discussed before conclusions on the work done are given followed by an outlook**.**

1.2 The Physics of Nano Dimensional Material

Over the last few years, advances in solid state physics have been characterized by a change from bulk crystal to a very small at least one of their three dimensions. Semiconductor nanocrystals are the subject of a rapidly developing field. It can be defined as crystals with dimensions ranging from 10- 100 nm; above this size, they are termed microcrystals. When the dimensions of a solid are reduced from a large size to the size of the characteristic lengths of electrons i.e. de Broglie wavelength λ_B**,** coherence length and localization length then the particles behave wave-like and the crystal size becomes smaller leading to the semiconductor energy levels to be more separated from each other and the effective band gap to increase, therefore new physical properties due to quantum effect is observed , such as : quantum conductance oscillations, quantum Hall effects, resonant tunneling single electron transport, etc. These properties are necessary to built nanostructure semiconductor heterojunction, superlattice, etc. [6].

Low dimensions materials are classified according to the number of dimensions in nanometer size into three types [7] :**Quantum wells, Quantum wires, and Quantum dots**

1.3 Electronic Structures of Nanomaterials

The electronic structure of materials is strongly depended on the nature of the material. In a three dimensional large size, the electronic structure is not restricted by the dimension of the material.

The wavelength of electron is much smaller than the typical length of the material and the density of states (DOS) dependence is a parabolic function on the energy. When the electronic motion is confined in one dimension, and it is free in the other two dimensions, its results in a creation of 'quantum wells'.

The electrons will be localized in the energy subbands therefore, in 2D system the density of states have to be square function and the exitonic absorption is much stronger because the interband transitions which is occurred in this system in contrast to 3D systems.

These interband transitions occur from an initial state in the valence band to final states in the conduction band and the absorption will appear at energies higher than 3D case since the energy difference between these states is larger than the energy band gap for semiconductor[6]. Figure (1.1) represents the band diagram of quantum well both in real and wave vector spaces.

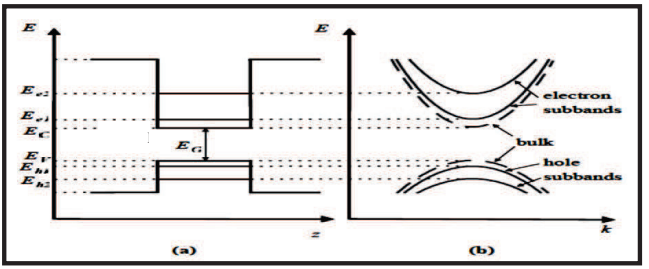

Fig. (1.1) Band diagram of a quantum well :(a) in real space(b) in k-space

In the case of a one-dimensional system (1D), i.e. when the electrons are free to move only in one direction, we get a situation where the (DOS) shows a Lorenzian line shape. Such situation can be seen in carbon nanotubes. If the electrons are confined to a point (QD system), we get a zero-dimensional system, where the electrons are not free to move at all. Here we get states which are molecular in nature. The situations is schematically depicted in Figure (1.2). From this figure, it can be noticed that the density of states is smoothly varying in bulk materials; it shows discontinuities in confined systems while to be steps in two-dimensional confinement, singularities in one-dimensional confinement and discrete lines in zero-dimensional confinement [8].

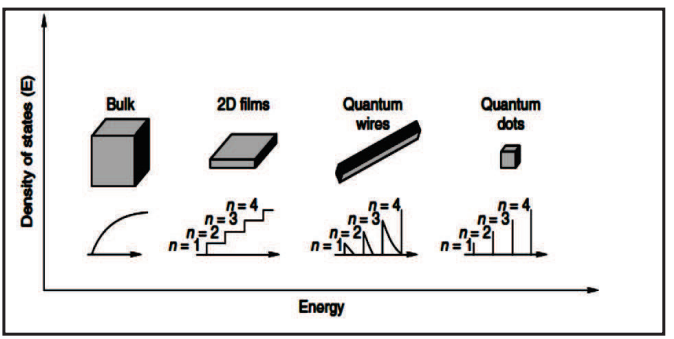

Fig.(1.2) Density of states as a function of energy for the four dimensional materials [6]

1.4 Conducting polymers

Conducting polymers are a prospective class of new materials that combine solubility, processability and flexibility of plastics with electrical and optical properties of metals and semiconductors. Conducting polymers are classified into four main types.

1. Conductively filled polymer (composites) the filling of polymer matrix, which is originally non conducting with a powder conductive medium such as metal or carbon gives rise to the conductivity [9]
2. Ionically conducting polymers (polymer electrolytes), they are organic polymers in which electric charge is carried by ions. These systems involve dissolution and solvation of salt in a polymer matrix, the ions are sufficiently mobile to move along the polymer when an electric filed is applied. The ion migration between coordination sites are generated by the slow motion of polymer chain segments. Polymer electrolytes normally show a low conductivity. These polymers are gaining importance in the battery industry [10,11].
3. Charge transfer polymer (CT), the conductivity arises from the formation of appropriate segregated stacks of electron donor and acceptor molecules and a certain degree of charge transfer between the stacks [12].
4. Conjugated conducting polymers. Owing to the delocalization of electrons in a continuously over lapped (π orbital) along the polymer backbone. [12,13]

1.5 Conjugated Polymer

A polymer chain characterized by an alternation of saturated and unsaturated carbon-carbon bonds, leading to the presence of non localized electrons {π –electrons} [14].The conjugated structure with alternating single and double bonds or conjugated segment coupled with atoms providing p-orbital for a continues orbital overlap seem to be necessary for polymers to become electrically conducing.

This is due to the conjugated structure not only provides a continues conduction path through the P- orbital over lapping along the polymer backbone

but also facilities the generation of charge carriers by either partial oxidation (p-doping) or partial reduction (n-doping)[15,16].

The most commonly studied conjugated polymers for the last three decades a large effort on the development of conducting polymers such as polythiophen (PT), polypyrrol (PPY), polyphenylene (PP), polyphenylene vinylene (PPV), polyasulfone (PS), and polyaniline (PANI)etc. [17,18]. Figure (1.3) shows the chemical structural formula of some commonly encountered conjugated polymers[19].

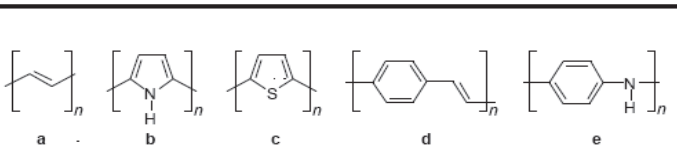

(a) Polyacetylene, (b) polypyrrole, (c) polythiophene, (d) polyphenylene vinylene, (e) polyaniline

Fig (1.3): Intrinsically conducting polymers[19]

The electrical conductivity of the intrinsically conjugated polymer systems have a range from those typical of insulators ($<10^{-10}$S/cm) to those typical of semiconductors such as silicon ($\approx 10^{-5}$S/cm) to those greater than (10^{+4}S/cm) nearly that of a good metal[19]. Figure (1.4) shows the variation of conductivity of some metals and doped conjugated polymers[20].

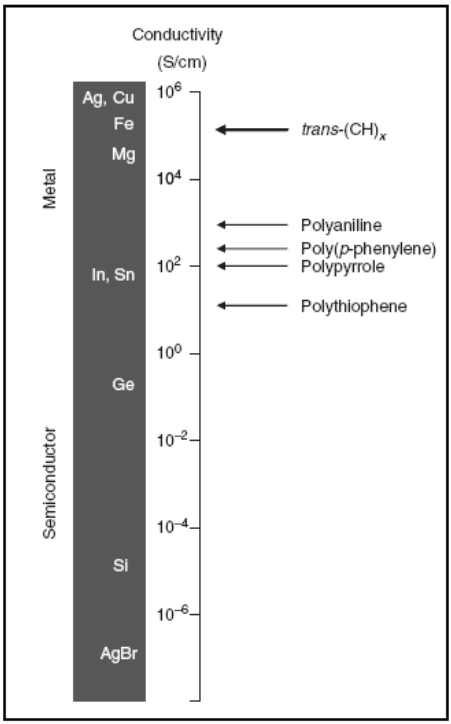

Fig. (1.4): Conductivity of some metals and doped conjugated polymer[20]

These polymers because of their good electrical and optical properties have been applied in a really impressive application range in different fields such as energy storage electromagnetic interference shielding[21] , light emitting diodes and photovoltaic devise [22], field effect transistors, plastic lasers, batteries[23] corrosion protection[24] and chemical and biological sensors [25].

1.6 Polyaniline (PANI)

Polyaniline (PANI) has been known for more than a century in its "aniline black" form, an undesirable black deposit formed on the anode during electrolysis involving aniline.

Among the conducting polymers, polyaniline is the most promising polymer due to its low cost, ease of preparation, chemical stability[26], controllable electrical conductivity as well as excellent environmental stability[27].PANI is

represented by the general following formula and structure, where B denotes a benzoid reduced unit and Q is a quinoid oxidized unit[28]as shown in figure (1.5).

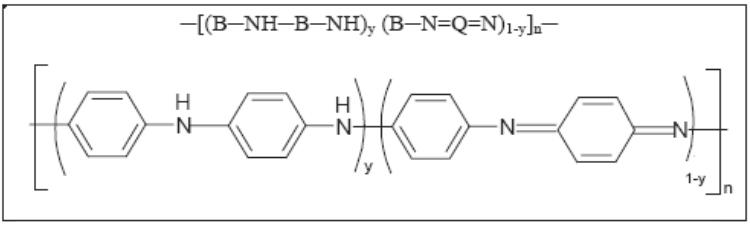

***Fig. (1.5) Structure of the polyaniline chain* [28]**

PANI is a typical phenylene-base polymer having a chemically flexible -NH - group in the polymer chain flanked on either side by a phenylene ring. The protonation, deprotonation and various other physico-chemical properties of PANI can be traced to the presence of the –NH- group [29].

PANI exists in various oxidation states characterized by the ratio of amine to imine nitrogen atoms[30]. When y = 1, the polymer is in the fully reduced leucoemeraldine (LE) state and is found to be insulating and yellow. The half oxidized polymer (y=0.5) is called emeraldine base (EB) and is insulating and blue. The only conducting state of PANI is the green colored emeraldine salt (ES), Which is the protonated form of EB[31].

Finally, pernigraniline base (PN) is the fully oxidized form of PANI (Y= 0) and is insulating and purple. All these oxidation states of PANI are shown in Figure (1. 6)[20] .

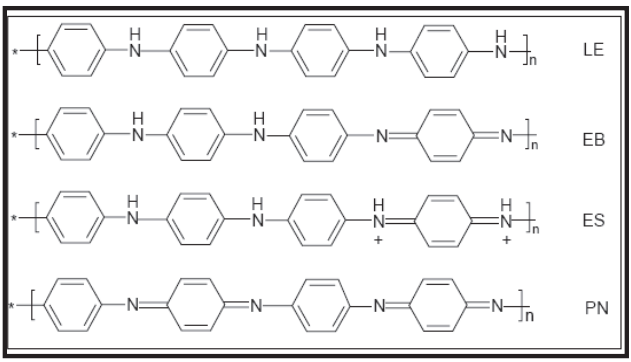

***Fig.(1.6) Different oxidation states of PANI , leucoemeraldine (LE), emeraldine base (EB), emeraldine salt(ES) and pernigraniline (PN).* [20]**

The ability of PANI to exist in various forms via acid/base treatment and oxidation /reduction, either chemically or electrochemically, has made PANI the most tunable member of the conducting polymer. PANI was found in wide variety of applications in different fields [32]. However, PANI has a rigid backbone originating from an extended conjugated double bond [33]. The rigid structure of PANI restricts its common usage and results in the insolubility, infusibility and incompatibility of this material with common polymers. This necessitates the modification of the structure of PANI. Therefore, during the past decade researchers have directed their attention to modify PANI structure and to overcome the difficulties associated with the use of PANI by using different approaches, for example, the utilization of a soluble precursor method, in which a processable precursor polymer is first prepared in an appropriate form and then chemically converted into the final conducting polymer[34]. Another approach is the formation of conductive blends/composites[35] or the formation of PANI filled interpenetrating polymer networks. Efforts have been made to improve the properties of PANI through the post treatment of PANI such as sulfonation or incorporation of N-alkylsulfonic acid pendant group (the use of functional dopants and the design of self-doping polymer [36]. Extensive studies on the polymerization of aniline (ANI) derivatives and/or the polymerization of ANI in the presence of another monomer (copolymerization) have also been carried out frequently in order to improve the properties of PANI. In recent years [37], due to the development of nanotechnology, PANI has been employed for studying nano composite materials in order to get new desired properties for practical application [38].

1.7 Different oxidation states of polyaniline

Unlike other know electro_conducting polymers, polyaniline can exist, depending on degree of oxidation, in different forms, known as: leuoemeraldine, emeraldine and perningraniline. Leucoemeraldine, eg. leucoemeraldine base, refers to fully reduced form; emeraldine, eg. Emeraldine base, is half-oxidized, while perningraniline, eg. perningraniline base, is completely oxidized form of polyaniline. The only conducting form of polyaniline is emeraldin salt, obtained by doping or protonation of emeraldine base[39-41] .

The unique feature of mentioned polyaniline forms is ease of its mutual conversions by both chemical and electrochemical reactions as it can be seen in

Figure(1.7) [42,43] .Apart from the changes in oxidation levels, all the transitions among polyaniline forms are manifested by color and conductivity changes[43].

The conducting protonated emeraldine in the form of green emeraldine salt, obtained as a product of electrochemical polymerization of aniline in acidic electrolytes, can be easily transformed by further oxidation to fully oxidized dark blue perningraniline salt, which can be treated by alkali to form violet perningraniline.

Emeraldine salt can also be reduced to transparent leucoemeraldine, or can be transformed by alkali to blue non conducting emeraldine. The two blue forms of polyanilne, perningranilne salt and emeraldine have different shades of blue[43].Both reduction of emeraldine salt to leucoemeraldine and oxidation to perningraniline states are followed by decrease in conductivity[44] .

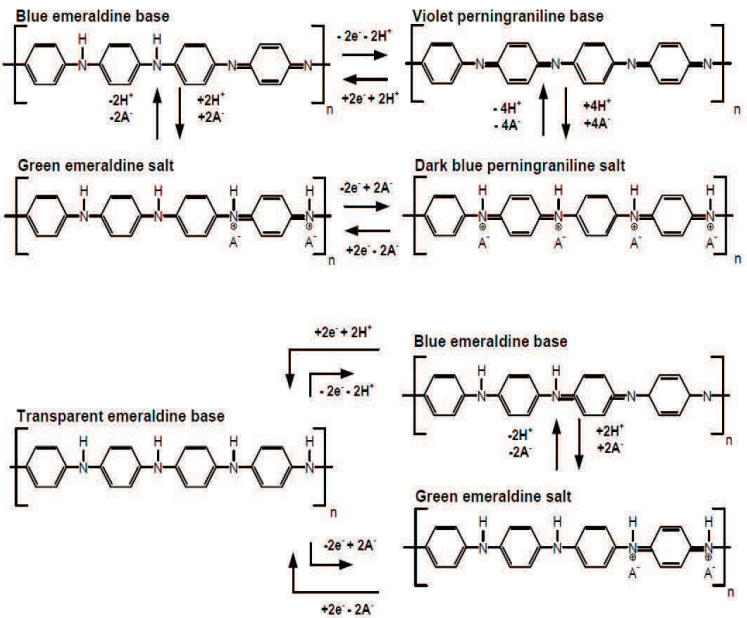

Fig. (1.7) Different forms of polyaniline [42,43]

1.8 Polyaniline conductivity

The mechanism of polyaniline conductivity differs from other electro conducting polymers, owing to the fact that nitrogen atom is involved in the formation of radical cation, unlike most of the electroconducting polymers whose radical cation is formed at carbon. On the other hand, nitrogen is also involved in the conjugated double bonds system. Therefore, electrical conductivity of polyaniline is dependent both on the oxidation and protonation degrees [41,45].As mentioned before, polyaniline is characterized by existence of various oxidation forms. Polyaniline in the form of emeraldine base can be doped (protonated) to conducting form of emeraldine salt. Emeraldine base, half oxidized form, is consisted of equal amount of amine (-NH-) and imine (=NH-) sites. Imine sites are subjected to protonation to form bipolaron or dicatione (emeraldine salt form). Bipolaron is further dissociated by injection of two electrons both from electron pairs of two imine nitrogen, into quinoid imine ring, and the third double bond of benzenoid ring is formed [44].

Unpared electrons at nitrogen atoms are cation radicals, but essentially they represent polarons. Figure(1.8) represents the polaron lattice, responsible for high conductivity of polyaniline in the form of emeraldine salt formed by redistribution of polarons along polymer chain [45].

Although both bipolaron and polaron theoretical models of emeraldine salt conductivity were proposed [46] , it was lately confirmed that, beside from the fact that few of spineless bipolarons exist in polyaniline, formation of polarons as charge carriers explained high conductivity of polyaniline [47,48] . As mentioned, unique property of polyaniline is conductivity dependence on the doping (proton) level [45].

The maximal conductivity of polyaniline is achieved at doping degree of 50%, which corresponds to polyaniline in the form of emeraldine salt [49] . For higher doping degrees some of the amine sites are protonated, while lower doping degrees means that some of the imine sites were left unprotonated[45] , explaining why, in the light of the polaron conductivity model, reduction of emeraldine salt to leucoemeraldine and oxidation to perningraniline states decrease the conductivity. The order of magnitude for conductivity varies from 10^{-2}S cm^{-1}, for undoped emeraldine, up to 10^{3} S cm^{-1} for doped emeraldine salt[50] .

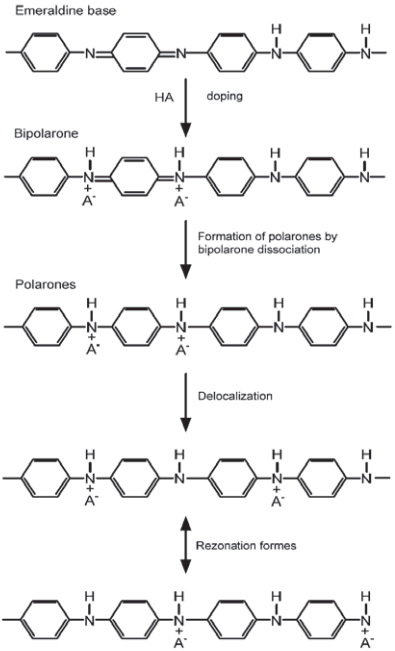

Fig. (1.8) Schematic presentation of conductivity for polyaniline [45]

Beside the fact that doping degree has the pronounced effect on the conductivity, various other factors such as: moisture amount [48,51] , morphology[52] , temperature [53] etc. were also found to had influence on the polyaniline conductivity.

1.9 PANI Synthesis

The ease and low cost of synthesizing PANI are attractive reasons why it is a primary candidate for the integration into new technologies. Intrinsically conducting polymers (ICP) are generally synthesized by chemical or electrochemical oxidation of a monomer where the polymerization reaction is stoichiometric in electrons.

1.9.1 Chemical Synthesis

Chemical synthesis has the advantage of being a simple process capable of producing bulk quantities of ICPs. Chemical polymerization is typically carried out with relatively strong chemical oxidants like ammonium peroxydisulfate, ferric ions, permanganate or bichromate anions, or hydrogen peroxide. These oxidants are able to oxidize the monomers in solution, leading to the formation of cation radicals. These cation radicals further react with other monomers or n-mers, yielding oligomers or insoluble polymer. There are two main limitations of the chemical oxidation technique, both related to the limited range of chemical oxidants available. The counter ion of the oxidants ultimately ends up as a dopant or codopant in the polymer. Hence it is difficult to prepare ICPs with different dopants. The limited range of oxidants also makes it difficult to control the oxidizing power in the reaction mixture and in turn the degree of over oxidation during synthesis. Both the type of dopant and the level of doping are known to impact upon final properties of the polymer such as molecular weight, crosslinking and, ultimately, conductivity [54,55]. Chemical synthesis of PANI is carried out by direct oxidation of aniline using an appropriate chemical oxidant such as hydrogen peroxide, ammonium persulfate, in acidic medium, in particular hydrochloric acid at a PH between 0-2.

The chemical polymerization of aniline was carried out in the presence of aqueous sulphuric acid solution. Appropriate amount of aniline 0.1 M is taken, to which H_2SO_4 acid was added into polymerization vessel and make a total volume of 100 ml. Then the vessel was placed on a magnetic stirrer. 20 ml of aqueous solution of $K_2Cr_2O_7$ oxidant at appropriate concentration was added slowly to the reaction medium by drop wise fashion for about 20 minutes using a dropping Funnel as shown in figure(1.9).

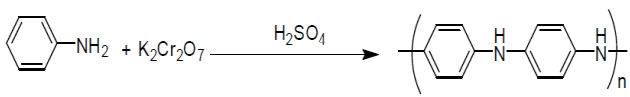

***Fig. (1.9)Scheme chemical polymerization of aniline*[56]**

At the end of polymerization reaction, final product was filtered, washed with dilute solutions of H_2SO_4 acid and dried at 60 C^{o} in vacuum, for 12 hours. The

synthesized polyaniline was finally grinded and the product is obtained in the form of fine green powder[56].

1.9.2 Electrochemical Synthesis

The electrochemical synthesis of conducting polymers, first demonstrated with polypyrrole [57], has proven important in the development of the field. Using this approach, semiconducting polymers have been obtained from a wide variety of monomers including thiophene, furan, carbazole, aniline, indole, azulene and polyaromatic monomers such as pyrene and fluoranthene. In general, chemical oxidation provides ICPs as powders, while electrochemical synthesis leads to films deposited on a working electrode. A wide range of anodes may be employed, including aluminum platinum, gold, carbon and iron. In the case of electrochemical method of synthesis, the potential is fixed or cycled [58]. The electrochemical synthesis of PANI offers some advantages over the chemical methods. The resulting product is clean, does not need to be extracted from the initial monomer / oxidant/solvent. This method offers the possibility of coupling with physical spectroscopic techniques for in situ characterization such as UV-visible, Raman spectroscopy and conductometry. [58]

1.10 Mechanism and kinetics of the electrochemical polymerization of aniline

Generally, electroconducting polymers are obtained by either chemical or electrochemical oxidative polymerization, although reductive polymerization was also reported[59,60]. Chemical polymerization is used when large quantity of polymer is requested. Electrochemical polymerization is favorable, since in the most cases the polymer is directly deposited on the electrode facilitating analysis. On the other hand, electrochemical polymerization is especially useful if polymer film electrode is needed. By proper design of the electrochemical experiment, polymer thickness and conductivity can be easily controlled. It is believed that electrochemical polymerization is consisted of three different steps:

1. first, oxidation of the monomer at anode lead to formation of soluble oligomers in the diffusion layer.
2. deposition of oligomers occurs through nucleation and growth process.

3. step is responsible for chain propagation by solid state polymerization[60]. Unfortunately, a general mechanism of electrochemical polymerization could not be established, since it was evidenced that various factors had influence. However, it was observed that first step of the electrochemical polymerization was formation of reactive cation radicals [60,61]. The next step, strongly dependent on the experimental conditions, is believed to be essential for the polymer growth [50] .The knowledge on the kinetics of the nucleation and growth process during electrochemical synthesis of electroconducting polymers is also of great interest, since it would be useful in control of the morphology, density, crystallinity etc. of the desired polymer.

1.10.1 Mechanism

Both the mechanism and the kinetics of the electrochemical polymerization of aniline were extensively investigated [59,62-68]. Electrochemical, similarly to chemical, polymerization of aniline is carried out only in acidic electrolyte, since higher pH leads to formation of short conjugation oligomeric material, with different nature[45] .As stated before, it is generally accepted that the first step of the polymerization process of aniline involves formation of aniline cation radicals, by anodic oxidation on the electrode surface, which is considered to be the rate-determining step[69,70] .

The existence of aniline radical cation was experimentally confirmed, by introducing molecules, (resorcinol, hydroquinone, benzoquinine etc.), capable of retarding or even stopping the reaction, which evidenced a radical mechanism[68] . The oxidation of the aniline monomer is an irreversible process, occurring at higher positive potentials than redox potential of the polyaniline [50].

The following step is dependent on numerous factors such as: electrolyte composition, deposition current density, or potential scan rate, nature and state of the anode material, temperature etc. [50].

There is a request for relatively high concentration of radical cations near the electrode surface. Radical cations can be involved, depending on reactivity, in different reactions. If it is quite stable, it may diffuse into the solution and react to form soluble products of low molecular weights.

On the other hand, if is very unstable, it can react rapidly with anion or the solvent, in the vicinity of the electrode and form soluble products with low molecular weights [71].

In favorable case, coupling of the anilinium radicals would occur, followed by elimination of two protons and rearomatization leading to formation of dimer (lately oligomer). The aniline dimer, or oligomer, is further oxidized on the anode together with aniline. The chain propagation is achieved by coupling radical cations of the oligomer with anilinium radical cation.

Finally, the counter anion originating from the acid, normally present in the electrolyte, dopes the polymer, meeting the request of electroneutrality. Figure.(1.10) presents schematically mentioned mechanism of aniline electrochemical polymerization[64,45].

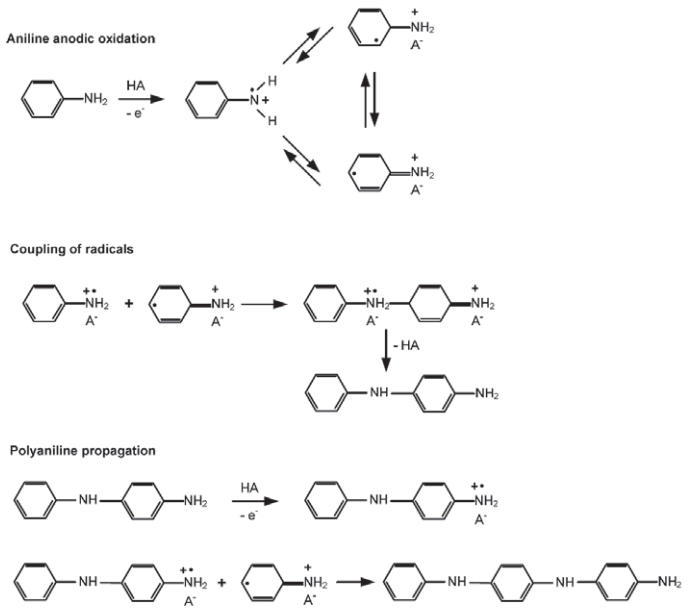

***Fig. (1.10) Schematic presentation of mechanism of electrochemical polymerization of aniline.*[64]**

Is evident that electrochemical polymerization of aniline is an autocatalytic process [50,72].

1.10.2 Nucleation and growth of polyaniline

Explanation of the kinetics of the nucleation and growth process during electrochemical synthesis of electroconducting polymers is usually relaying on the metal deposition theory [61,60]. According to the theory, two kinds of nucleation process exist, instantaneous and progressive, with three types of growth referring to: one-(1D), two- (2D), and three- (3D) dimensional processes.

Instantaneous nucleation implies constant number of nuclei, growing without the further formation of nuclei. In the case of progressive nucleation, nuclei are constantly generated. 1D growth implies growth in only one direction, e.g, perpendicular to the electrode surface. In 2D growth, the nuclei has preference to grow parallel to the electrode surface, while 3D growth is characterized by the similar rates for these processes perpendicular and parallel to the electrode are quite similar[60] .

It was shown, mostly based on potentiostatic experiments that several stages of polyaniline growth during electrochemical polymerization of aniline were involved, proceeding through different mechanism [67].Cyclic voltammetry studies indicated that polyaniline growth was strongly dependent on type and concentration of anion in the electrolyte [70](Zotti et al.,1988). Studies on the early stages of the polyaniline growth indicate progressive nucleation of the polyaniline film, with 2D or 3D growth mechanism or 3D instantaneous nucleation, depending on electrolyte concentration and composition [65,73,67].

In the case of perchloric acid, depending on monomer concentration, the nucleation process proceeds from progressive, at lower, to instantaneous nucleation at higher concentration [67]. At advanced stage, characterized by exponential current increase, 1D growth was assumed, resulted in continual branching and formation of the open structure [74].

1.11 Factors affecting electrochemical polymerization of aniline

Electrochemical synthesis of electroconducting polymers is strongly dependent on numerous parameters involved, such as: nature of the doping anion, electrolyte composition(affecting morphology, order of the polymer rate growth, nature and the composition of the solvent to nucleofilic solvent would react with cation radicals formed by monomer oxidation on the anode) and electrode material[60,50,40,45].

1.11.1 Doping anions

As mentioned above electrochemical polymerization of aniline, is practically always carried out in strong acidic aqueous electrolytes. Doping anions incorporated in polyaniline originate from the acid, and represent its conjugated base. The dopant anions are inserted during electrochemical polymerization fulfilling the request of electroneutrality, and therefore their concentrations are on the stoichiometric levels, for its reasonable that their presence have strong influence on, polyanilne morphology, conductivity, and electrochemical activity and the polymerization process itself[63,73,66,40] .

The order of the polyaniline growth was also proved to increase with the size of the dopant anion[59]. It was shown that addition of polyelectrolytes in polymerization electrolyte resulted in insertion of these molecules as dopants [45].

1.11.2 Electrolyte composition

As mentioned previously, electrochemical polymerization of aniline is usually performed in aqueous electrolytes. There is limited number of studies referred to electrochemical polymerization in non-aqueous solvents[66].

Various alkyl substituted anilines were electrochemically polymerized in both acetonytrile(CH_3CN) and dimethylsulfoxide(DMSO)($(CH_3)_2SO$),their conductivities were also very low suggested that there were not in the typical state of the emeraldine salt[75] .

Successful electrochemical co-polymerization of aniline and pyrrole was also carried out in acetonitrile. It was also observed that resulted polyaniline had exhibited good electrochemical activity in solutions with pH12, and also considerably wider window of the detectable color changes at higher pH values, this effect was explained by the fact that used ionic liquid possessed high buffer capacity, which improved the redox activity and the electrochemical activity in broader pH range[76] .

Apart from the strong influence of the solvent, the presence of other components in the electrolyte solution, used for electrochemical polymerization of aniline, also had influence, primarily, on the morphology of the deposit[50] . It was shown that presence of alcohols in the electrolyte would lead to polyaniline in the form of nanofibers agglomerated into interconnected network, FTIR spectra

of the resulted polymer revealed strong interactions between alcohol and polyaniline molecules[77] .

1.11.3 Electrode material

Electrochemical polymerization of aniline is easily performed at so called inert electrodes, such as: platinum, gold, various graphite, carbons or indium-tin-oxide glasses, according to previously described mechanism. But the fact that relatively high electrode potential is required for oxidation of aniline, restricts the usage of other materials. The electrochemical polymerization of aniline on active metals is usually considered for application in corrosion protection [78]. The problem connected to electrochemical polymerization onto active metals is either dissolution, or formation of nonconducting passive layer, on the potentials necessary for oxidation of aniline.

In the case of iron and steel the potential at which polymerization starts is in the region of active dissolution, leading to lost of the metal and contamination of the electrolyte, therefore it necessary to find a suitable electrolyte that would enable strong passivation of the metal without suppressing further electrochemical polymerization.

The most common electrolyte used to electrochemical deposition of polyaniline on steel and aluminum is oxalic acid [79] . The use of oxalic acid permitted formation of passive layer consisted of iron oxalate, on which aniline polymerize.

1.12 Deposition methods of thin PANI films

Different methods exist to deposit PANI onto a substrate. The most common are electrochemical deposition, dip-coating, spin-coating and drop-coating. However, deposition methods like thermal evaporation , Langmuir–Blodgett (LB) and self assembly techniques have also been described.

1.12.1. Electrochemical deposition

This deposition method is performed either in organic or in aqueous solutions. Three electrochemical methods can be used to PANI synthesis:

(i) galvanostatic method when applied a constant current,

(ii) potentiostatic method with a constant potential,

(iii) potentiodynamic method where current and potential vary with time.

Whatever the method is, a three-electrode assembly composes the reactor vessel: a working electrode on which the polymer is deposited, a counter electrode also named auxiliary electrode (platinum grid) and a reference electrode (in most cases, a saturated calomel electrode (SCE)).

The more common working electrode is a platinum one, but PANI depositions have also been realized onto conducting glass (glass covered by indium-doped tin oxide (ITO) electrode), Fe, Cu, Au, graphite, stainless steel [80].

Polyaniline can be then peeled off from the electrode surface by immersion in an acidic solution. Compared to chemical synthesis, this route presents several advantages [81] as cleanness because no extraction from the monomer–solvent–oxidant mixture is necessary, doping and thickness control via electrode potential, simultaneous synthesis and deposition of polyaniline thin layer. The drawback is that electropolymerization is restricted by the use of conducting substrate, no deposition can be obtained on insulating surface.

Electrochemical deposition is the most convenient method to deposit conducting polymer films. The thickness of the film can be controlled by the total charge passed through the electrochemical cell during film growing process. Moreover, the film can be deposited on patterned microelectrodes [82]. Of course, the deposition must be carried out on a conducting substrate. However, if the insulating gap between the neighboring electrodes is close enough (~several tens of micrometer), the growing film can cover the insulated gap and connect electrodes [83].

1.12.2 Dip-coating.

When dipping a substrate into a chemical polymerization solution, part of the polymer will be deposited onto its surface [84, 85]. This process occurs on different substrates, and the thickness of the film is usually controlled by dipping time. Another similar process involves alternatively immersing a substrate into the monomer and oxidant solutions. The adsorbed monomer will be polymerized on the surface of substrate [86,87].

1.12.3 Spin-coating.

Spin-coating is a simple method for preparing films from soluble conducting polymers. In this process, the conducting polymer solution is spread on a rotating substrate [88, 89].

After evaporation of solvent, a thin film was formed. Repeating above process is feasible, which can control the thickness of the film. Concentration of the solution and rotating rate of the substrate are also play important roles in adjusting the thickness of the formed film. This method can coat conducting polymers on both conducting and insulating substrates.

1.12.4 Langmuir-Blodgett (LB) technique.

LB technique is a famous method to produce a thin film of polymer and surfactant. The operation of LB technique has been described in many books and literatures. Two different ways are reported to deposit a conducting polymer film by LB technique: directly depositing polymer and depositing monomer followed by polymerization on the substrate. A LB film is ultrathin (monomolecular layer), and a thick film can be obtained by repeating the procedure of LB deposition[90].

1.12.5 Layer-by-layer (LBL) self-assembly technique.

By alternative immersing the substrate into a polymeric anion solution and a polymeric cation solution, an alternative composite film (layer by layer) consists of the two polymeric electrolytes is fabricated [91, 92]. Doped conducting polymers, such as PANI, bring positive charge on their backbone, which allow it possible to deposit with a polymeric anion. The thickness of the LBL film depends on the number of repeating times.

1.12.6 Thermal evaporation.

This technology can be realized by heating conducting polymer under vacuum, and the evaporated conducting polymer deposits on the target substrate. The thickness of the film is determined by the evaporation duration [93].

1.12.7 Vapor deposition polymerization.

This technology consists of two steps: prepare an oxidant film and then place the film into monomer vapor [94]. The monomer diffuses into the film and polymerized on it. This technique is useful not only in preparing a pure

conducting polymer film, but also in coating composite films of different conducting polymers.

1.12.8 Drop-coating.

A polymer solution is drop dried [95,96], or some drops of the monomer and oxidant solutions are dropped and reacted on a substrate. This technology is rather simple. However, the resulting film is usually not uniform.

1.12.9 Other methods

An electric field induced electrochemical polymerization can fabricate patterned conducting polymer film. The polymerization of pyrrole occurs between an electrode gap (5 mm) when a voltage is applied in the saturated vapor of pyrrole [97]. Colloidal suspension of PANI is controlled to directionally deposited on microelectrodes at controlled voltages [98]. For soluble conducting polymers, inkjet-print also is a convenient method for producing thin films [99]. Some researchers also packed conducting polymer powders into pellets to fabricate the active layers [100, 101].

1.13 Solubility of PANI

The protonated emeraldine salt form of PANI is insoluble in aqueous solutions and most common organic solvents. It is soluble in concentrated sulfuric acid[102].When the emeraldine salt is deprotonated to the insulating emeraldine base, it can be solubilised in a number of organic solvents [103,104,105] such as methyl pyrrolidinone (NMP), dimethyl formamide (DMF), dimethyl sulfoxide (DMSO), *m*-cresol, chloroform (CCl_3H) and tetrahydrofuran (THF). The process of deprotonation effectively removes the cationic charges upon the backbone, reducing the polymers ionic character making it more amenable to dissolution.

1.14 Carbon Nanotubes

In 1960 carbon Nanotubes were observed from Bacon at Union Carbide in Parma [106], he began carbon arc research to investigate the properties of carbon fibers. He studied the melting of graphite under high temperatures and pressures and he investigated carbon nanotube by SEM in 1960. He presented the observation of carbon nanowhiskers of his material under the same investigation and he proposed a scroll like-structure [106]. In 1976, Endo *et.al* produced and

imaged nanotubes under high resolution transmission electron microscopy (HRTEM) [107].

In the mid of 1985, Kroto *et al*. [108] reported the synthesis of cyanopolyynes from laser vaporization of a graphite target and they discovered a family of large 60–carbon atom. These molecules were designed and built by Fuller and thus, were referred to as 'Fullerenes'.

Fullerenes are large, closed shell–cage clusters with high gas–phase stability which have been discovered by the mass spectrometer of evaporated carbon samples in carbon soot.

The most famous Fullerenes is C^{60}, is referred to "Buckminster Fullerene", or "bucky ball," and its structure is shown in Figure(1. 11).

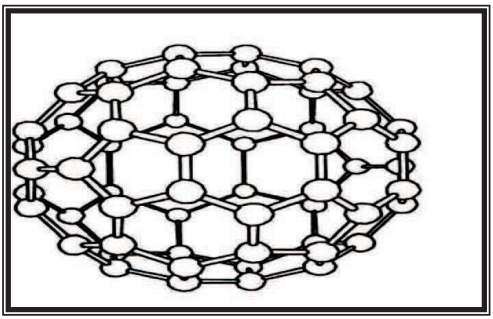

Fig. (1.11) Buckminster Fullerene or 'Buck ball' structure[109]

The first reported observation of carbon nanotubes was made by Ijima at Nagoya University in 1991(Japanese)[110]using a high–resolution electron transmission microscope (HRTEM). Iijima discovered multi-walled nanotubes while studying carbonaceous deposited from a direct current arc discharge between graphite electrodes in a helium environment at 3273 K. These carbon filaments have a small diameter (a few nanometers) and a large length (several microns) and were referred to as carbon nanotubes, as in Figure (1.12). Two years after (in 1993), Iijima and Ichihashi[111] and Bethune and coworkers[112]simultaneously observed single walled carbon nanotubes (SWNTs).

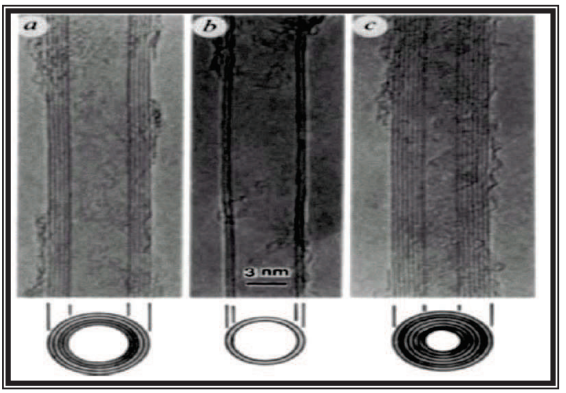

Fig.(1.12) Electron micrographs of microtubules of graphitic carbon by Iijim :a. Tube consisting of graphic sheets .b. Two-sheet tube. c. Seven-sheet tube [111]

1.15 Structure of Carbon Nanotubes

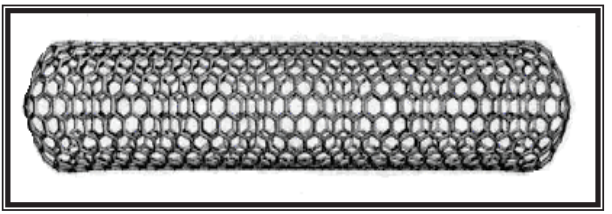

Fig.(1.13) Molecular model of a carbon nanotube capped by six pentagons in each end [113]

The discovery of carbon nanotubes pioneered a new direction in carbon research that complemented the activities on the fullerene research front. Unlike the fullerene structure, where carbon atoms form a sphere, carbon nanotubes are cylindrical structures contain a hexagonal network of carbon atoms rolled up to form seamless cylindrical tubes either infinite in length or with caps at each end by pentagonal carbon rings. A molecular model of carbon nanotubes closed on both ends by six hemispherical pentagons is shown in Figure(1.13) [113].

Carbon forms diamond, which is composed of tetrahedral bonded carbon atoms, under conditions of extreme temperature and/or pressure as shown in Figure (1.7). The four valence electrons in carbon are shared equally and exhibit

sp^3 hybridization (sp^3 C-C bond length ~ $1.56A^0$), whereby four bonds are directed towards the corners of a regular tetrahedron to form extremely isotropically , rigid three dimensional structure and hence , it is the hardest substance known and it has the excellent heat conduction properties (about five times better than copper)[115] . In graphite, only three valence electrons are shared covalently between neighbors in x-y plane and the fourth is allowed to be delocalized among all atoms and this is resultant to compose of sheets of triagonal bonded carbons atoms arranged in hexagonal sheets called graphite sheets, then sp^2 hybridization occurs, of bonding builds a layered structure with strong in plane bonds and weak out of plane bonding of the van der Waals bond due to the p_z orbital is present in the x-y plane and a van der Waals bond due to the p_z orbital in the z-axis[106], i.e. the free electrons in the p_z orbital of the graphite lattice are delocalized and move within the lattice framework .Consequently, graphite is a soft, grey material due to its ability to slide along plane with high electrical conductivity and also is the thermodynamically stable bulk phase of carbon. Unlike the sp^3 hybridized diamond in which all electrons localized in sp framework, it behaves as an insulator, optical transparency and is only kinetically stable [106] . The tetrahedrally bonded diamond and triagonal bonded graphite structure are shown in Figure(1.14) and Figure(1.15) respectively[116] .

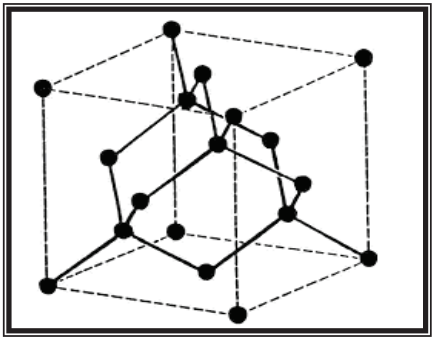

Fig. (1.14) Tetrahedrally–bonded structure of diamond, [116]

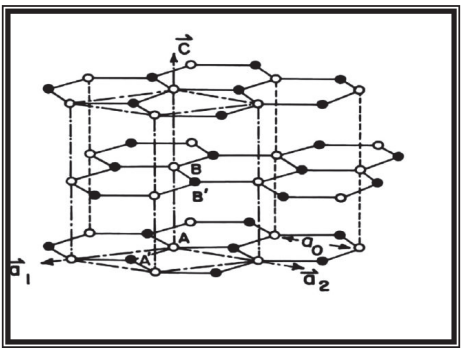

Fig.(1.15) Trigonally–bonded graphite structure[116]

The sp^3 and sp^2 hybridization scheme in the C–C structure is depicted by Fig.(1.9)

.

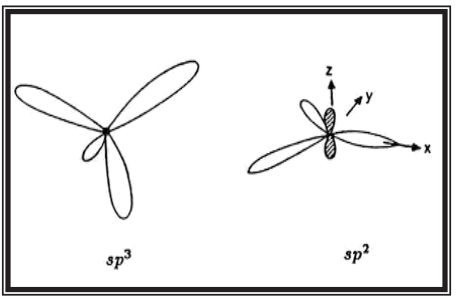

Fig.(1.16) sp^3 and sp^2 hybridization scheme in C–C structure[116]

1.16 Types of Carbon Nanotubes

The two main categories of carbon nanotubes exist, the single–walled carbon nanotubes (SWNTs) and multi–walled carbon nanotubes (MWNTs) depending on whether the tubes walls are made of one layer (graphene tubes) or more than ones (graphitic tubes) [117] .

1.16.1 Single Walled Carbon Nanotube (SWNT)

SWCNTs are regarded cylindrical in shape and composed of singular graphene sheet rolled in cylinder walls Figure(1.17) with diameters ranging from 0.4 to 3 nm and due to difference in the length and diameter, their physical and chemical properties differ. It is consisted of two separate regions, with distinct physical and

chemical properties . The first is the side wall of the tube and the second is the two hexagon cups [118]

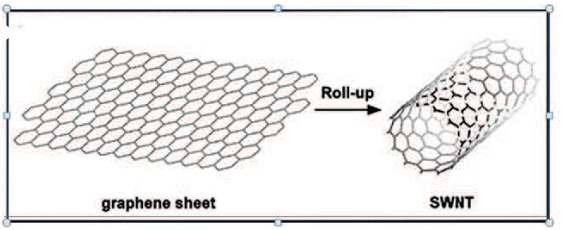

Fig(1.17) Single walled Carbon Nanotube

1.16.2 Multi Wall Carbon Nanotubes (MWNTs)

MWCNTs which are the most general case, are a group of concentric SWCNTs Figure(1.18) often capped at both ends, with different diameters in the range from several nanometers up to 200 nm[119]. These concentric nanotubes are held together by van der Waals bonding. MWNTs form complex systems with different wall numbers, structures, and properties and additional features such as: tips, internal closures within the central part of the tube, and the properties are also very different. Compared with multi walled nantubes, SWCNTs are expensive, clean and difficult to obtain, but they have been of great interest owing to their expected novel electronic, mechanical, and gas adsorption properties.

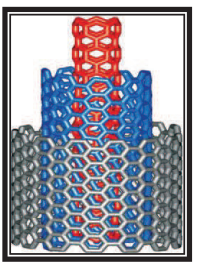

Fig.(1.18)Theoretical model for a multi walled carbon [119]

1.17 Properties of Carbon Nanotube

Carbon nanotubes have gained in interest as nanoscale materials due to their exceptional, outstanding properties. There are tubular carbon molecules with exciting and fascinating properties compared to the parent planar graphite due to the unique structure, topology dimensions of the nanotubes, high Young's

modulus, ultimate strength, high electric and thermal conductivity. Moreover, CNTs provide a remarkable model of 1D system . The properties are greatly dependent on how sheets have been rolled up, the tube and length diameter, aspect ratio (ratio between diameter and length) and the nanotube morphology[121] . More details on the properties of carbon nanotubes are presented below.

1.17.1 The Mechanical Properties

The small sizes and high surface-to-volume ratios of one-dimensional nanostructures endow for CNTs a variety of interesting and useful mechanical properties as well as, the high strength of C–C covalent bonds in carbon nanotubes makes them one of the strongest materials in nature and gives carbon nanotubes their unique strength, and thus, carbon nanotubes are one of the stiffest and most robust synthesized structure. CNTs have a very high Young's modulus being over (1-5) TPa for MWNTs, nearly five times greater than steel , high tensile strength of (10- 200) GPa [122].

1.17.2 The Electrical Properties

Carbon nanotubes possess unique electrical properties because of the diameter being in the nanometer range gives rise to quantum effects and this quantum confinement of electrons normal to the carbon nanotube axis, resulting in electron propagation occurring only along the carbon nanotube axis. Theoretical studies predicted a strong dependence of the electrical conducting properties of carbon nanotubes on their molecular structure, so that the carbon nanotube can either be metallic or semiconducting, depending on their helicity and diameter.

MWNTs behave like quantum wires due to the confinement effects on the tube circumferences. The conductance of carbon nanotubes is given by [119]:

$$G=G_0M=(2e^2/h)M \quad \text{..... (1.1)}$$

where $\mathbf{G_0=(2e^2/h)= 12.9(k\Omega)^{-1}}$ is the quantum unit of the conductance, *e* is electron charge, h is Planck's constant, M is an apparent number of conducting channels including electron-electron coupling and intertube coupling effects in addition to intrinsic channels.

Multi walled carbon Nanotubes(MWNTs)are quite often found to be one-dimensional conductors with a high electrical conductivity even $>10^3$ $(\Omega\ cm)^{-1}$ .The metallic properties of the MWNTs are due to their multiple-shell structure consisting of tubes with various electrical properties**.** The electrical current that could be passed through a multi wall nanotube corresponds to a current density in excess of 10^7 A/cm^2 [123].

1.17.3 The Optical Properties

Besides the mechanical and electrical properties, CNTs exhibit interesting thermal and optical properties. Because of the one dimensional electronic structure, electronic transport in SWNTs and MWNTs occurs ballistically (i.e. without scattering) over long nanotube lengths, enabling them to carry high currents with essentially no heating. Phonons also propagate easily along the nanotube. The experimental measurements of the optical absorption of carbon nanotubes show that there are several groups of absorption peaks and each group is closely related to the nanotube geometry[116,117].

The energy band gap of semiconducting CNTs highly depends on the nanotube diameter and is given by [124] :

$$E_{gap}=\frac{2\gamma_0 a_{c-c}}{d} \quad \text{.....(1.2)}$$

Where γ_0 denotes the C-C tight binding overlap energy (2.45eV), $a_{C\text{-}C}$ is the nearest neighbor C-C distance (~1.42 Å), and d is the diameter of a nanotube.

Also, band gaps depend on specific possible chiral vectors in terms of the integers (m, n) indices , for small gap semiconducting carbon nanotubes $m - n =$ 3i where i is integer, the energy gap in the range of 2–50 meV for d = 3–0.7 nm. These nanotubes are usually called small-gap semiconducting or semimetallic nanotubes. The small band gaps are expected to have nontrivial consequences to the electrical properties of SWNTs.

For semiconducting carbon nanotubes , when $m-n \neq 3i$, the band gap can vary from ~2.5 eV to below 0.5 eV. Devices consisting of such nanotubes display strong dependence on both the temperature and the gate bias, and therefore have great potential to be used as building blocks for nanoelectronic systems**.**

1.17.4 Chemical Properties

In comparison to a graphene sheet, the chemical reactivity of carbon nanotubes is greatly enhanced by the curvature of the CNT surface and directly related to the pi-orbital mismatch caused by an increase curvature. Therefore, a distinction must be made between the sidewall and the end caps of a nanotube , a smaller nanotube diameter results in increased reactivity. The solubility of carbon nanotubes in different solvents can be controlled by the covalent chemical modification of either the sidewalls or the hemispherical end caps[125].

Because of the non-polar nature of the carbon bonds, carbon nanotubes are insoluble in water. SWNTs can be made to form stable suspensions in certain organic solvents like toluene, dimethyl formamide (DMF), and tetrahydrofuran (THF), but they are generally insoluble in any medium without chemical modification or coordination with surfactant Nanotubes are subject to the rules of carbon chemistry [126].

1.17.5 Thermal Properties

All nanotubes are expected to be very good thermal conductors along the tube, exhibiting a property known as "ballistic conduction" but good insulators laterally to the tube axis. It is predicted that CNTs will be able to transmit up to (6000W/m.K) at room temp. Compare this to copper, which only transmit 385W/m.K. The temperature stability of carbon nanotubes is estimated to be up to 2800ºC in vacuum and about 750ºC in air[127].

1.18 Carbon Nanotube Synthesis

Carbon nanotube can be synthesized using different techniques involving gas phase processes. These processes provide access to the high synthetic temperatures required for carbon nanotube production. Three main methods of producing carbon nanotubes are: the electric arc discharge, laser vaporization and chemical vapor deposition. Other techniques include electrolytic synthesis, solar production method etc. are being developed to find more economical ways of producing the unique and novel materials.

1.18.1 Laser Ablation Technique

In 1996, Smalley *et.al* [128] reported the synthesis of carbon nanotubes using laser vaporization of a carbon target to synthesize SWNTs. The laser vaporization technique involves the use of a pulsed or continuous laser to vaporize a graphite target, in an oven of 1473 K; the oven is filled with helium or argon gas in order to keep the pressure at 500 torr and containing a small amount of transition metal particle catalysts. An oven laser vaporization apparatus is shown in Figure(1.19).

The laser vaporizes the metal–graphite target and nucleates carbon nanotubes in the shockwave just in front of the target, while flowing argon gas sweeps the vapor and nucleated nanotubes, which continue to grow, from the furnace to a water-cooled copper collector [119].

Multi–walled carbon nanotubes are generated by this method when the vaporized carbon target is pure graphite whereas the addition of transition metals (Co, Ni, Fe or Y) as catalysts to the graphite target results in the production of SWNTs

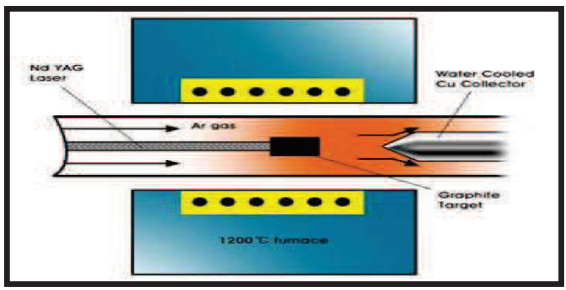

. ***Fig. (1.19) Schematic laser vaporization*** **apparatus**[125]

1.18.2 Chemical Vapor Deposition (CVD)

CVD was first reported to produce defective MWNTs in 1993 by Endo et.al. The CVD process encompassed a wide range of synthesis techniques, from gram-quantity bulk formation of nanotubes material to the formation of individual aligned SWCNTs on SiO2 substrates for use in electronics [129].

CVD has become the most important commercial approach for manufacturing carbon nanotubes. CVD is known as irreversible deposition of solid from gas or

a mixture of gases through a heterogeneous chemical reaction. The principle of this technique is shown in Figure (1-20) [130] .

The process for CNT production by CVD usually involves gaseous carbon feed stock which is flowed over transition metal nanoparticles at medium to high temperature (550 to 1200°C) and reacts with the nanoparticles to produce CNT as shown in figure (1.20). Depending on these conditions, (feed stack and catalyst), the yield can exceed 99% [129].

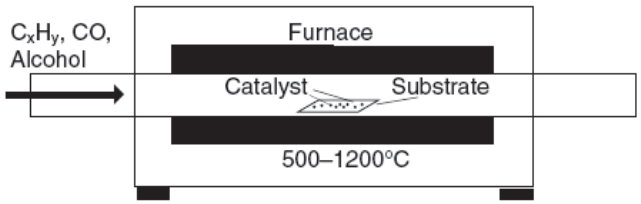

***Fig. (1.20): Diagram of a CVD furnace* [129].**

There are different techniques for the carbon nanotubes synthesis by using CVD, such as plasma enhanced CVD, thermal CVD, and alcohol catalytic[131].

1.18.3 Electric Arc Discharge

The arc-discharge technique is the most easiest way and the first method employed by Iijima[110] for the production of both SWNTs and MWNTs. It was originally employed in fullerene synthesis.

The carbon nanotubes which were first observed as need like structure ranging from 4 to 30 nm in diameter and up to 1mm in length were grown on the cathode surface of an electric arc discharge chamber[125].

This method creates nanotubes through arc discharge of two graphite electrodes with different diameter ranging from 5nm to 20 mm placed end to end separated by approximately 1mm under an inert gas atmosphere. Typically synthesis conditions for the carbon arc discharge method employ a direct current (50 to 120A) power supply (an arc welder can be used) and a low voltage discharge (12 to 25V) operating in an inert gas in contrast with the low–current, high voltage glow discharge (electrical current passing through a gas vapor of electrode material[125]. The arc voltage has to be near the ionized potential of the

gas or vapor. The magnitude of the current required is proportional to the diameter of the electrode as a higher current needed to vaporize larger electrodes. A typical electric arc discharge apparatus is shown in Figure (1.21).

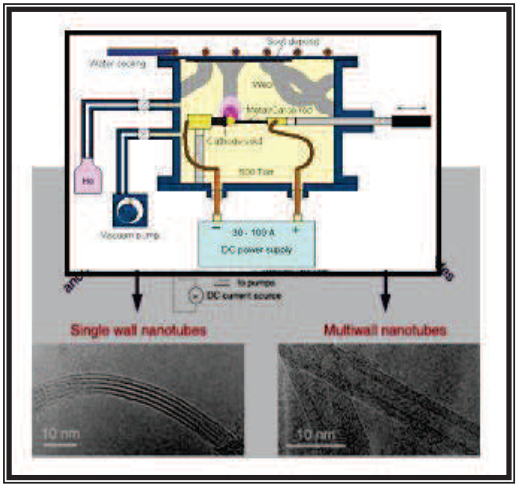

***Fig.(1.21) Schematic of an arc discharge chamber with TEM Pictures for carbon nanotube*[125].**

When direct current (D.C.) is passed between two electrodes immersed in a chamber containing gas, the glow will be formed and creates a high temperature discharge. The discharge vaporizes one of the carbon electrodes (anode) to form a rod shaped deposited on the other electrode (cathode), the carbon nanotubes form mainly where the current flows and the inner region of the electrodes, where the most copious tubular harvest is obtained, has an estimated temperature of 2737-3373 K[116].

Multi-walled carbon nanotubes are the main products generated by the electric arc discharge technique if both electrodes are graphite, while SWNTs are synthesized by co-evaporation of hollow graphite anode mixed with transition metals such as iron (Fe), cobalt(Co), nickel(Ni), Molybdenum(Mo) and Yttrium(Y) etc. In electric arc discharge, the results are mixture components and required separation and purification of CNTs from the soot and other impurities present in the cured reaction products [115] . The cost of producing carbon nanotubes through the arc discharge method is quite expensive because of the

high–purity graphite electrodes, metal powders and high–purity inert (Helium/Argon) gases employed in the production process [118].

1.19 Purification of Carbon Nanotubes

Consequently, various purification techniques have been devised in order to improve the quality and yield of carbon nanotubes obtained. These purification methods employed in the post–syntheses processing of carbon nanotubes include oxidation, acid treatment, annealing, micro filtration, Ultrasonication, ferromagnetic separation, fictionalizations and chromatography techniques. The purification procedures used are stated below:

1.19.1 Oxidation

The oxidative treatment of carbon nanotubes in air/oxygen removes carbonaceous impurities, such as amorphous carbon, and helps to expose the catalytic metal surface enclosed in the carbon nanotube for further purification techniques. The main purpose of the oxidative treatment is the high ability of the carbon nanotubes being oxidized during impurities oxidation [125].

1.19.2 Acid Treatment

Acid treatment of SWNTs is used to remove metal catalyst. The surface of the metal must be exposed by oxidation or sonication followed by the solvation of the metal catalyst on exposure to an acid. The SWNTs remain in suspended form. When using a treatment in HNO_3, the acid only has an effect on the metal catalyst. It has no effect on the SWNTs and other carbon particles. If a treatment in HCl is used, the acid has also a little effect on the SWNTs[136].

1.19.3 Annealing

Due to high temperatures (873–1873) K the nanotubes will be rearranged and defects will be consumed. The high temperature also causes the graphitic carbon and the short fullerenes to pyrolyse. When using high temperature vacuum treatment (1873 K) the metal will be melted and can also be removed [125].

1.19.4 Ultrasonication

This purification technique involves the separation of particles due to ultrasonic vibrations whereby agglomerates of different nanoparticles undergo forced vibration and become more dispersed. The separation of the particles is highly dependable on the surfactant, solvent and reagent used[115].

1.19.5 Magnetic Purification

In this purification technique, ferromagnetic (catalytic) particles are mechanically removed from their graphitic shells. The as-produced SWNTs suspension is mixed with inorganic nanoparticles (mainly ZrO_2 or $CaCO_3$) in an ultrasonic bath to remove the ferromagnetic particles from their graphite shells. Then, the particles are trapped with permanent magnetic poles, followed chemical treatment, to obtain high purity SWNTs. Figure.(1.22) shows a schematic diagram of the apparatus for magnetic purification[138] .

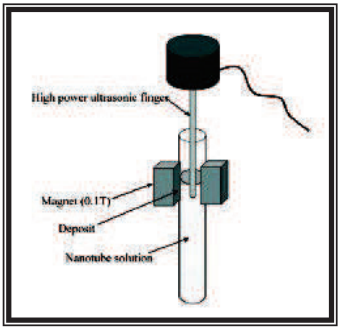

Fig.(1.22) Schematic diagram of the apparatus for magnetic purification [125]

1.19.6 Microfiltration

Microfiltration technique, based on size or particle separation, separates coexisting carbon nanospheres (CNS), metal nanoparticles, polyaromatic carbons and fullerenes from single walled carbon nanotubes. It involves the suspension of CNS, metal nanoparticles and SWNTs in an aqueous solution using a cationic surfactant. The carbon nanotubes are subsequently trapped using a membrane filter, while other nanoparticles (metal nanoparticles and carbon nanospheres) pass through the filter [137].

1.19.7 Chromatography

This technique is mainly used to separate small amounts of SWNTs into fractions with small size (length and diameter) distribution. The process involves running SWNTs over a column with porous material, through which the SWNTs will flow [115].

1.20 Polyaniline–Carbon nanotube composites

Electroactive polymers have been an area of immense interest over the past 36 years since the first discovery of conducting polyacetylene in 1977 by Shirakawa et al. [138]. Extensive research on several conjugated polymers including poly(*p*-phenylene), polyaniline (PANI), polypyrrole, polythiophene, polyindole,polycarbazole, polyfluorene, poly(*p*-phenylenevinylene), and their substituted derivatives have led to their applications in rechargeable batteries, microelectronics, sensors, electrochromic displays, light-emitting and photovoltaic devices [139,140]. Among the various conjugated polymers, PANI Figure(1.23) has received special recognition owing to its good stability and interesting redox behavior [141-144]. In the past few years, several novel ethodologies have been developed for the preparation of nanostructured PANI in the form of dispersions, nanowires, nanofibers, and nanotubules [146-148].

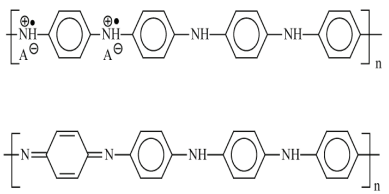

***Fig (1. 23)scheme ES forms and EB*[141]**

The discovery of fullerenes[110] and carbon nanotubes (CNTs) [112] has led to an explosion of research in nanoscience and nanotechnology. In fact, the focus in nanoscience has since shifted from synthesis to applications. A logical extension is to find new combinations of the existing materials as hybrid materials, blends, and nanocomposites for exploitation of their complementary properties[148-150].

In this context, there has been a new surge of interest in developing conducting polymer–CNT composites as novel futuristic materials. One main reason for this

is that common applications of the two components offer the possibility to observe synergetic effects. Already, various studies have proved that certain discrete properties of the components of conjugated polymer–CNT composites are enhanced, thus validating their high suitability for some technological applications [151].

This review focuses mainly on the extensive literature published since 1999, on the preparation characterization, and applications of PANI–CNT nanocomposites. The possible interactions between PANI and CNT that may be responsible for enhancement in certain properties of the composites are highlighted. Wherever applicable, the literature on CNT composite materials with substituted derivatives of PANI is also included.

1.21 Preparative Methods

Since the first report in 1999 on the efficient electropolymerization of aniline on CNT whiskers [152], a number of innovative methodologies have been developed for preparing PANI–CNT composites. A general scheme of the common preparative methods is given by figure(1.24).

Apart from direct solid-state mixing [153] and dispersal of CNTs in PANI solutions of *N*-methyl-2-pyrrolidinone[154] or HCl [155], several chemical and electrochemical procedures have been reported. A simple method is in situ chemical polymerization of aniline in an acidic dispersion of multiwall carbon nanotubes (MWNTs) or single-wall carbon nanotubes (SWNTs) in the presence of an oxidant at low temperature[156,157].

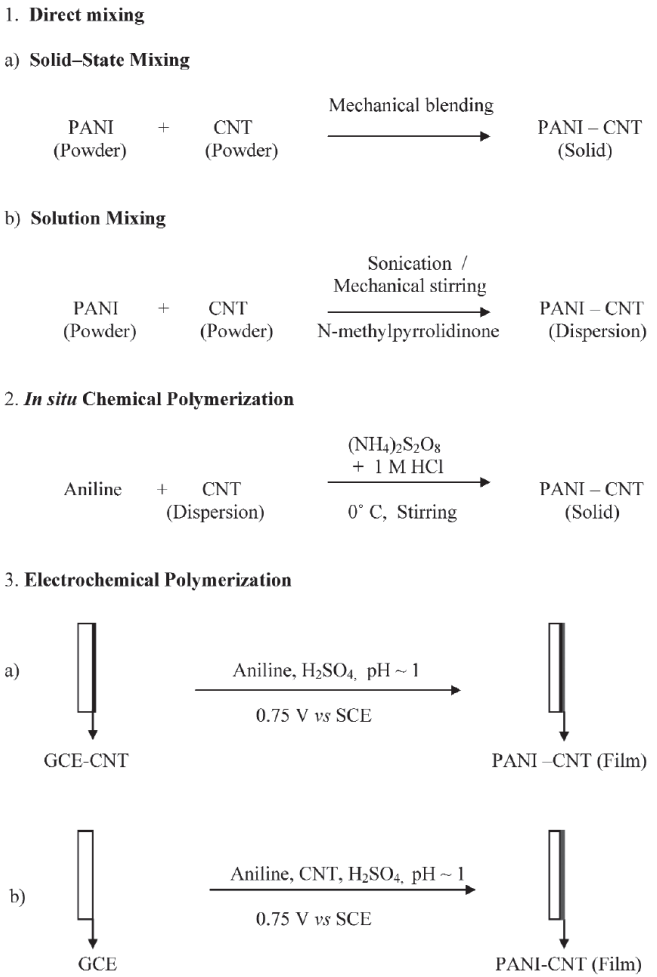

Fig(1.24) Generalized scheme of preparative methods of PANI–CNT composites where GCE represented (Glassy carbon Electrode) [156]

1.22 Interactions Between PANI and CNTs

The electrical, thermal, and mechanical properties of PANI–CNT composites are intermediate between pure PANI and CNT but vary depending on CNT content and the extent of its integration with PANI. However, it is exceptional that the electrochemical properties of these composites are tremendously

enhanced compared to the two individual components. For example, despite the same surface area, the electrochemical growth, redox and capacitive currents of the composites are several-fold higher compared to the values obtained on pure PANI Figure (1.25)[158,159] .

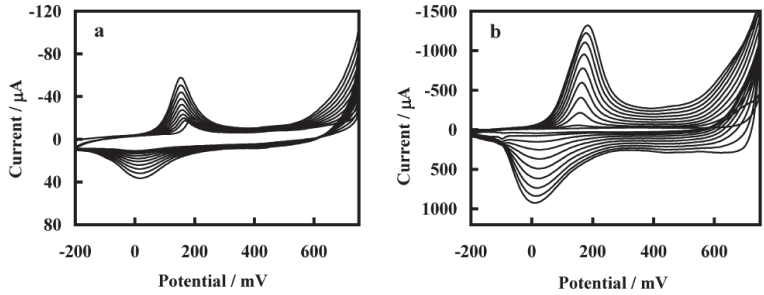

Fig.(1.25) Current enhancement during cyclic voltammetric growth of PANI at (a) GCE (0.07 cm²) and (b) CNT/GCE (0.07 cm²); electrolyte: 0.5 M aniline in 1 M H_2SO_4; sweep rate: 50 mV s^{-1}.[158]

Several studies have dealt with the various possible interactions between PANI and CNT in the composites. One of the first suggestions has been the attachment of aniline radicals, generated during electrochemical oxidative polymerization, onto the CNT lattice especially at defect sites resulting in local deposits which grow in size and finally become interconnected to form a multilayer coating[160].

The FTIR spectra of pure PANI and PANI/MWNT composites are presented in Figure (126) [161] .

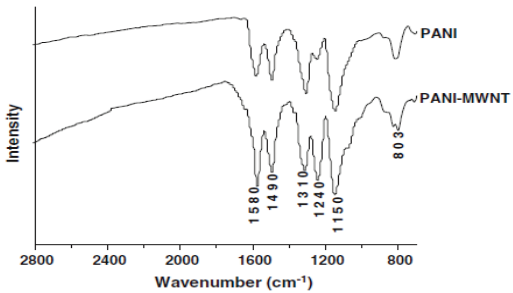

Fig.(1.26) FTIR spectra for PANI and PANI/MWNT composites [161]

The bands situated 1490 cm^{-1} and 1580 cm^{-1} are attributed to benzoid and quinoid ring vibrations, respectively[162,163]. It's commonly observed for PANI that the quinoid band at 1580 cm^{-1} is less intense than that of the benzenoid band at 1490 cm^{-1}. As shown in spectrum of PANI/MWNT composites, an inverse 1580/1490 cm^{-1} intensity ratios was exhibited. These data reveal that PANI in the composite is richer in quinoid units than the pure PANI. This fact may suggest that PANI–MWNTs interactions promote and stabilize the quinoid ring structure. As shown in Figure (1.27) the interaction between polyaniline and MWNTs may result in (charge transfer)[164] .

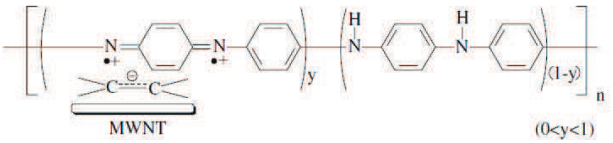

Fig (1.27) scheme illustration of interaction between PANI and MWNT [164].

The p-bonded surface of the carbon nanotubes might interact strongly with the conjugated structure of polyaniline, especially through the quinoid ring [165]. Such selective interaction of the carbon nanotubes with the quinoid ring of PANI has been reported in previous literature[164,165]. The peak at 1240 cm^{-1} is attributed to C–N stretching + ring deformation + C–H bending vibration mode[163,166,167]. Detected as a weak band in the spectrum of pure PANI, its enhancement in PANI/MWNT composites indicates more vibrational units associated to C–N bonds. The new covalent C–N bonds are mainly formed between the imine nitrogen atoms of the repeating units of PANI and the carbon atoms of carbon nanotubes. An appropriate microscopic picture for these composites is that of a carbon nanotube wrapped with the polymer [162,165,167].

1.23 Sensing Principles

Chemical sensors transform the concentrations of analytes to other detectable physical signals, such as currents, absorbance, mass or acoustic variables. After exposing to the vapor of an analyte, the active sensing material of the sensor interacted with the analyte, which causes the physical property changes of the

sensing material. The interactions between the analytes and sensing materials are multiform, according to different analytes and different active materials, and they are discussed in the following sections.

1.23.1 Interactions between gas molecules and conducting polymer films

Chemical reactions between analytes and conducting polymers. As described above, the physical properties of conducting polymers strongly depend on their doping levels. Fortunately, the doping levels of conducting polymers can be easily changed by chemical reactions with many analytes at room temperature, and this provides a simple technique to detect the analytes. Most of the conducting polymers are doped/undoped by redox reactions; therefore, their doping level can be altered by transferring electrons from or to the analytes. Electron transferring can cause the changes in resistance and work function of the sensing material. The work function of a conducting polymer is defined as the minimal energy needed to remove an electron from bulk to vacuum energy level. This process occurred when PPy, PTh and in some case PANI films exposed in NH_3, NO_2, I_2, H_2S and other redox-active gases [168-176]. Electron acceptors, such as NO_2 and I_2, can remove electrons from the aromatic rings of conducting polymers. When this occurs at a p-type conducting polymer, the doping level as well as the electric conductance of the conducting polymer is enhanced.

An opposite process will occur when detecting an electro-donating gas. However, this mechanism has not been understood clearly. Ammonia is an electron-donor; when PPy reacts with ammonia, its electric resistance dwindles down sharply. However, after washing with dry nitrogen or air, the resistance of the sensing layer can be totally or partly recovered. Following reactions are possibly involved in the ammonia sensing process[177,178]:

$$PPy^{+} + N\ddot{H}_3 \rightarrow PPy^{0} + NH_3{}^{+} \quad Adsorption \ldots\ldots\ldots (1.3)$$

$$PPy^{0} + \ddot{N}H_3{}^{+} \rightarrow PPy^{+} + \ddot{N}H_3 \quad Desorption \ldots\ldots\ldots (1.4)$$

1.23.2. Chemiresistors

Chemiresistors are the most common type of sensors[179-181]. They can be fabricated through a cheap and convenient process [183]. A chemiresistor is a resistor, whose electric resistance is sensitive to the chemical environment .

Chemiresistor consists of one or several pairs of electrodes and a layer of conducting polymer in contacting with the electrodes, as illustrated in Figure (1.28).

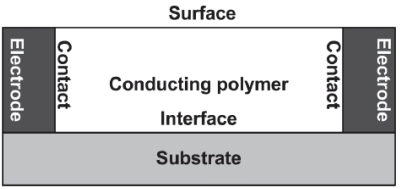

Fig.(1.28). Configuration of chemiresistor[182]

The electrical resistance change of the sensing material is measured as the output, so a simple ohmmeter is enough to collect the data. Usually, a constant current or potential is applied on the sensor, and the measuring signal is potential or current change, respectively. To improve the performance, interdigitated electrodes widely used[183-185] , and a typical one was shown in Figure (1.29). This type of sensor is simple but efficient.

Fig(1.29) Interdigitated electrodes (IDE). The dark pattern is conducting electrode and the white part is insulating substrate [178]

An equivalent circuit diagram is presented in Figure.(1.30) [186]. The change in any parts of the sensor will cause a consequential change of overall resistance of the device. Of course, the most important part is the bulk resistance. For a doped conducting polymer, its conductivity consists of three component:

$$\frac{1}{\sigma} = \frac{1}{\sigma_c} + \frac{1}{\sigma_h} + \frac{1}{\sigma_i} \dots\dots\dots\dots\dots\dots\dots\dots\dots\dots\dots\dots\dots\dots (1.5)$$

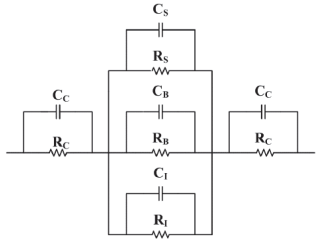

Fig.(1.30). Equivalent circuit diagram of the IDE shown in Figure (1.29)[186].

where σ is overall conductivity,σ_c the intermolecular conductivity, σ_h the intrmolecular hopping conductivity and σ_i the ionic conductivity, respectively.

This is achieved by swelling the polymer, changing crystallinity, forming H-bonds and dipolar dipolar interactions, σ_i is controlled by mobility of counter ions, which is effected by the interaction between the ions and analytes. The contact resistance was studied by Mirsky et al. [187,188].

They designed a four-point Interdigital electrode to reduce the contact resistance and enhance the response of a chemiresistor. Other researchers reported that the sensors based on conducting polymer nanofibers have a worse performance than those of ordinary films.

Alternating current (AC) also has been used as the signals of chemiresistor sensors[180,189]. When AC current is applied, the capacitance and inductor should be included in equivalent circuit model. Both of these two variables are related to gas interaction with the sensing film. . The peak position is unique for different gases and useful in distinguishing them[190,191].

1.24 Basic Characteristics of Chemiresistor Gas Sensors

The electrical resistance of a chemiresistive sensor change drastically (increase or decrease) when exposed to the molecules of analyzing gas .increase or decrease in resistance depends on the nature of sensor material(n-type or p-type)and the gas (reducing or oxidizing).Atypical response curve ,that is, variation of resistance of sensor with time of exposure and with drawal of analyzing gas is schematically depicted in figure (1.31).

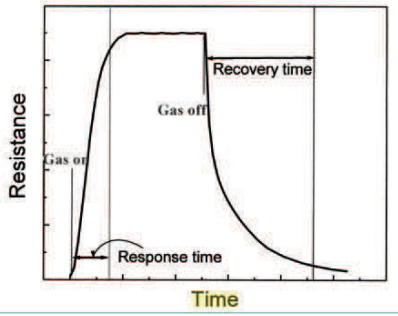

***Fig(1.31)Schematic response curve of a chemiresistive gas sensor*[192]**

The response curve of sensor is characterized by following five parameter (Sensitivity, Response time, Recovery time, Selectivity, and Long time stability)[192].

(i)Sensitivity

The Sensitivity (*S*) of a sensor can be defined by many ways . The often used definitions of S are the following

a) A ratio of resistance in air to that in gas

$$S = \frac{R_{air}}{R_{gas}} \dots\dots\dots\dots\dots\dots\dots\dots\dots\dots\dots\dots\dots\dots\dots\dots\dots\dots (1.6)$$

A high value of S for a particular gas indicates that the material is very good sensor.

b) sensitivity percentage

$$S(\%) = \left(\frac{R_{air} - R_{gas}}{R_{gas}}\right) x100 \dots\dots\dots\dots\dots\dots\dots\dots\dots\dots\dots\dots (1.7)$$

A positive value of S implies film resistance decrease on gas exposure and vice versa.

(ii)Response time: the response time is the time interval over which resistance attains fixed percentage (usually 90%) of final value when the sensor is exposed to full-scale concentration of the gas [192].

(iii)Recovery time: this is the time interval, usually referred as T10, over sensor resistance reduces to 10 % of the saturation value when the sensor is exposed to full-scale concentration of gas and then placed in the clean air. A good sensor should have a small recovery time so that sensor can be used over and over again.

(iv)Selectivity: Usually most chemiresistive sensors exhibit significantly high value if sensitivity for many gases under similar operating conditions. The selectivity or specificity of sensor towards an analyzing gas is expressed in terms of dimension that compares the concentration of the corresponding interfering gas that produces the same sensor signal. This factor is obtained by:

$$\text{Selectivity} = \frac{\text{Sensitivity of the sensor for interfering gas}}{\text{Sensitivity toward the desired gas}} \dots\dots\dots\dots\dots (1.8)$$

(v)Long term stability :this is the ability of the sensor to maintain its properties when operated continuously for long duration in hostile environment .The good sensors are expected to work for several years without showing a drift in any of the above four parameters.

All these five parameters depend on the sensing material, the interaction between the gas and sensor, the sensor operating condition etc, In order to control these parameters scientific understanding of gas-sensor interaction, and various new technological concepts and novel materials have been developed .

1.25 Determination of sensing parameters

In order to record the response curve of a chemiresistor gas sensor, the resistance or conductance of the sensor element is measured in air and in presence of a known amount of analyte gas. The response curve are recorded using following two methods

(i)Dynamic (flow-through) method: The concept of this method is schematically shown in figure(1.32). Here the response curve is recorded under a continuous flow of a known amount of analyte gas. The concentration of analyte gas (Gas-1)is controlled by mixing it with a carrier gas (Gas-2:N2 or Ar)using mass flow controllers(MFC). For recovery measurements, the MFC of analyte gas is switched off. The advantage of this method is that the sensor response can be recorded repeatably as a function of different concentration [192] .

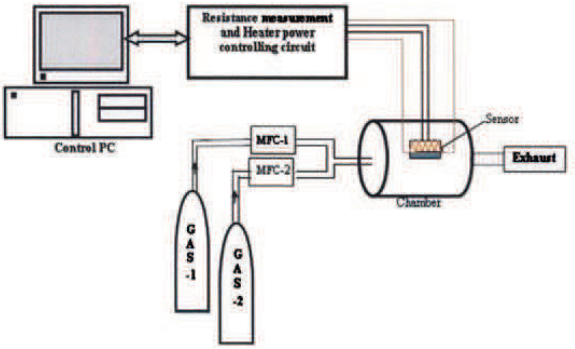

Fig(1.32)Schematics of sensor testing method using (MFC)controlled [192]

(ii)Static environment method: in this method, the sensor element is mounted in an enclosed test chamber of a known volume as shown in figure. (1.33)

In order to measure the sensor resistance in a desired concentration of analyte gas, a known amount of gas injected into the housing using a micro-syringe. The recovery of the sensor is studied by removing the sensor from housing and exposing it to air[192] .

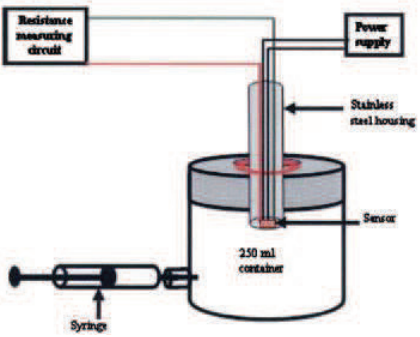

Fig[1.33]static environment method (a known amount of gas injected in container having fixed volume) [192]

Since the sensing properties are a function of temperature ,a heater is often used to increase the temperature of the sensor element .The resistance of sensor can be directly measured by using a multimeter .However, in most of the cases ,a simple sensor circuit ,as shown in figure(1.34) ,is used for the determination of the sensor resistance .

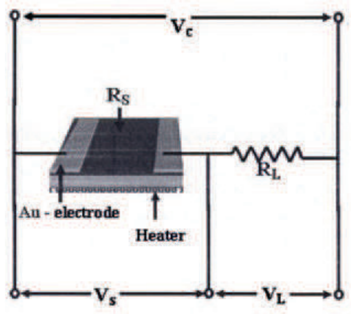

Fig(1.34) A circuit for determination of the resistance of the gas sensor.[192]

Here ,a load resistance(R_L)is connected in series with the sensor resistance (R_s).A voltage source (V_c)is applied to the combination to provide the current (I_s) which drops voltages V_s and V_L across the sensor and load respectively . the output voltage is usually measured across the load ,which is given by:

$$V_L = \frac{V_C R_L}{R_L + R_S} \quad \text{...(1.11)}$$

The sensor resistance (R_s) is obtained from equation (1.11)

$$R_s = R_L\left(\frac{V_c}{V_L} - 1\right) \quad \ldots\ldots\ldots\ldots\ldots\ldots\ldots\ldots\ldots\ldots\ldots. (1.12)$$

1.26 Literature Survey

1.26.1 Synthesized of PANI

Many organic ICPs have been reported since the first synthesis of doped polyacetylene in **(1977)** [138] by **Shirakawa et al**, who reported high conductivity in oxidized, iodine-"doped" polyacetylene. This discovery, along with the extensive research in this area, eventually culminated with the award of the 2000 Nobel Prize in Chemistry to MacDiarmid, Heeger, and Shirakawa for *"The discovery and development of conductive polymers"*.

Pron *et al*.(1989) [193] reported that the competing degradation reactions of the polymer in chemical polymerization was slower than in electrochemical polymerization. This suggests that under proper reaction conditions the side reactions are negligible in chemical polymerization as compared to electrochemical polymerization.

Sambhu Bhadra *et al*. **(2007)**[194]Were synthesized the polyaniline (PANI) powder was formed (0.15M of aniline and 1M of HCl)in distilled water at room temperature in a single compartment electrochemical cell, and synthesized chemically keeping the composition and temperature same as electrochemical process but adding equimolar amount of ammonium peroxydisulfate as an oxidizing agent. Result shows that the electrochemically synthesized PANI (ECS- PANI) has somewhat lower conductivity, higher solubility, more benzenoid rings than quinoid rings, lower crystallinity, higher band energy, and higher particle size than that of chemically synthesized PANI (CS- PANI) . Table (1.3)shown the different in properties of electrochemical and chemical synthesized of polyaniline.

Table (1.3) Different in properties of ECS-PANI and CS –PANI[194]

Properties	ECS-PAni	CS-PAni
DC conductivity	1.7×10^{-4} S/cm	6.3×10^{-4} S/cm
Solubility of PAni per 100 g of DMF at room temperature	0.37 g	0.06 g
Quinoid to benzenoid ratio in PAni	0.8	1.1
Band energy for the third band (*c*)	2.06 eV	1.98 eV
Particle size from SEM	20–40 μm	0.1–1.0 μm

S. Mu and Y. Yang (2008)[195]were synthesized polyaniline nanofibers by using cyclic voltammetry at different potential scan rates, in the presence of ferrocenesulfonic acid. The potential scan rate controlled the formation and growth of polyaniline nuclei, which plays a key role in controlling nanofiber sizes. The average diameters of nanofibers decreased from about 130 nm to about 80 nm as the potential scan rate increased from 6 to 60 mV s^{-1}. They first observed an ordered change in the following spectra with the nanofiber sizes of polyaniline .The spectra of the X-ray diffraction indicated that the partially crystalline form existed in the polyaniline nanofibers and that the crystallinity of polyaniline increased with decreasing diameter of polyaniline nanofibers.

M.M. Gvozdenovi´ca *et al*. **(2011)**[196] were synthesized PANI electrode was formed by electrochemical on graphite electrode(S = 0.64cm^2) from aqueous solution of 1.0 mol dm^{-3} HCl containing(0.25 mol dm^{-3}) aniline , at constant current density of (2.0mA cm^{-2}) . cyclic voltammetry and galvanostatic measurement for study the influence of citrate ions on charge/discharge capability and cycling efficiency. It was observed that, for anodic potential 0.32V, higher electrode capacity of PANI electrode in chloride/citrate electrolyte was obtained, comparing to chloride electrolyte. It was suggested that influence of both chloride and citrate anions had exhibited influence on electrochemical behavior of PANI electrode in citrate containing electrolyte.

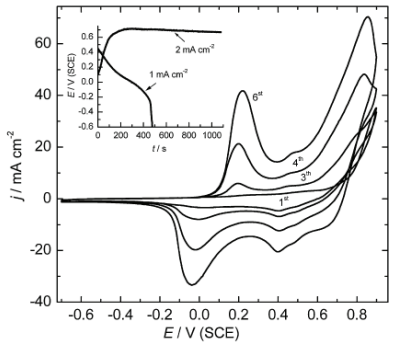

Fig (1.35) Cyclic voltammogram of PANI electrode in 1.0 mol dm^{-3} HCl and 0.25 mol dm^{-3} aniline(scan rate =20 mV s^{-1}).insert: Galvanostatic curve of electrochemical polymerization of aniline at graphite electrode in 1.0 mol dm^{-3} HCl and 0.25 mol dm^{-3}aniline, j=2.0 mA cm^{-2} ,and dedoping by j=1.0 mA cm^{-2}[196]

Aniline electrochemical polymerization occurs together with doping by chloride anions, according to[196]:

(PANI)n +nyCl−→ [PANIy+(Cl$^-$)]n +nye$^-$ …….(1.13)

where y refers to doping degree (ratio between the number of charges in the polymer and the number of monomer units).

1.26.2 Carbon nanotube

Iijima in **(1991)**[110] was the first who discovered the MWNTs in the soot of negative graphite electrode produced by arc discharge. In 1992, **Ebbesen** and **Ajayan**[27] achieved growth and purification of MWCNTs and found that these nanotubes have diameters around 5-30 nm and lengths around 10μm. In 1993[20] Iijima's group as well as Bethune and coworkers [21] found that the use of transition metal catalyst in the arc discharge leads to nanotubes with only single shell. In 1996, **Smalley's** group [128] grows SWNTs using laser ablation technique on graphite rode.

Journet *et al*. (1997)[197] produced a large quantities of single walled carbon nanotubes by an arc discharge under helium pressure(660 Torr) between two electrodes of a graphite in which a hole in anode electrode had been drilled and filled with a mixture of metallic catalyst (Ni–Co, Co–Y, or Ni–Y) and graphite powders. The products were characterized by SEM, HRTEM, XRD and Raman spectroscopy analysis.

Kataura *et al*. (1999) [198] reported synthesis of SWCNTs by arc discharge and the optical absorption spectral were measured. They observed three absorption bands due to optical transition like density of states which characteristic SWCNTs range from IR to visible region .The first and second peaks are due to optical transition in semiconductor at energy 0.68 eV and 1.2 eV and the third peak is due to metallic nanotube at energy 1.7 eV.

Park *et al*. (2001) [199] prepared purified multi–walled carbon nanotubes by electric arc discharge, through thermal annealing in air. The annealing apparatus consists of two quartz tubes, whereby the inner tube, which contains the MWNTs, is simply rotated by the outer tube. The samples were annealed at 1033 K under ambient air with supply of sufficient amount of oxygen.

Yutaka Maniwa *et al*. (2001) [200] studied X-ray diffraction of (MWNT) grown by arc discharge in hydrogen atmosphere. They noticed that (002), (100), and (004) peaks are indexed on the basis of the hexagonal graphite as shown in Fig. (1.36). The effect of the annealing temperature (298,473,673 and 873) K on the X-ray diffraction pattern of MWCNTs was investigated. They are also found that the interlayer distance d increases with increasing the annealing temperature. On the other hand, the (100) peak does not change by elevating temperature. From the figure, Q represents the wave vector transfer and Q is defined by $(4\pi\sin\Theta)/\lambda)$.

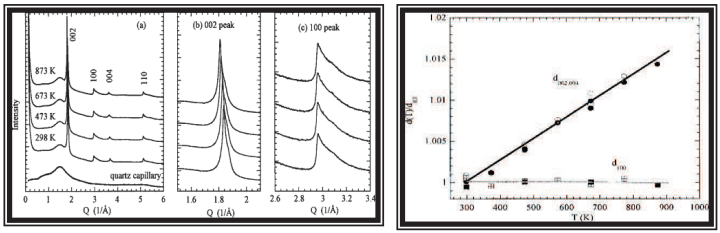

Fig.(1.36)Temperature dependence of interplane and in-plane d spacing at 298 K in

Jung *et al*. (2003) [201] reported the synthesis of multi walled carbon nanotubes using the arc discharge technique, in which the conventional vacuum arc discharge chamber replaced by a liquid nitrogen filled chamber. The diameter of anode is 8 mm and cathode is 10 nm and the distance between them was adjusted until arc discharge occurred and direct current 80 A at 20-27.5 V was supplied using a power supply. The synthesized MWNTs have a diameter range of 20–50 nm and high production 70% **.**

Debasis *et al*. (2004)[202] synthesized CNTs filled by Palladium nanoparticles using arc-discharge technique and show that the indexed diffraction pattern confirmed that the peak corresponding to carbon binding energy lie at 0.2846 eV from EDXA spectrum.

Ambrosio *et al.* (2005) [203] grew MWNT by CVD technique. They presented an investigation that the films have important photonic effect as a function of the wavelength in a large spectral interval (200-1800) nm. The energy gap varies from (0.4 -6) eV leading to sensitivity to the electromagnetic radiation, potentially from UV to IR. They observed that the maximum value of quantum efficiency occurs in the UV region at wavelength equal to 355 nm and then decreases in the infrared region.

Hicks *et al*. (2007) [204] have fabricated diode SWNT devices using Au and Al, as the asymmetric metal using chemical vapor deposition (CVD) process. The films were grown using an iron catalyst on substrate of single crystal silicon. They observed that these devices exhibit current rectification with maximum forward-biased current capacities range between 8 μA and 841 μA. The bias voltage range was from -3V to +3V.

1.26.3 PANI /MWNTs composite for chemical sensing

Y.Wanna *et al*. (2006)[205].Were developing of nanofibers composite PANI/CNT fabrication by electro spinning technique for CO gas sensors .The sensors were tested for CO sensing at room temperature with CO concentrations in the range of 100-500 ppm . in comparisons to PANI prepared by solvent casting technique with no CNT inclusion the sensitivity of nanofiber composite was increase by more than two orders of magnitude and response /recovery times were reduced by more than the factor of 3.

Shabnam et al (2006)[206] were studied response of camphorsulfonic acid (CSA)doped polyaniline nanofibers exposed to hydrogen concentrations . Hydrogen causes a reversible decrease in the resistance of thin film of (CSA)doped polyaniline. For a 1% mixture of hydrogen in nitrogen a 3% decrease in resistance was observed. Figure (1.37)exhibits response of (CSA) doped polyaniline nanofibers film exposed to 1% H_2

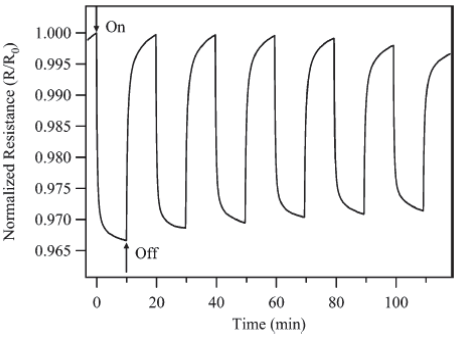

Fig(1. 37) response of (CSA)doped polyaniline nanofibers to 1% H_2[206]

REZA *et al*. (2010)[207]synthesized (PANI/MWNTs)composite by an in situ chemical oxidative polymerization method and characterized physically using (SEM)as shown in Figure(1.38 a)and electrochemical behavior of the composites in acidic solution (HCl)using cyclic voltammetry Figure(1.38 b)

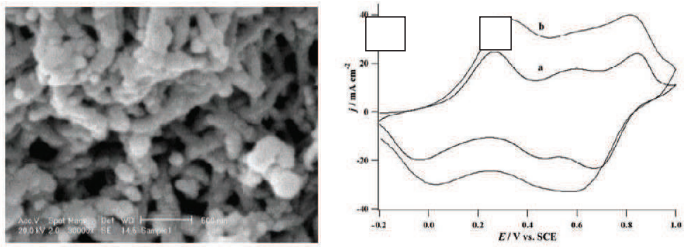

Fig (1.38)(A) (SEM) image of PANI/MWNTs composite (B) cyclic voltammograms of a)PANI-MWNTs and b)PANI composite electrodes in 0.5 M HCl at a scan rate of 50 mV/s)[207]

Subodh Srivastava *et al*. (2010) [208]Were studied the composite thin films of polyaniline with multiwall carbon Nanotubes (MWNT)and single wall carbon nanotube for Hydrogen gas sensing application .They were founded the response of these composite films for hydrogen gas by monitoring the charge in electrical resistance at room temperature. In Figure(1.39)was observed the (SWNT/PANI)and (MWNT/PANI) composite film show a higher response as compare to pure PANI.

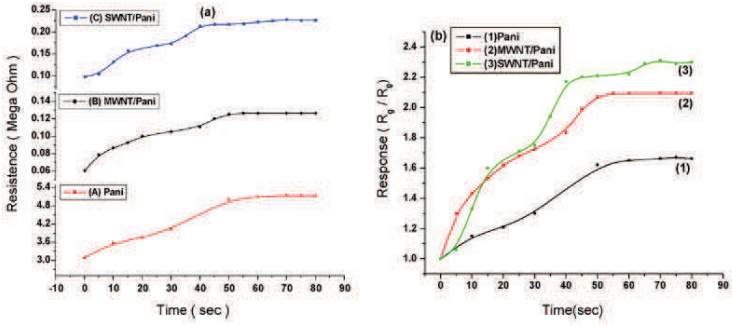

***Fig(1. 39)the fig shown (a)variation in resistance of composite films as a function of time with 2%hydrogen concentration in air at 1.3 atm exposure (b) plot of response of composite films as a function of time with 2%hydrogen concentration in air at 1.3 atm exposure*[208].**

Inho Kim *et al*. (2010)[209].were fabricated a gas sensor for the detection of carbon monoxide (CO)and ammonia(NH_3) gas using (SWNT)and (PANI) composite .the SWNTs were dispersed in sodium dodecyl sulfate(SDS)and were applied over interdigitated electrodes(IDE).the sensor showed faster response to the CO gas than the NH_3 gas . The CO increased the conductance of the

composite, while NH_3 showed opposite response. The composite were more adsorptive to co than NH_3.

Wen-bo Li *et al*. (2011)[210]Were synthesized multishell Nanotubes of polyaniline and carbon via a template approach .The polyanilne –carbon Nanotubes show enhanced dispersibility in water and can be used us a functional material of electrochemical capacitors with improve performance. The cyclic voltammogram of PANI-CNT composite nanotubes is relatively deferent from that of pristine CNTs as shown in Figure(1.40). For the CNTs, only capacitive current was observed, no peak attributable to the presence of any redox-active species Fig. (1.40 a) was observed. As shown in Figure(1.40b), the PANI-CNT composite tubes have in-creased electroactivity which have two anodic peaks at 0.14 and 0.58 V and two cathodic peaks at -0.12 and 0.30 V, respectively.

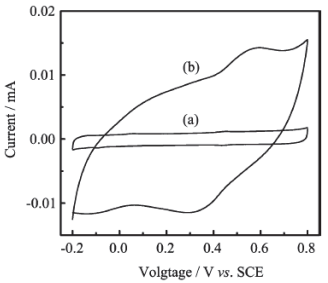

***Fig. (1.40) Cyclic voltammograms of CNT (a) and PANI-CNT(b). Measured in 1 mol/L H_2SO_4 with a scan rate of 10 mV/s*.[210]**

Yaozu *et al*.(2011)[211] reported synthesize single-walled carbon nanotube/polyaniline composite nanofibers for use as high-performance chemosensors.. Chemosensors fabricated from the composite nanofibers synthesized with a 1.0 wt % SWCNT loading respond much more rapidly to low concentrations (100 ppb) of HCl and NH_3 vapors compared to polyaniline nanofibers alone (120s vs 1000 s). Upon exposure to 100 ppb HCl vapor for 1 min, the film resistance dramatically decreases from >200 MΩ to 430 kΩ, and then increases to 3.8 MΩ after 3days of storage in N_2. After two successive 1 min exposures of 100 ppb NH_3 vapor, the resistances increase to 27.5 and 74.0MΩ, respectively. Upon exposure to HCl vapor for another minute, the resistance decreases dramatically from 74.0 MΩ to 610 kΩ. Continued gas phase cycling (i.e., doping/dedoping) experiments indicate that the nanofibrillar composite

ultrathin films show highly reversible sensitivity to acid doping and base dedoping

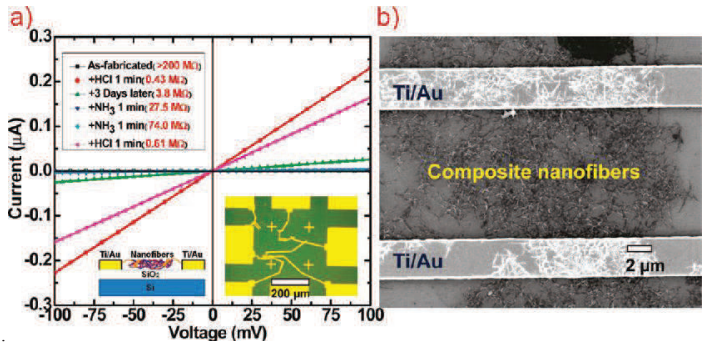

Fig (1.41). (a) Typical I-V curves of nanofibrillar 1.0 wt % SWCNT/polyaniline composite films upon exposure to alternating vapors of HCl and NH_3. The insets show the geometry of the device: (left) front view and (right) top view. (b) A zoomed-in SEM image of the device[211].

Chapter Two

Process Requirements Necessary

2.1 Introduction

In this chapter, the preparation and synthesis conditions of Polyaniline , Carbon Nanopowder(CNpowder), and Polyaniline/MWNTs (MWNTs purity 95% were produced via the chemical vapor depositon method(CVD) ,average outer diameter 20-30 nm and the length of 10-30 μm purchased from (Cheap Tubes Inc. USA).the prepared Composite were deposited on stainless steel (SUS304)substrate by electrochemical method for liquid sensing test. On the other hand, polyaniline and Polyaniline/MWNTs were also deposited on gold (Au) interdigitated electrode(IDE) by spin coating method for gas sensor fabrication . The analysis methods of the above fabricated films are dealt with in this chapter. This chapter also describes the study of the structural, electrical properties as shown in the scheme of the experimental flow chart Figure (2.1).

2.2 Chemicals and Materials

The following chemicals and materials are listed in table (2.1). A chemical and materials have a highest purity for synthesizing the Polyaniline, CNpowder and Polyaniline/multi wall carbon Nanotubes (MWNTs) composite were produced via the chemical vapor depositon method (CVD) , purchased from (Cheap Tubes Inc. USA)the main properties lested in table (2.2).

Table (2 .1): Employed chemicals and materials with their supplier companies

Chemicals and materials	Molecular weight M.wt(g/mol)	Specific gravity (Sp.gr)	Purity (%)	Company origin
Aniline ($C_6H_5NH_2$)	93.13	1.023	90%	Sigma Aldrich U.K
Sulfuric Acid(H_2SO_4)	98.07	1.84	98%	(GCC) U.K
Hydrochloric Acid (HCl)	36.5	1.18	37%	Sigma Aldrich U.K
Ammonia(NH_3)	17.03	0.91	25%	BDH U.K

Dimethyl sulfoxide DMSO(CH_3)$_2$SO	**78.139**	**1.0955 at 25 ^oC**		**BDH U.K**
Deionized distilled water	**Conductivity 10 µs/cm from Dept. of chemistry(University of Baghdad)**			
Graphite Rod	**C_GR-04-R purity of 99. 99% American Elements**			
Stainless steel SUS (304)	**(thickness 1mm) Density 8000 kg/m^3**			
Interdigitated Electrode (IDE)	**(Au)IDE(0.1" X 0.1")with micro Heater Synkera technologies inc. USA**			

Table (2.2): MWNTs Properties

Outer Diameter	**20-30nm**
Inside Diameter	**5-10nm**
Ash	**<1.5 wt%**
Purity	**>95 wt%**
Length	**10-30um**
Specific Surface Area	**110 m^2/g**
Electrical Conductivity	**>100 S/cm**
Bulk density	**0.28 g/cm^3**
True density	**~2.1 g/cm^3**

2.3 Instrumentations

The different instruments and apparatus are used in process as listed in Table (2.3).

Table (2.3) Origin, function and specification devices

Item	*Function*	*Device type*	*Original*	*Specification*
1	Ultrasonic Cleaner	Ultrasonic Cleaner	Bransonic 3510 R-DTH USA	Ultrasonic Cleaner with Digital Timer/Heater 5L Capacity
2	Electrochemical Station for : (i)potentiostatic (ii)glvanostatic (iii)open circuit potention	Potentiostat	WENKING M Lab Bank Electronik-Intelligent controls GmbH Germany	Max. Current per channel =± 100 mA Max. CE voltage= ± 20 V Current Ranges 7 Current Resolution 100 pA
3	Agitation	Magnate stirrer	Germany	220V, 50 Hz, 415 watt. Stirrer and heater. Digital Timer
4	Evaporation System	Coating unit	Edward 306 A England	Rotary 10^{-2}mbar Diffusion $<10^{-3}$mbar
5	Power supply	Power supply	Hp 6216A England	(0-30) V (0-500)mA
6	Digital multimeter DMM	AVO meter	Victor 86D Malaysia	(400uA/4000uA40mA/400mA/4A/ 10A) (400Ω/4kΩ/40kΩ/400kΩ/4MΩ/40MΩ)
7	Computerize I-V measurement	I-V meter	Keithley 2361 trigger controller USA	Six trigger input Six trigger output One 8-bit digital input port One 8-bit digital output port
8	Deposition	Spin coater	VTC-100 USA	(500-8000) rpm
9	Vacuum portable unit	phlegm suction unit	Suction unit7E-A China	(0- 0.075) MPa,
10	Temperature measurement	IR Temperature Sensor	Rayomatic 14814-2 Eurotron IRtec Co.Ltd UK	Divergence =(21mm) at distance (600mm) Temperature rang (-25 – 1000)°C
11	PH measurement	PH meter	Hanna H19812 Italy	pH(0.0 to 14.0) pH EC (0.00 to 4.00)mS/cm TDS (0 to 1999) ppm (mg/L)
12	welder	AC/DC welder	Champion ELITE	DC: 40–225 amps AC: 50–260 amps

13	Analysis and characterization	FT-IR	FT-IR Shimadzu spectrophotometer model 8300	solid KBr discs Maximum Resolution 0.5cm^{-1}
		XRD	Shimadzu 7000 Japan	40 kV, 30 mA
		SEM	Hitachi FE-SEM model S-4160, Japan	0.5 - 20 kV
		AFM	AA3000, Angstrom Advanced Inc. USA	220V, Resolution: 0.26nm lateral, 0.1nm vertical

2.4 Electrochemichal system

The electrochemical system consist of potentiostat ,cell ,and electrodes.

2.4.1 The potentiostat

Electrochemical experiments were performed on potentiostat[WENKING M Lab Bank Electronik-Intelligent controls GmbH]as shown in figure(2.2).M Lab is multichanal potentiostat /galvanostat are organised on hardwere board conacted to personal computer by RS 232 cable. M Lab has three operation modes for each channal:(i)Potentiostatic mode (ii) Glvanostatic mode (iii) Open circute mode

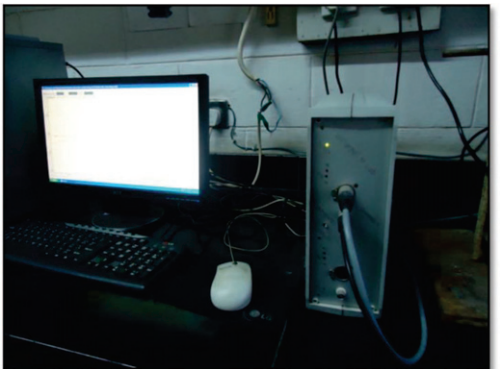

Fig (2.2)Weking M Lab multichanal (potentiostat/glvanostat)

2.4.2 Cells

Volume and design of a cell are determined by the type and size of the working electrode and the goal of a certain measurement: Large electrodes require large volumes of the solution (usually, not necessary). Fast measurements are require small electrodes and small cell volumes. However, these are coarse rules and not laws. But, it shows that a really universal cell which delivers best result under all conditions cannot be realised. However, you will find so - called "universal cells" on the market. They got the designation because they offer convenient work for many different applications, as long as the working electrode area is in the order of some cm^2. They are made of glass; they have enough openings to insert different types of electrodes, thermometers, gas injectors or other auxiliary equipment. Such a universal cell consists of a glass beaker with plane sleeve; volume may be 0.25 L to 1 L.

2.4.3 Electrodes

There are three electrodes in the system can function as:

1. Ag/AgCl used as Reference Electrode (RE) to determine the working electrode potential according to the potential of reference electrode.
2. Counter Electrode (CE) or Auxiliary electrode consist of high purity Platinum metal (Diameter 6 mm, length 10cm).
3. Working Electrode (WE) consist of Diskfix an easy-to-exchange fixture for electrodes made from sheet material. The maximum electrode diameter is 28 mm, maximum Thickness of 3 mm. For smaller electrodes, masks are available to insert specimens with 1 cm^2, 2 cm^2, and 4 cm^2. Both round and octagonal specimens can be used.In experimants a stainless steel (SUS 304) flat sheet (disk shape diameter 24 mm with thikness 1mm). The area of the exposed surface to the electrolyte solution is $1cm^2$ was used as subtrate -working electrode (WE)and reference electrode (RE) are illesturated in figure (2.3) , a platinum rod and sturated calomel electrode (SCE)were used as counter and reference electrode ,respectively .

The two electrode (sus 304 and platinum rod) are cleaned by potential cycling between -100mV and 1500 mV at 30mV/s in 0.3 M H_2SO_4 until astable cyclic voltammogram was obtained.

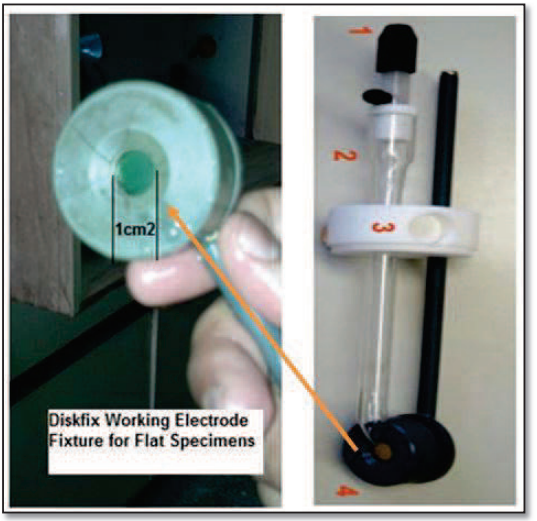

Fig. (2.3) working and reference electrodes(1. Reference electrode, 2. Protection tube and Haber-Luggin – capillary, 3.D-Top for DN cell tops, 4. Diskfix, here with mask 1 cm²)

The electrochemical cell should be connected to the instrument through a cable supplied individual wires showen in table (2.4).

Table (2.4)electrochemical cell connections

Electrode	Colour
Counter Electrode (CE)	Yellow
Working Electrode (WE)potential	Black
Working Electrode (WE)current	Black
Ground	Grey
Reference Electrode (RE)	Green

A complete setup of cyclic polymerization process is shown in figure(2.4).

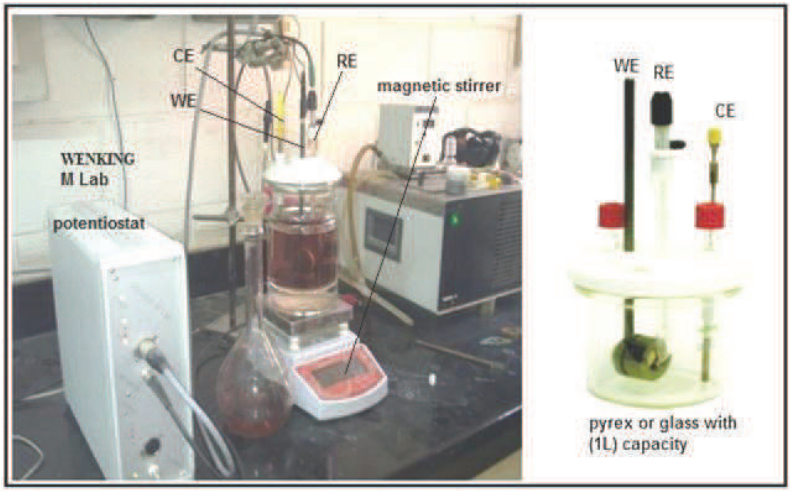

Fig (2.4) The complete system setup of cyclic polymerization process

2.4.4 Preperation of Substrate

Stainless steel SUS 304 disk with diameter of 24 mm and thickness of 1mm was used as substrate (working electrode).The substrate was polished by SiC abrasive paper from 300 to 800 grits .After it had been dipped in HCl(5%) for 5 minutes , it was washed by distilled water then rinsed with acetone in ultrasonic bath before each experment.

2.4.5 Preperation of PANI electrolyte

Aniline monomer was purified by distilled under reduced pressure(0.05 MPa) and stored in darkness before use. The distillation system in figure (2.5) contains the following

(i) chiller for colding water to 5 ^{0}C

(ii) heater for boiling Aniline

(iii) condenser

(iv) vacuum portable unit for reducing pressure to 0.05 MPa

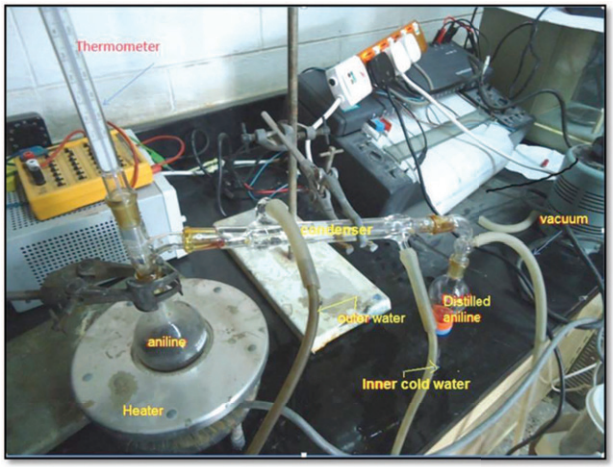

Fig (2.5) Distillation system of Aniline

PANI electrolyte was prepeared with two ways selected acids as following:

(i) 0.1 M distilled aniline in solution of concentrations of (0.1 M,0.2 M and 0.3 M) HCl .

(ii)0.1 M distilled aniline in solution concentration of (0.1 M ,0.2 M and 0.3 M) H_2SO_4.

For example the preperation of solution contains(0.1 M of aniline with 0.3 M of H_2SO_4)The steps are following.

preperation of 0.1 M/L distilled aniline for i.e it was done by

$$n(mol) = \frac{wt(g)}{m.wt\left(\frac{g}{mol}\right)} \dots\dots\dots\dots\dots\dots\dots\dots\dots\dots\dots\dots\dots\dots\dots\dots (2.1)$$

Wher e n ,wt and m.wt are concentration, mass and molecular weight of solution respectively, is the mass and is

$$0.1\ mol = \frac{wt(g)}{93.13\ (\frac{g}{mol})}$$

wt =9.3 gm dissolved in 500ml distilled water

For preperation of 0.3 M/L of H_2SO_4.

$$0.3\ mol = \frac{wt\ (g)}{98.07\ (\frac{g}{mol})}$$

wt=29.421 gm dissolved in 500 ml distilled water

2.4.6 Cyclic voltammetry

Cyclic voltammetry (CV) is a potentiodynamic electrochemical technique. The potential is varied linearly versus time between an initial potential (E initial) and a final potential (E final) via a change in the current being measured with respect to the change in voltage. The resultant current-potential plot is called a cyclic voltammogram [Figure (2.6)].

This technique is used to investigate the electrochemical behavior of electroactive conducting polymers and also provides useful information on the mechanisms of polymer growth.

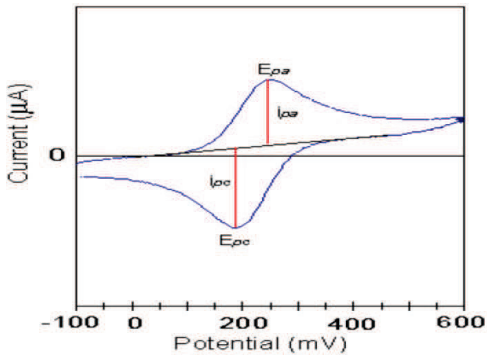

Fig.(2.6) A typical cyclic voltammogram showing an oxidation peak at Epa with a Maximum anodic current (ipa) in the forward scan, and a corresponding reduction peak at Epc with a maximum cathodic current (ipc) in the reversed scan

In this book, cyclic voltammetry was used to investigate the redox properties of conducting polymers. This technique was also used for potentiodynamic polymerization of aniline in the presence of different dopants. Cyclic voltammetry was carried out in a three electrode cell using a working electrode (stainless steel SUS 304) with a platinum mesh auxiliary electrode and an Ag/AgCl (3M NaCl) reference electrode. The potential was varied between -100mV and 1500mV for depositing PANI and PANI/MWNTs and from -1000mV to 1000 for liquid sensing.

2.5 Preparation of Carbon Nanopowder Films by Arc Discharge Technique

2.5.1 Evaporation System

The evaporation system consists of two graphite rods (American Elements C_GR-04-R purity of 99. 99%) of different diameters 3mm and 7mm used as anode and cathode electrodes respectively. The design and shape of the rods are illustrated in Figure (2.7b).

These two electrodes were installed in the center of the vacuum chamber of coating unit, type Edward 306A, end to end separated by approximately 1mm and all other arrangements necessary for evaporation process such as the evaporation source, substrate holder and radiation heater are fixed inside the chamber.

As for evaporation deposited films of carbon Nanopowder , the substrate consists of glass slide which are placed at a normal distance (h) of 5 cm to the graphite rods.

The coating unit used in this work is shown in Figure (2.7a).The chamber represents the first part unit, the second part is the pumping system which consists of two evacuation pump (stages) , the first stage is the rotary pump for roughing stage where the vacuum can reach 10^{-2} mbar ,the second stage is the diffusion pump which produces very low pressure down to (10^{-3}-10^{-6}) mbar. A welding generator and filtering bridge were used to confrere AC/DC current. Consequently, this welding generator gives current range of (40-100) A**.**

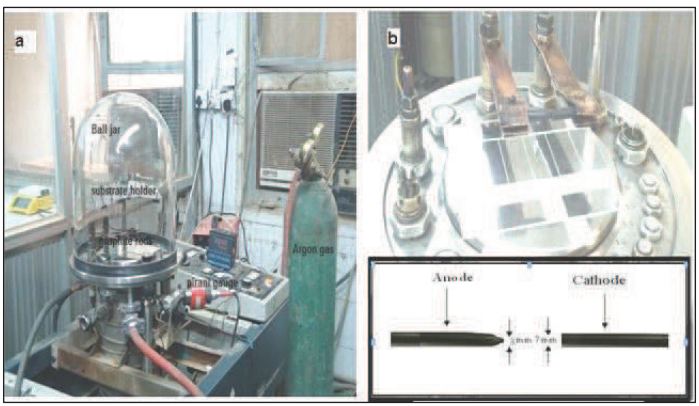

Fig.(2.7)Evaporation system (a)shape of electrode(b)

2.5.2 Synthesis of Carbon Nanopowder

Arc discharge evaporation method in a high vacuum and low pressure was used to evaporate graphite. This method is a direct deposition technique in which the material is deposited by vaporization after plasma is produced. After the arc was carried out, much soot was deposited on the chamber wall.

This method must be carried out with care and precision as flow:

When the system is pumped down to a pressure of $2*10^{-6}$ mbar , then it is broken out by entering the Argon (Ar) gas was fed into the chamber using a valve control, the pressure reached 10^{-3} mbar which is monitored by using penning gauges, the power was turned off, and the passage of direct current creates raising temperature discharge between the two graphite electrodes because in DC arc discharge technique the cathode was used always larger than anode in the diameter about 3mm and 7mm as an anode and cathode electrodes, respectively. The DC current of approximately 60 A and voltage of 25 V was applied between two electrodes.

The current density of cathode was significantly smaller than that of the anode; hence there was a notable temperature gradient between the anode and the cathode. This temperature gradient to the heat of the graphite rod and the plasma was produced; result in the evaporation of the one of graphite electrodes (anode) to form rod shape on the cathode and chamber wall. After the arc was carried out, carbon anions arrived at the cathode, there were deposited there and formed several forms of carbon which include Nanopowder , then the current was switched off and the samples were left in the high vacuum for one day, then the air was admitted to the chamber, and the films were taken out from coating unit to in the desiccators until the measurements were performed made. .The soot was collected from the chamber wall and taken out to the purification treatment.

2.5.3 Purification of Carbon Nanopowder

When the powder was collected from the chamber, it contained amorphous carbon and this is purified as following:

Firstly the soot was placed in a beaker containing of 5ml conc. $HNO_3$and 10ml distilled water stirred in at 323 K for 90 minutes. The sample was washed with distilled water, dried and dispersed in ethanol under sonication and filtered using

filter paper. To separate the amorphous carbon from carbon Nanopowder, the samples were collected on a filter paper.

2.6 Preperation of PANI /CNpowder composite electrolyte

CNpowders synthesized by arc discharge technique (0.25 wt%,0.5 wt% and 1% wt) were added to aniline and the mixture was heated at reflux for 3 hours . The reflux system illustrated in figure (2.8) was a liquid reaction mixture placed in a vessel open only at the top. This vessel is connected to Vigreux condenser, such that any vapors given off are cooled back to liquid, and fall back into the reaction vessel. The vessel is then heated vigorously for the course of the reaction. The purpose is to thermally accelerate the reaction by conducting it at an elevated temperature.

The 0.1 M of (0.25 wt%,0.5 wt% and 1% wt) CNpowder-aniline solution was added to 0.3 M H_2SO_4 for the fabrication of PANI/CNpowder films by electrochemical method.

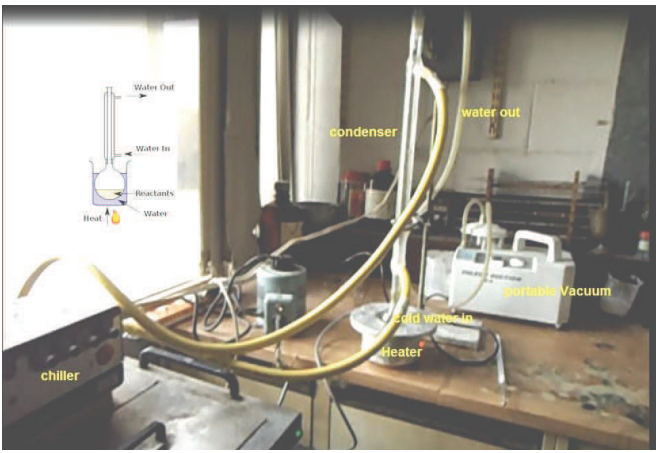

Fig.(2.8)image of The reflux system

2.7 Preperation of PANI/MWNTs composite electrolyte

Multi Wall Nanotubes (MWNTs) (0.25wt%,0.5wt% and 1wt%) were added to aniline and the mixture was heated at reflux for 3 hours . The 0.1 M of (0.25 wt%,0.5 wt% and 1% wt) MWNTs -aniline solution was added to 0.3 M H_2SO_4 for fabrication of PANI/MWNTS films by electrochemical method.

Dissolution of either CNpowders or MWNTs in aniline can be observed by color change of the solution with continuous heating .The original colorless aniline solution first becomes brownish and then turned dark red. After it had been cooled to room temperature and settled for 24 h with a small undesolved quantity of CNpowders and MWNTs were precipitated from CNpowders - aniline solution.

2.8 Fabrication of gas sensing devices

In its final form ,PANI and PANI/MWNTs composite resemble a dark powder which cannot be employed directly for sensing applications must be dispersed in a suitable solvent in order to apply it to a surface such as IDEs. The type of metallic IDEs gold (Au) 2 x 2 mm^2 (synkera technologies inc. USA)as shown in figure (2.9).

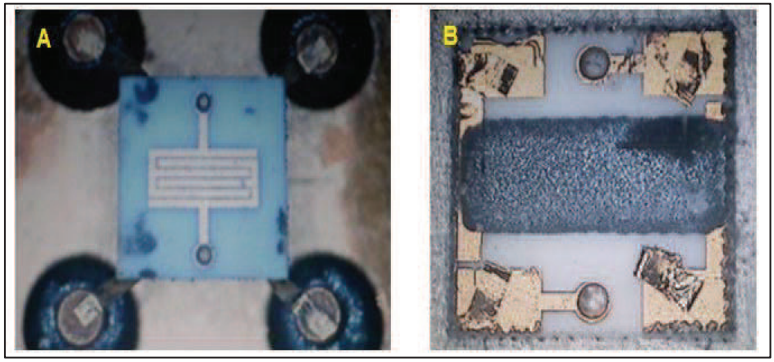

Fig(2.9) (A) .Top view synkera gold IDE(2 x 2 mm^2)(B) Bottom view micro-heater underneath IDE

PANI and PANI/MWNTs composite were dispersed in a Dimethyl sulfoxide (DMSO)($(CH_3)_2SO$) solvent (0.05 grams powder per mL solvent) . The mixture was then placed in a sonication bath for approximately three hours in order to obtain a uniform suspension. Small pipettes were used to transfer the solution ,and drop small amounts onto gold IDEs spin coating (1000 revolution per minute(rpm) and 2000 rpm for 30 second)was used to distribute the solution over the IDEs surface using VTC-100 vacuum spin coater as shown in figure(2.10).

Fig(2.10)Photography of the spin coater type VTC- 100

In order to measure the gas sensing characteristics of the sensor at a room temperature ambient atmosphere, the sensor element was packed with a stainless steel mesh cap as shown in figure (2.11a). The sensor temperature was controlled by modulating the power of the micro-heater underneath the alumina substrate. The temperature of the gas sensor at various heater powers was measured using an IR temperature sensor (Rayomatic 14814-2, Eurotron IRtec Co., Ltd.).

Varying the heater power between 50 and 400mW resulted in the sensor temperature variation from 60 to 370 ºC shown in figure (2.11 b). Prior to the measurements, the sensor was heated at a power of 400mW for 6h to remove any organic content before deposition process.

The sensor was again contained within a quartz tube kept at room temperature. The same above procedure was followed during these gas sensing measurements.

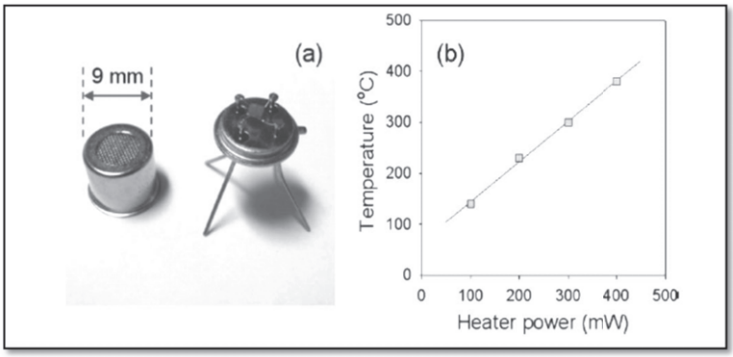

Fig.(2.11) (a)sensor structure and (b)sensing temperature as heater power

2.9 Gas sensor testing system

A schematic cross sectional view of the gas sensor testing system, test chamber and photos of the mounted sensor and test chamber illustrated schematically in figure (2.12), and the system photograph figure (2.13) respectively. The testing chamber unit consists of vacuum quartz tube cylindrical shape as test chamber of diameter 25mm and of height 120mm with the top base made removable. A multi-pin feed through at the top base of the chamber allows for the electrical connections to be established to the heater assembly as the sensor electrodes.

The PC-interfaced multimeter of type Victor 86D is used to register the variation of the sensor resistance exposed to predetermined air-hydrogen gas maxing ratio. The chamber can be evacuated using rotary pump to a rough pressure of (0-0.075 MPa) a gas mixing manifold is incorporated to control the maxing ratios of the test and carrier gases prior injected into the test chamber

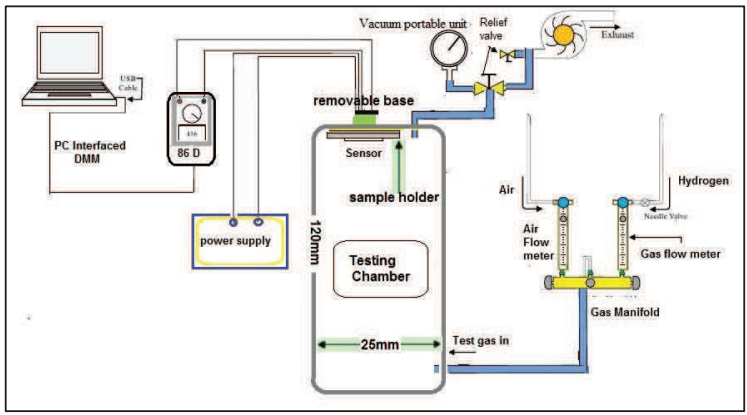

Fig. (2.12)Gas sensor testing system

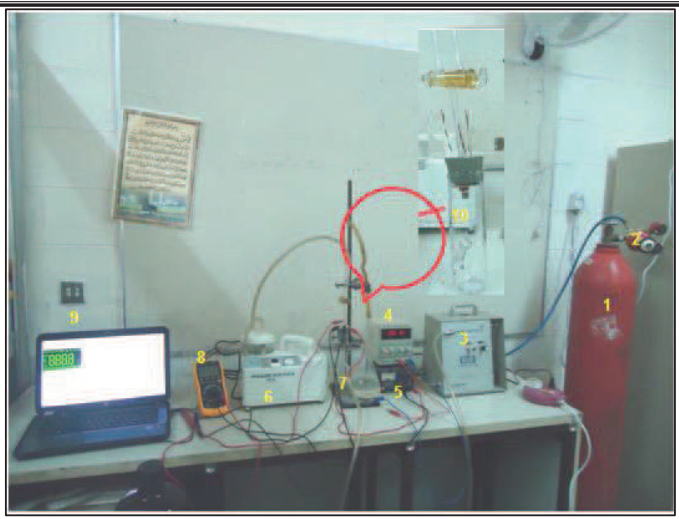

Fig(2.13)A photo of the sensor testing system (1.Gas container of H_2 2.Regulator of H_2 gas 3.Mixture manifold gases 4.Power supply 5.Power supply for heate of sensor 6.Portable vacuum unit (0-0.075 MPa .7.Testing chamber 8.Digital multimeter 9.Personal computer 10.Testing chamber magnified)

The mixing gas manifold is fed by zero air and test gas through a flow meter and needle valve arrangement .This arrangement of mixing scheme is done to ensure that the gas mixture entering the test chamber is premixed thereby giving the real sensitivity.

A schematic diagram of the electrical circuit used for gas sensor measurements is illustrated in figure (2.14).

When the sensor is connected as shown in the basic circuit ,output across the resistor (V_{RL})increase /decrease as sensor's resistance (R_s) decrease/increases, depending on the analyte gas concentration and its type i.e. reducing or oxidizing .A DC. Power supply feeds on an adjustable bias voltage V_b from (0 to 15)V across the sensor resistance R_s and corresponding current of the circuit is measured via the digital multimeter DMM whose signal directly being interfaced to the pc for further analysis . The power supply for control heating with the graph refer to figure (2.11 b).

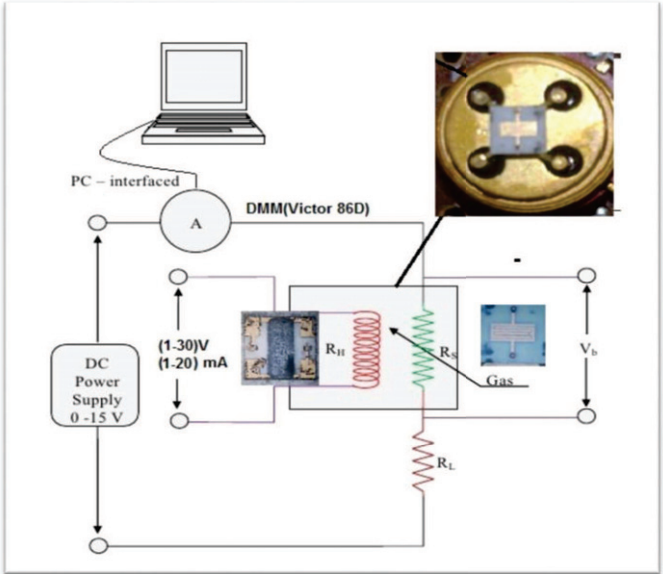

Fig.(2.14) Schematic diagram of the electrical circuit are used for gas sensing

2.10 Measurements

2.10.1 Thickness Measurement

Arc discharge deposited films used for optical or other purpose must normally be deposited to specific thickness. Optical method was used for thickness measurements as follows:

The thickness of PANI, carbon nanopowder, multiwall carbon Nanotubes, and PANI/MWNT composite thin films was measured by using an optical interferometer by employing He-Ne laser (0.632μm) with incident angle of 45° as shown schematically in Figure (2.15). This method depends on the interference of the laser beam reflected from thin film surface and then substrate, the films thickness (t) was determined using the following formula[212]:

$$t = \frac{\Delta x}{x} \cdot \frac{\lambda}{2} \quad \text{..... (2.2)}$$

Where x is the fringe width, Δx is the distance between two fringes and λ is the wavelength of laser light.

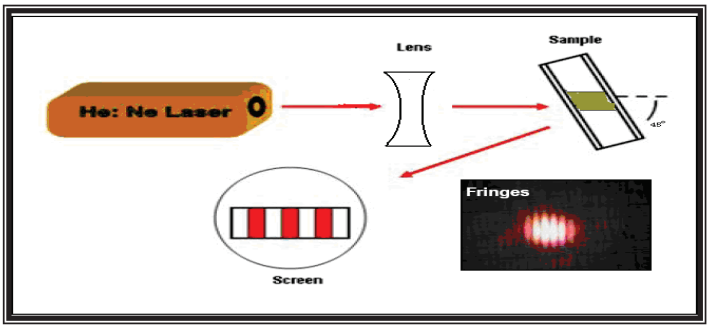

Fig. (1.15) The schematic diagram of the film thickness [212]

2.10.2 Structure Identification

The main purpose of these measurements is to investigate the type of structure and the morphology of the prepared powder and deposited films.

2.10.2.1 X-Ray Diffraction Investigations

The structure of PANI ,CN powder fabricated by arc discharge technique, and MWNTs purity 95% were produced via the chemical vapor depositon method(CVD) ,average outer diameter 20-30nm and the length 10-30 μm purchased from (Cheap Tubes Inc. USA), AND PANI/MWNTs composite have been examined by x-ray diffraction measurements at low angle of diffraction.

X-ray diffractmeter Shimadzu XRD 7000 in Ministry of Industry and Minerals (Iraqi geological survey board) (Voltage 4 kV 30 mA)maxima Ni filter scan speed 10 deg/min resolution with capper K_α radiation of wavelength λ =1.54 Å was used for measurements ,the scanning angle (2θ)varied in the range $(10\text{-}90)^0$ with speed of 2cm/min. Figure (2.16) shows the x-ray diffractrometer system.

The inter planer distance $d_{(hkl)}$ for different planes was determined by using Braggs law $n\lambda = 2d\sin\Theta$ [213], where n is the reflection order and by comparing $d_{(hkl)}$ value with the International Centered Diffraction Data (ICDD) card for PANI, carbon nanopowder, Multiwall carbon Nanotubes, and PANI/MWNT composite we have examined the structure of their powders and thin films.

The particle size (D) of these materials was calculated from Scherre relation [214]:

$$D = \frac{K'\lambda}{\beta' \cos\theta} \quad \text{..... (2.3)}$$

Where D is the crystallite size, λ is the x-ray wavelength used which is equal to 1.54 Å ,β' is the angular line width at half maximum of intensity, θ is the Bragg's diffraction angle and K' is a constant with a value of 0.9.

2.10.2.2 FT-IR Spectroscopy

The FT-IR spectra measurements of PANI and PANI /MWNTs composite for determine the bond . The I-R absorption spectra were recorded by double beam Fourier Transform Infrared Spectroscopy using FT-IR Shimadzu spectrophotometer model 8300, Japan, with potassium bromide source in the range of wave number (4000-400) $cm^{-1}$with resolution 0.5 cm^{-1}.

2.10.2.3 Scanning Electron Microscopy (SEM) Investigations

The scanning electron microscopy examinations were carried out for PANI, carbon nanopowder, Multiwall carbon Nanotubes, and PANI/MWNT composite thin films prepared on stainless steel substrate under different conditions. Samples were analyzed for structure morphology and nanostructure using Hitachi FE-SEM model S-4160 in University of Tehran - College of Engineering (Electricity engineering and Computer Dept).

The magnification in the zoom ranges is (10-100) kx. The acceleration voltage applied to the electron gun can be varied from (20-40) kV. Fig.(2.18) shows SEM system for morphology measurements.

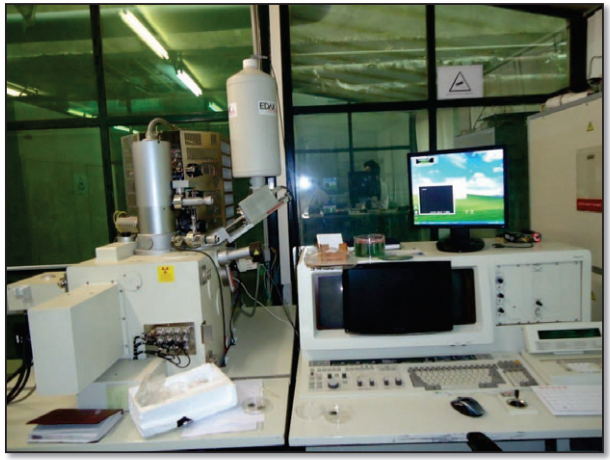

Fig (2.17) photography image of SEM system for morphology measurements Hitachi FE-SEM model S- 4160

2.10.2.4 Scanning Probe Microscope system (SPM)

Atomic Force Microscope (AFM) measures the interaction force between the tip and surface. The tip may be dragged across the surface, or may vibrate as it moves. The interaction force will depend on the nature of the sample, the probe tip and the distance between them.

Samples were analyzed for structure morphology and nanostructure of PANI, carbon nanopowder, Multi Wall carbon Nanotubes, and PANI/MWNTs composite using AA3000 Scanning Probe Microscope (atomic scale of resolution 0.26 nm lateral and 0.1nm vertical)with multi functions Atomic Force Microscope (AFM),Scanning Tunnelling Microscope(STM),and Lateral Force Microscope(LFM) Figure (2.18) Shows the SPM AA3000.

Fig (2.18) Scanning Probe Microscope (SPM AA3000)

2.11 Electrical Properties

I-V characteristics of PANI ,PANI/CNpowder (0.25 wt%, 0.5wt% and 1wt %)composite ,and PANI/MWNTs (0.25wt%,0.5 wt % and 1wt % CNTs) composite have been measured at room temperature by sensitive computerized electrometer type Keithley 2361 trigger controller at University of Tehran - College of Engineering (Electricity engineering and Computer Dept)as showed in figure(2.19) .

Fig (2.19) Photography of Keithley 2361 trigger controller system

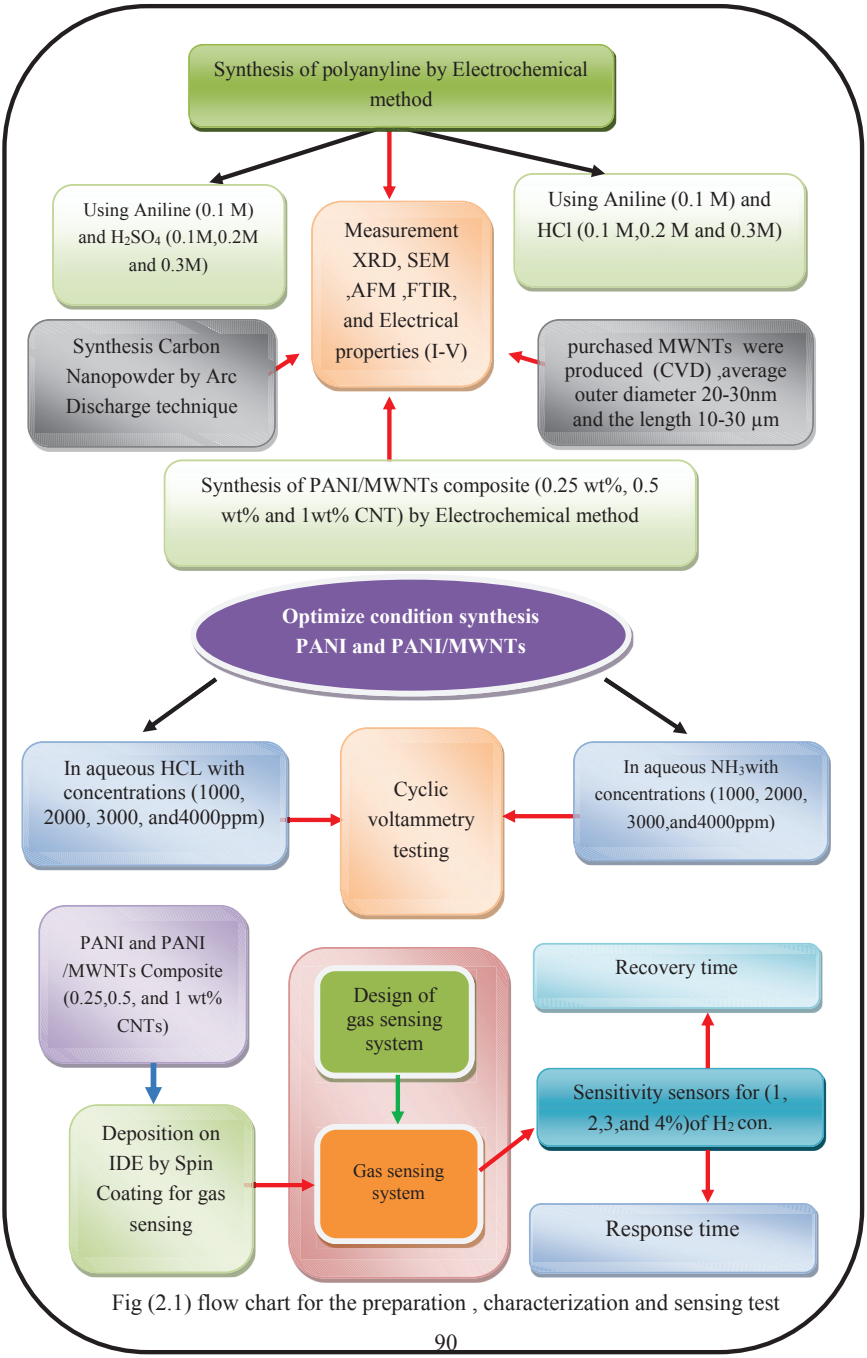

Fig (2.1) flow chart for the preparation , characterization and sensing test

Chapter Three

Sensors Techniques Results and Discussion

3.1 Introduction

The result and analysis of the experimental measurements, which involve fabrication of nano materials such as (polyaniline nanofibers by electrochemical method and carbon nanopowder by arc discharge technique) .The structure and morphology of the materials fabricated are characterized by means of scan electron microscopy, Atomic Force microscopy analysis, and x-ray diffraction. Moreover, the electrical measurement of PANI, PANI/CNpowder, and PANI/CNTs devices are presented .In addition, the liquid and gas sensitivity of the sensors fabricated by the nano materials have been determined and discussed.

3.2 Electrochemical Fabrication of PANI nanofibers

Depositions of polymer films were carried out electrochemically by varying acid concentrations as well as monomer (distilled aniline) on stainless steel (SUS 304) electrode.

3.2.1 Fabrication of PANI Nanofibers in Aniline/HCl electrolytes

Figures (3.1a-c) show cyclic voltammogram with potential range (-100mV to 1500mV) and scan rate 30 mV/s for six repetition of PANI films obtained at constant monomer concentration(0.1M distilled aniline) in concentrations 0.1 M ,0.2 M and 0.3 M HCl respectively at scan rate 30mV /s with six repetition at room temperature .The polymerization takes place by oxidation at 700-1300 mV while potential is increasing followed by a de-protonation at 500–150 mV in the reverse direction of potential.

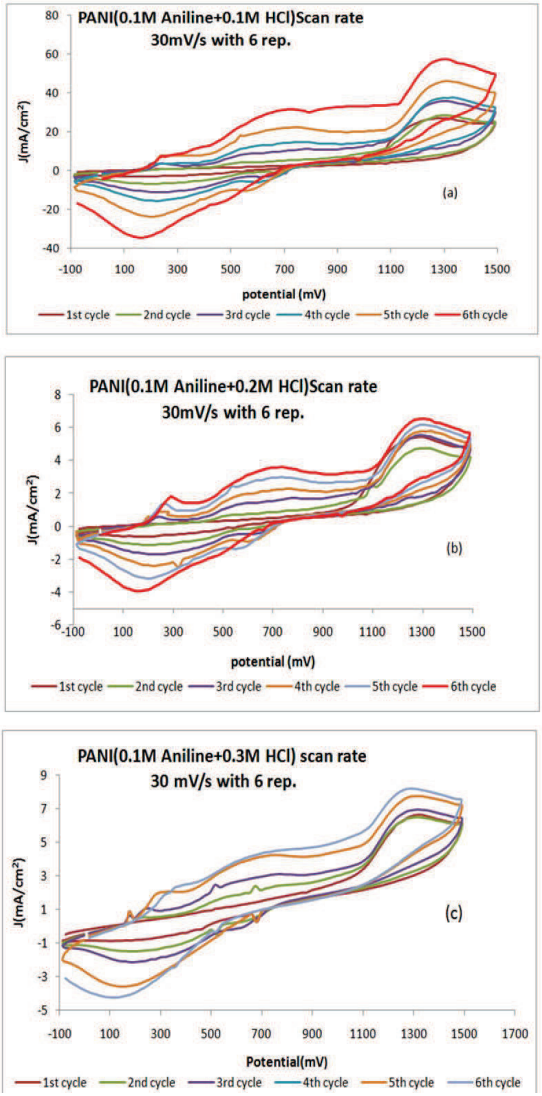

Fig(3.1)cyclic voltammograms of PANI fabricated from (a)(0.1 M aniline+0.1 M HCl)(b)(0.1M aniline +0.2 M HCl)and(c)(0.1M aniline +0.3 M HCl) scan rate 30 mV/s with 6 rep. at room temperature

Table (3.1) gives the peak current densities obtained in different cycles during polymerization at different HCl concentrations and constant aniline concentration 0.1M . It is observed that the current density in 1st cycle for almost double to the

current density in 6th cycle for lower HCl concentration of 0.1M and 0.1M aniline, while the other concentrations do not show any notable change current density. The deposition yielded a green film of polyaniline specially at 0.1 M HCl .

Table (3.1) Peak deposition current densities of different deposition cycles at 0.1 M aniline and different HCl concentrations

HCl concentration (M)	Peak current density at 1st cycle (mA/cm^2)	Peak current density at 2nd cycle (mA/cm^2)	Peak current density at 3rd Cycle (mA/cm^2)	Peak current density at 4th cycle (mA/cm^2)	Peak current density at 5th Cycle (mA/cm^2)	Peak current density at 6th cycle (mA/cm^2)
0.1	29.9	28.5	35.9	37.7	46.19	57.37
0.2	5.4	4.75	5.5	5.79	6.16	6.16
0.3	6.6	6.46	6.92	7.34	7.72	8.71

Figure (3.2) gave the SEM images of PANI films obtained from the systems with different HCl concentrations. When the HCl concentration was as low as 0.1 M, a film constructed with nanoparticles (diameter from 60 to 100 nm) could be obtained Figure (3.2a). As the HCl concentration was increased, microfibers would be generated Figure (3.2b). However, when the HCl concentration reached 0.3 M, serious nano particles without nanofibers could be observed Figure (3.2c). It showed that a lower HCl concentration would accelerate the agglomeration of the freshly formed PANI, because in the fixed reaction space, stronger interaction between the resulting PANI would occur when 0.1 M HCl were used.

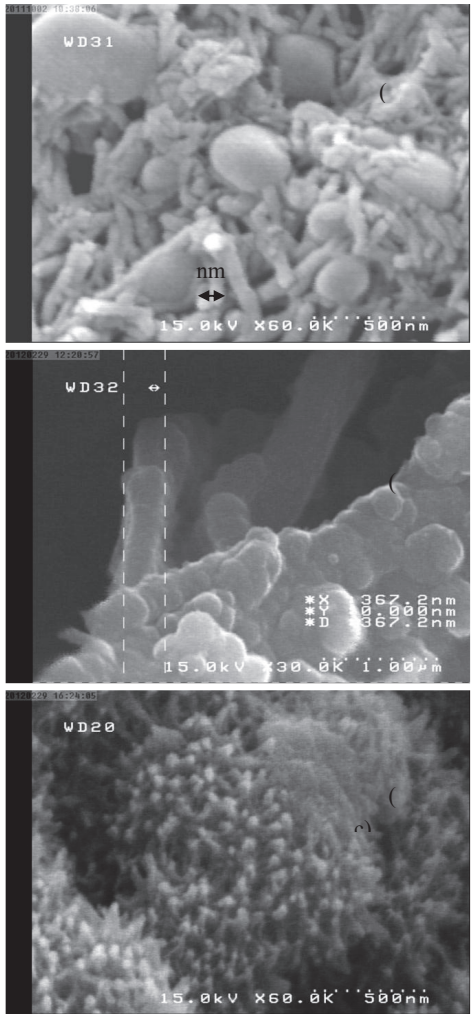

Fig(3.2)SEM images of PANI films obtained from different HCl concentration (a)0.1M,(b) 0.2M , and(c) 0.3M with 0.1M aniline

Steps involved in the possible mechanism of the oxidative electropolymerization of aniline to polyaniline are given in figure (3.3)[215].

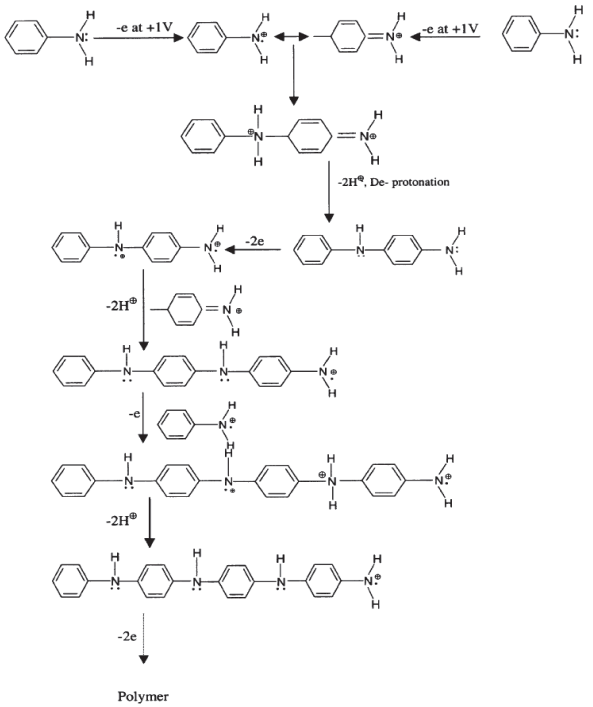

Fig(3.3) Mechanism of oxidative electropolymerization of aniline[215]

The polymerization takes place by oxidation at (700-1300) mV while potential is increasing followed by a de-protonation at (500–150) mV in the reverse direction of potential.

The polymer films obtained by varying the HCl concentration, however, do not show any notable change in current densities deposition at 0.2 M and 0.3 M .The fast rate of deposition current density(J) at lower HCl concentration 0.1M could be ascribed to higher proton concentration and hence higher protonation rate of the film.

The chloride ion (Cl^-) from the electrolyte enters the polymer film in the oxidative polymerization and remains in the polymer chain as dopant and

contributes to oxidation/reduction by accepting/contributing one electron, which makes the polymer conducting, this result also have been reported by Pharhad Hussain [215] .

3.2.2 Fabrication of PANI Nanofibers in Aniline/ H_2SO_4 electrolytes

Figures 3.4(d-e)shows similarly the cyclic voltammograms of PANI films recorded at 0.1 M distilled aniline in concentrations 0.1 M, 0.2 M, and 0.3 M H_2SO_4 respectively.

The polymerization takes place by oxidation at (700-1300) mV while potential is increasing followed by a de-protonation at (500–150) mV in the reverse direction of potential for 0.1 M and 0.2 M H_2SO_4 concentrations and at (200-100) mV in the reverse direction of potential for 0.3 M.

Table (3.2) gives the peak current densities obtained in different cycles during polymerization at different H_2SO_4 concentrations and constant aniline concentration 0.1M. It is observed that the current density in 1^{st} cycle for almost four times to the current in 6^{th} cycle for higher H_2SO_4 concentration of 0.3 M and 0.1M aniline, while the other concentrations do not show any notable change current density. The deposition yielded a green film of polyaniline especially at 0.3 M H_2SO_4.

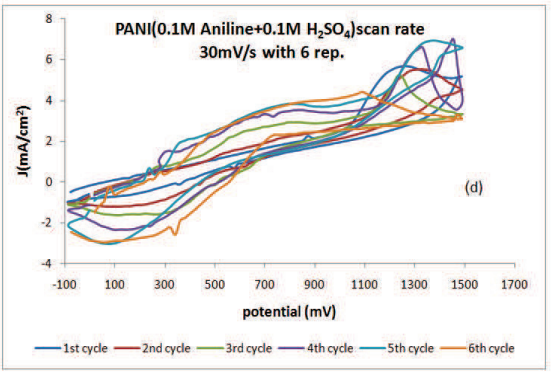

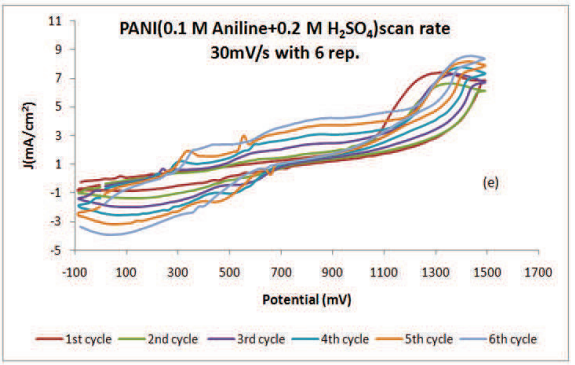

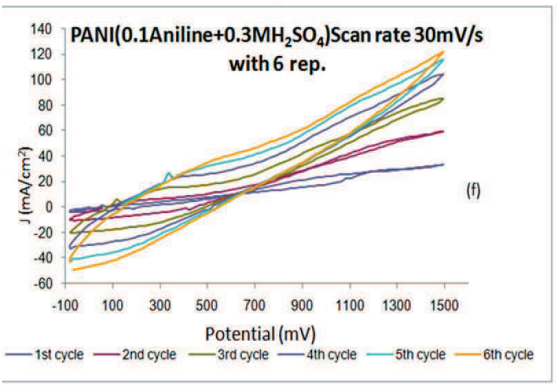

Fig(3.4)cyclic voltammetry of PANI fabricated from (d)(0.1 M aniline+0.1 M H_2SO_4), (e)(0.1M aniline +0.2 M H_2SO_4), and(f)(0.1M aniline +0.3 M H_2SO_4) scan rate 30 mV/s with 6 rep. at room temperature

Table (3.2) peak deposition current densities of different deposition cycles at 0.1M aniline and different H_2SO_4 concentrations

H_2SO_4 concentration (M)	Peak current density at 1st cycle (mA/cm^2)	Peak current density at 2nd cycle (mA/cm^2)	Peak current density at 3rd Cycle (mA/cm^2)	Peak current density at 4th cycle (mA/cm^2)	Peak current density at 5th Cycle (mA/cm^2)	Peak current density at 6th cycle (mA/cm^2)
0.1	5.67	5.53	5.2	6.98	6.94	4.41
0.2	7.41	6.6	7.29	8.7.76	8.13	8.52
0.3	33.4	59.3	84.8	104.2	115.5	121.6

Figure (3.5) shows the SEM images of PANI films obtained from the systems with different H_2SO_4 concentrations. When the H_2SO_4 concentration was as high as 0.3 M, a film constructed with nanofibers (diameter from 50 to 70 nm) could be obtained Figure (3.5 c). As the H_2SO_4 concentration was decreased, microfibers would be generated Figure (3.5 b). However, when the H_2SO_4 concentration reached 0.1 M, serious no nanofibers could be observed Figure (3.5 a). It showed that a higher H_2SO_4 concentration would accelerate the agglomeration of the freshly formed PANI, because in the fixed reaction space, stronger interaction between the resulting PANI would occur when 0.3 M H_2SO_4 were used.

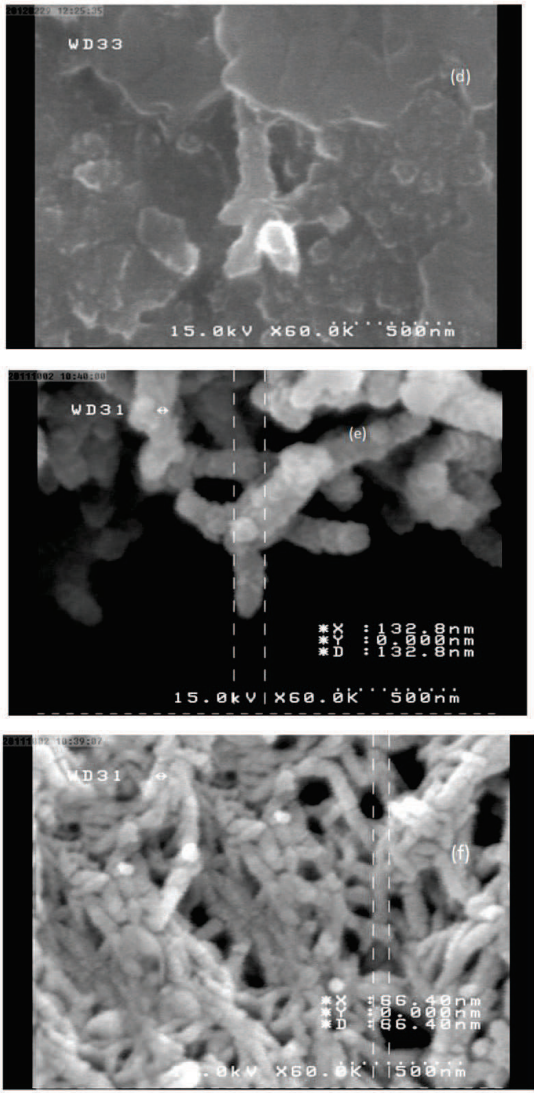

Fig(3.5) SEM images of PANI films obtained from different H_2SO_4 concentration (a)0.1M ,(b) 0.2M , and(c) 0.3M with 0.1M aniline

The polymer films obtained by varying the H_2SO_4 concentration, however, do not show any notable change in current densities deposition at 0.1 M and 0.2 M.

The fast rate of deposition current density (J) at higher H_2SO_4 concentration 0.3 M could be ascribed to higher proton concentration and hence higher protonation rate of the film.

The sulfate ion (SO_4^-) from the electrolyte enters the polymer film in the oxidative polymerization and remains in the polymer chain as dopant and contributes to oxidation/reduction by accepting/contributing one electron, which makes the polymer conducting[215] .

Deposition electrochemically of two varying acid HCl and H_2SO_4 (concentrations 0.1 M, 0.2 M and 0.3 M) with 0.1 M aniline demonstrated a process of two concentrations with incomplete polymerization for 0.1 M HCl while a complete process was observed with 0.3 M H_2SO_4 .Such observations were confirmed by SEM analyses by investigating the formation of aggregations .Figure(3.2 a) illustrates growth of nanofibers with 0.1 M HCl as well as aggregation zones ,on other hand, Figure (3.5c) shows such nanofiber growth with no aggregation zones when 0.3 M H_2SO_4 was involved.

Since the current density has an influence on the quality of polymerization and its electrical conductivity, the formation cycles were studied in terms of acid type and concentration .As shown in table (3.1), the current density (J) of the first cycle was found to be half that of the sixth cycle at 0.1M HCl, meanwhile, at 0.3 M H_2SO_4 the ratio of (J) for the first and sixth cycles was found to be 1/4 as listed in table (3.2). Such conditions justified the adoption of the 0.3 M H_2SO_4 for the required optimum processes.

3.2.3 Effect of scan rate varying on the nanofibers PANI fabrication

The effect of scan rate variation with pH=4 and (0.1 M distilled aniline +0.3 M H_2SO_4) for the six cycles was also inspected .Figures (3.6, 3.7, 3.8, 3.9, and 3.10) refer to the PANI fabrication with scan rate (20mV/s, 30mV/s, 40mV/s, 50mV/s, and 60 mV/s) respectively. The current density was found to be optimum at 30 mV/s and less for the other scan rates. Therefore, this scan rate on the sixth repetition were considered as optimum for the preparation process of PANI/ carbon nanopowder composite and PANI/ carbon Nanotubes composite.

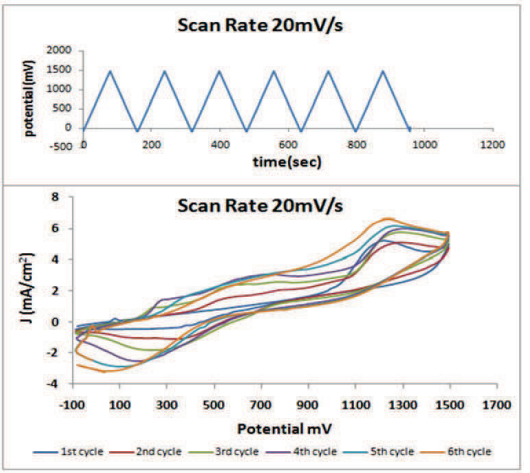

Fig. (3.6)cyclic voltammograms of SUS(304) electrode in PANI electrolyte (0.1M aniline +0.3M H_2SO_4)(pH=4.0) (from -100 to 1500mV)scan rate 20 mV/s at room temperature.

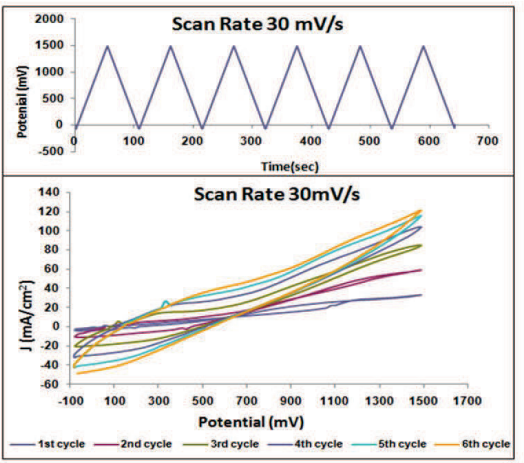

Fig(3.7)cyclic voltammograms of SUS(304) electrode in PANI electrolyte (0.1M aniline +0.3M H_2SO_4)(pH=4.0) (from -100 to 1500mV)scan rate 30 mV/s at room temperature.

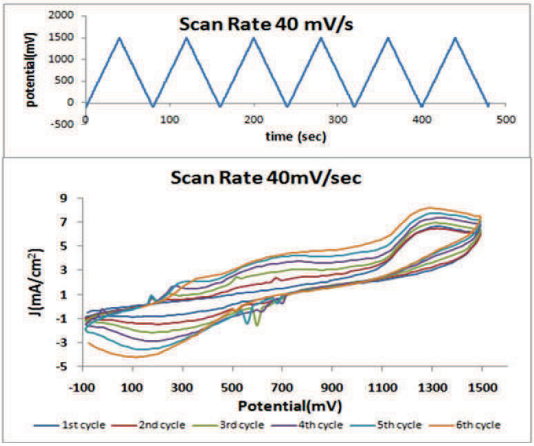

Fig(3.8)cyclic voltammograms of SUS(304) electrode in PANI electrolyte (0.1M aniline +0.3M H_2SO_4)(pH=4.0) (from -100 to 1500mV)scan rate 40mV/s at room temperature .

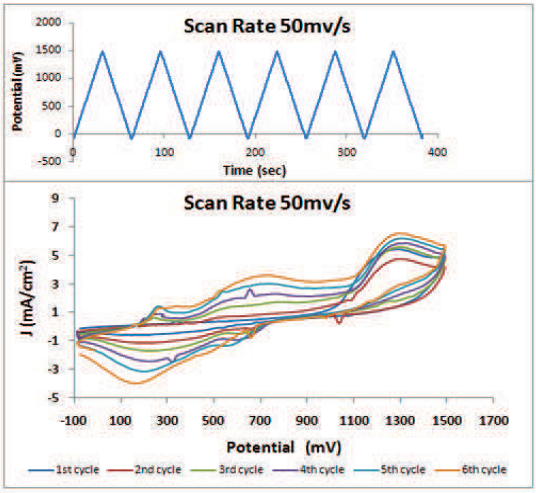

Fig(3.9)cyclic voltammograms of SUS(304) electrode in electrolyte (0.1M aniline +0.3M H_2SO_4)(pH=4.0) (from -100 to 1500mV)scan rate 50 mV/s at room temperature.

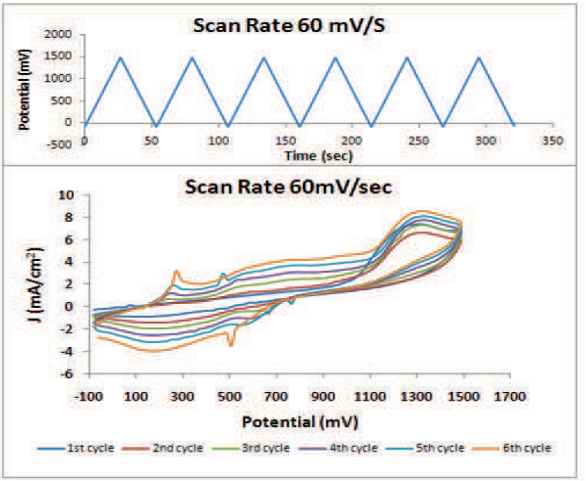

Fig(3.10)cyclic voltammograms of SUS(304) electrode in electrolyte (0.1M aniline +0.3M H_2SO_4)(pH=4.0) (from -100 to 1500mV)scan rate 30 mV/s at room temperature.

3.3 Characterization of fabricated PANI nanofibers

PANI nanofibers fabricated by electrochemically at scan rate 30 mV/s with six repetition characterized as:

3.3.1 Fourier Transformation Infrared spectra (FT-IR) of PANI synthesis

The electropolymerization of 0.1 M aniline was carried out in 0.3 M H_2SO_4 at 30 mV/s with six repetition .Figure (3.11) gives a typical Infrared spectra of the PANI product where the main absorption peaks shows 3468 cm^{-1} it is possible assign asymmetric stretching vibration of NH_2. The N-H stretching in benzoid-NH-benzoid(B-NH-B) ,the broad band at 3310 cm^{-1} to hydrogen bonded NH and 3178 cm^{-1} to terminal quinoid =NH (Q=NH). The 2943 cm^{-1} represented C-H stretching region. The absorption peak observed at 1647.21 cm^{-1} were attributed to C=C stretching in aromatic nuclei Absorption bands at 1477.4 cm^{-1} evidenced to C=N stretching in aromatic compounds. The polymer shows absorption bands at 1300-1200 cm^{-1} which confirms the C-N stretching of primary aromatic amines .The 1141 cm^{-1} band is vibrational mode

$(B-\overset{+}{N}H=Q)$ or $(B-\overset{+}{N}H-B)$ which is formed in doping reaction. This band is very intense and broad which may be attributed to an existence of positive

charges[216] . The absorption peaks at 1546.91cm^{-1} assigned to the quinoid structure does not revealed any significant changes for all polymer samples, that concludes that the polymers were prepared using di and tri basic acids. It has been reported that H_2SO_4 may interact with PANI by donating either hydrogen sulfate, $(HSO_4)^-$ or sulfate, $(SO_4)^{-2}$ anions as dopant anions. Many authors agreed that $(HSO_4)^-$ dopant anions are present in PANI/H_2SO_4 [56]

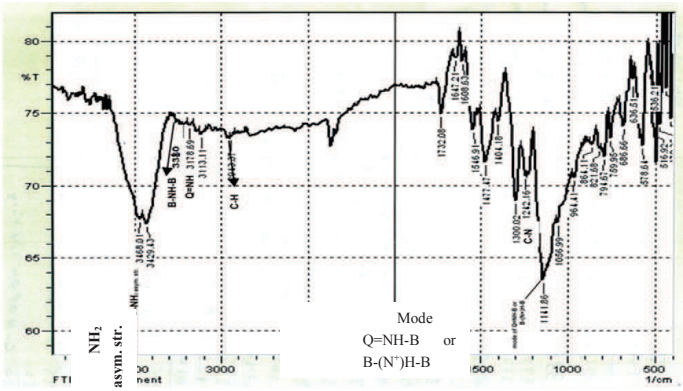

Fig(3.11) Infrared spectra of PANI synthesized from (0.1 M aniline +0.3 H_2SO_4) at scan rate 30 mV/s with 6 repetition

3.3.2 Crystallographic structure polyaniline

Typical XRD patterns of PANI fabricated by (0.1 M aniline +0.3 H_2SO_4) at scan rate 30 mV/s with six repetition shows in figure 3.12 and are given data of crystalline information. It was revealed find highly oriented along 2θ (43.46 ^{0}, 50.66 ^{0}, and 74.47 ^{0}) this information have no card matching data, Figure (3.13) provides the data requires to calculate the particle size from *(Scherrer formula* [213]). Table (3.3) represent the value of (2θ) of the strong three peaks and particle size of polyaniline nanofibers calculated by *Scherer formula*.

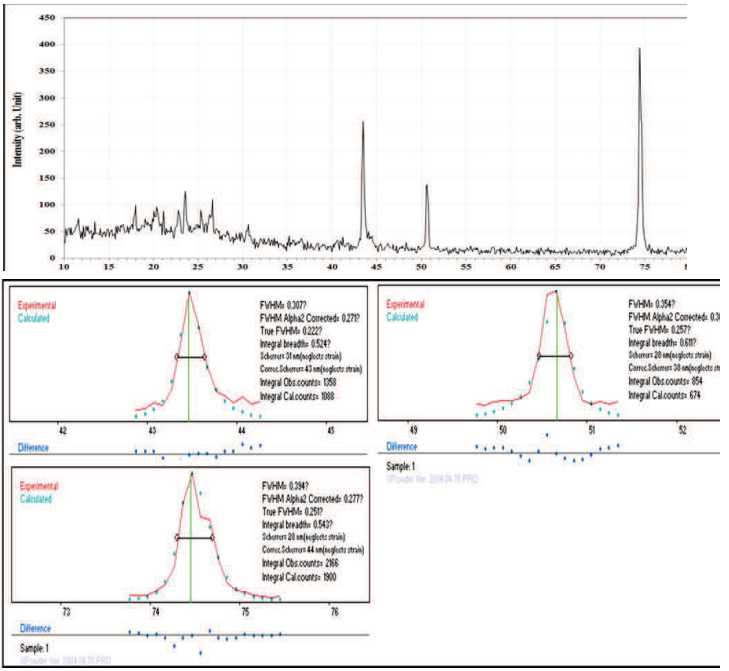

Fig(3.13) Full Width Half Maximum of three peaks in fig(3.12)

Table (3.3) *Represent the value of (2θ) of the strong three peaks and particle size of polyaniline nanofibers calculated by Scherrer formula*

Peak No.	2θ (Deg.)	d Exp.[Å]	FWHM (Deg.)	Particle Size (nm)
1	43.46	2.0824	0.222	36.3
2	50.66	1.8020	0.257	32.2
3	74.45	1.2744	0.251	37.4

3.4 Characterization of Fabricated CNpowder

Carbon Nanopowder was fabricated by arc discharge technique at deposition pressure of (10^{-6} mbar Argon gas) on glass substrates. Arc discharge method in a high vacuum and low pressure was used to evaporate graphite. This method is a direct deposition technique in which the material is deposited by vaporization

after plasma is produced. After the arc was carried out, soot was deposited on the chamber wall .The soot was collected from the chamber wall and taken out to the purification treatment. The characterized of CNpowder of the soot as received and purified examined as:

3.4.1 Crystallographic structure of CNpowder

Figure (3.14) showed x-ray diffraction of CNpowder as received from chamber and that purified by acid-treated prepared at a pressure 0f (10^{-6} mbar Argon gas) the figure reveals find highly oriented along the c-axis giving a peaks at $2\theta = 26.58^0$ and 54.69^0 which belongs to (002) and (004) respectively for purification CNpowder by acid treated which agreement with reference to Joint Committee on Powder Diffraction Standards (JCPDS) No.56-159[217].

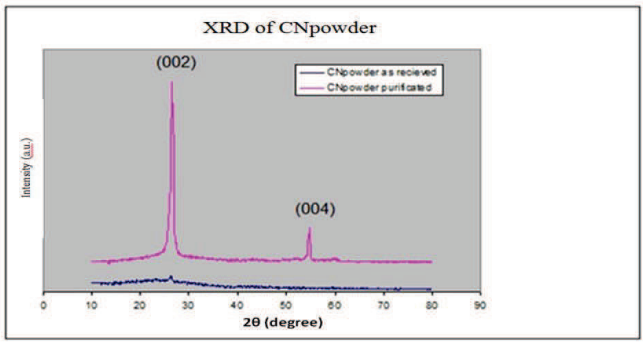

Fig(3.14)X-Ray Diffraction of CNpowder for as fabricated and purified by nitreic acid-treated prepared at pressure (10^{-6} mbar Argon gas)

The peak at $2\theta = 26.58^0$ which was strong and sharp ,was corresponding to(002)reflections of CNpowder .The interplanar spacing was calculated to be $d_{(002)}$=3.351 Å the other peak which was corresponding to (004) at $2\theta = 54.692^0$.The interplanar spacing was calculated to be $d_{(004)}$=1.677 Å .The average particle size of the nanoparticles of CNpowder purified by HNO_3 treated was estimated by using the standard Scherrer formula[213], table 3.3 indicated for the particle size estimation[218] .

Table (3.4) Represent the value of (2θ) of the strong two peaks and particle size of purified CNpowder calculated by Scherrer formula

Peak No.	2θ (Deg)	FWHM (Deg)	hkl	d_{hkl} (Å)	Particle Size(nm)
1	26.580	0.538	002	3.351	14
2	54.692	0.197	004	1.677	43

3.4.2 Morphological characteristics of CNpowder

The powder fabricated of two types were examined by Atomic Force Microscope (AFM) and Scanning Electron microscope (SEM).

3.4.2.1 CNpowder as received from chamber

AFM images of CNpowder as received from chamber was shown in figure (3.15).The Granularity normal distribution of the particles collected as a result of the preparation of CNpowder, where the size of the particle rate ranged up to 60nm .

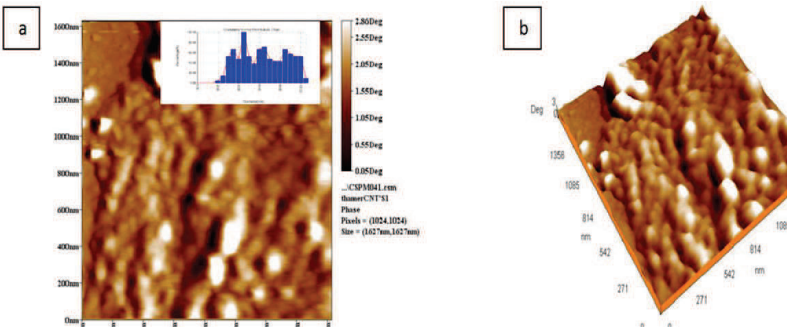

Fig (3.15)AFM images of the untreated CNpowder(a)Two dimensions and (b)Three dimensions

SEM images of untreated CNpowder are shown in Figure (3.16). The diameters were measured and found to be about 60 nm and the side walls were non uniform because more amorphous carbon in the structure.

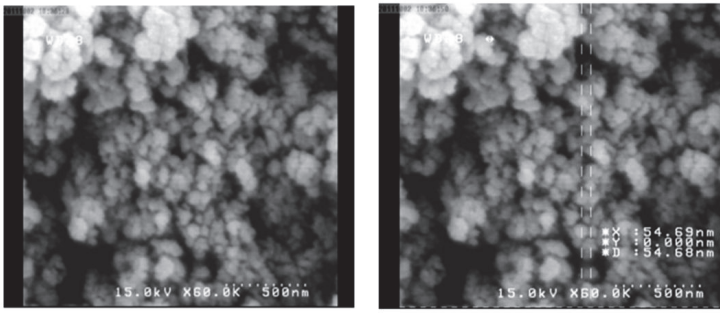

Fig (3.16) SEM images of untreated CNpowder magnified 60000 times showed the particle size

3.4.2.2 Purification of CNpowder by nitric acid

In order to dissolve the amorphous carbon must be the purified CNpowder treated by nitric acid. Figure (3.17) shows(AFM)images of the treated powder(a) two dimension and (b) three dimension .The Granularity normal distribution of the particles collected as a result of the preparation and purified of CNpowder ,where the size of the particle rate ranged up to 50nm[218].

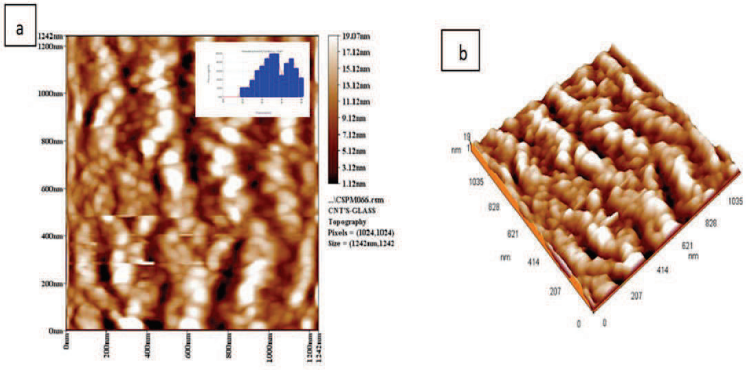

Fig (3.17) AFM images of the treated CNpowder (a) Two dimensions and (b) Three dimensions

SEM images figure (3.1٨) shows morphological of purified CNpowder treated by nitric acid magnified 60000 time and shown the Particle size about 50 nm.

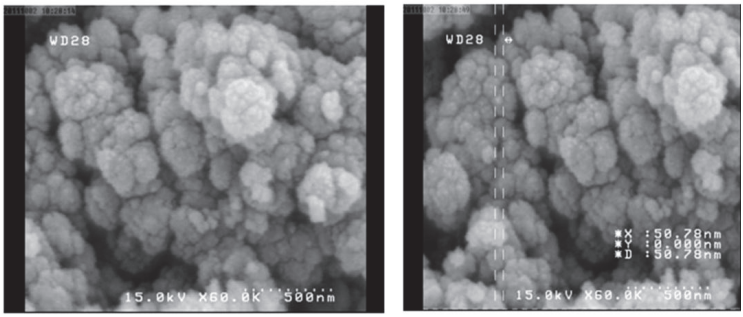

Fig.(3.18) ***SEM images of treated CNpowder by nitric acid magnified 60000 times shown the particle size***

3.5 Fabrication of PANI/CNpowder composite

The fabrication process involved a cyclic voltammogram, morphology, and current-voltage characteristics as discuss below.

3.5.1 Cyclic voltammetry

Figures (3.19),(3.20), and(3.21) show a typical cyclic voltammogram with potential range (-100mV to 1500mV) and scan rate 30 mV/s for six repetition of PANI(0.1M aniline+0.3 M H_2SO_4)/0.25 wt% CNpowder ,PANI/0.5 wt% CNpowder and PANI/1 wt% CNpowder composite respectively on SUS(304) stainless steel electrodes .

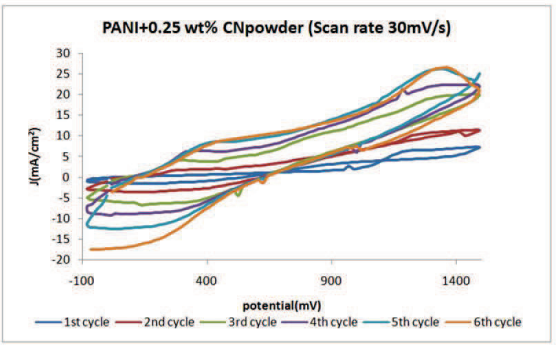

Fig (3.19)PANI+0.25 wt% CNpowder composite fabricated at scan rate 30mV/s with six repetition

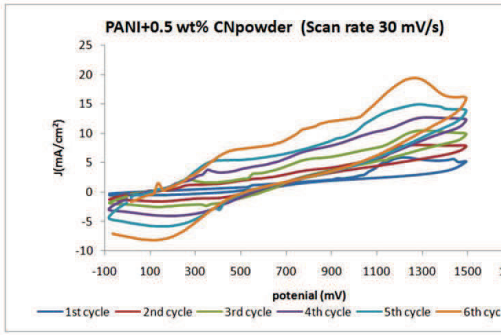

Fig (3.20) PANI+0.5 wt% CNpowder composite fabricated at scan rate 30mV/s with six repetition

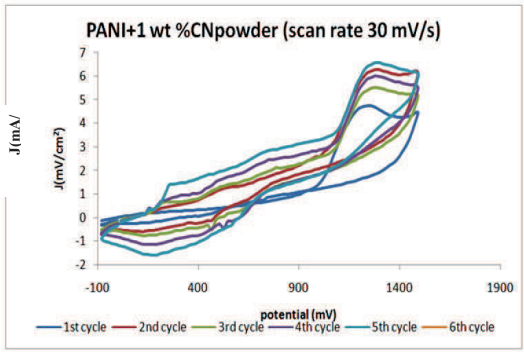

Fig (3.21) PANI+1 wt% CNpowder composite fabricated at scan rate 30mV/s with six repetition ***scan***

Its was found that an adition of CNpowder on PANI reduces deposition current density (J) and such reduction is enlarged with more addition of CNpowder as demonstrated in figures(3.19, 3.20, and 3.21) an comparison with PANI alon figure(3.4 f)

3.5.2 Morphology of PANI/CNpowder film

SEM images (figure 3.22) shows morphological of PANI (0.1M aniline+0.3 M H_2SO_4)/1 wt% CNpowder composite film synthesis from electrochemical with

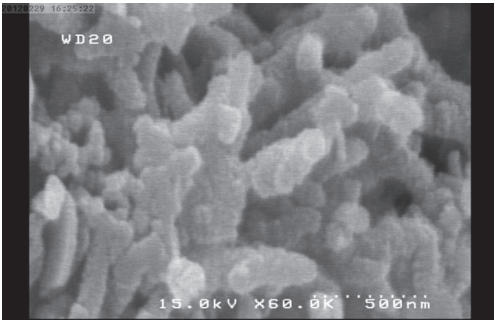

Fig (3.22) SEM of PANI/ 1wt% CNpowder synthesized at scan rate (30mV/s) with six repetition

cyclic voltammogram potential range (-100mV to 1500 mV) at scan rate (30mV/s)with six repetition on SUS(304)stainless steel electrode.

3.5.3 Current-Voltage Characteristics of PANI and PANI/CNpowder Composite

The I-V characteristic of PANI and PANI/CNpowder composite and electrical resistance show from figures (3.23), (3.24a) and (3.24b). I-V curves provide information on the electrical resistance of each individual sample. Lower resistance recorded for the PANI samples (0 addition Fig. (24b)). The resistance was found to be increased with the increasing proportion rate of the carbon nanopowder. The reason behind that is the formation of discontinuities with the PANI nano fibers with subsequent electrical bad conduct, these observations were agreements with reported by Chuizhou Meng et al[220]; one can conclude that the addition of CNpowder results in an increase in the electrical resistance. Such undesirable increase of the resistance was excluded from consideration in chemical sensing.

The reason behind this may be the existence of some intersections in the randomly growing PANI giving rise to an enlargement in the fiber diameter as illustrated in the SEM image figure (3.22).

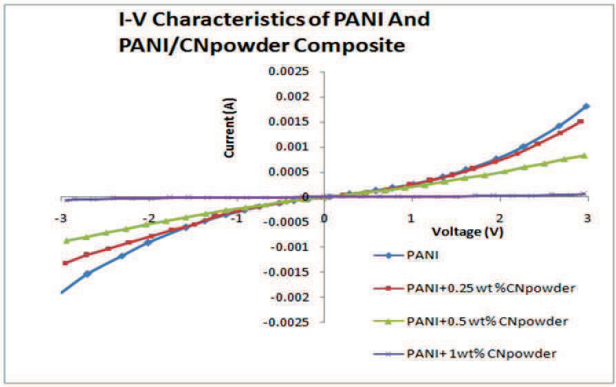

Fig (3.23) Current-Voltage characteristic of PANI, PANI+0.25, 0.5, and 1 wt% CNpowder composite

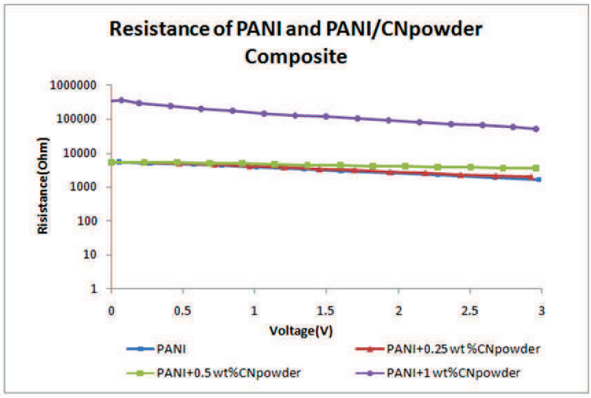

Fig (3.24a)Resistance of PANI, PANI+0.25, 0.5, and 1 wt% CNpowder composite

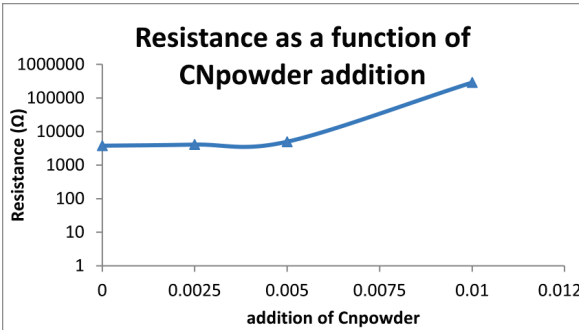

Fig (3.24b)Resistance as a function of CNpowder at applied voltage

3.6 Fabrication of PANI/Carbon Nanotubes composite

cyclic voltammogram with potential range (-100mV to 1500mV) and scan rate 30 mV/s for six repetition was carried out for PANI(0.1 M aniline+0.3 M H_2SO_4)/0.25 wt% CNTs , PANI/0.5 wt% CNTs and PANI/1 wt% CNTs composite fabrication using purchased MWNTs supplied by (cheap tubes Inc). The main characteristics of MWNTs were deduced throughout the steps.

3.6.1 Characterization of Purchased MWNTS

In order to ensure the required properties of the composite materials, the fabrication was carried out by as indicated in the following sections.

3.6.1.1 Crystallographic Structure of MWNTs

Figure (3.25) showed x-ray diffraction of CNTs. The figure reveal find highly oriented along the c-axis giving a peaks at $2\theta = 25.87^0$ and 53.85^0 which belongs to (002) and (004) respectively, the other peaks at $2\theta = 37.89^0$, 64.420 oriented along (021) and (203) so the peaks at $2\theta = 42.7^0$, 44.15^0 ,77.6^0 oriented along (100), (101), and (110) respectively.

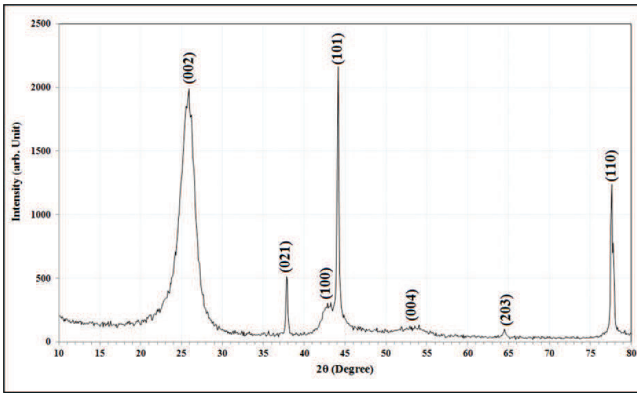

Fig(3.25)XRD of purchased CNTs

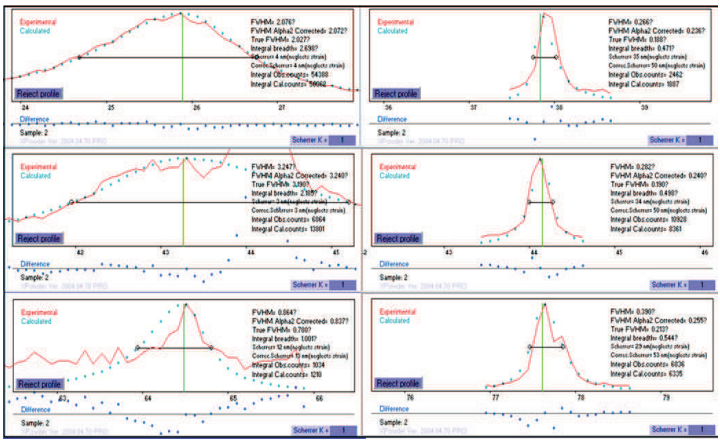

Fig(3.26) Full Width Half Maximum of main six peaks in fig(3.25)

The peak at 2θ=25.87^0 which was strong and broad, was corresponding to (002) reflections of CNTs .The interplanar spacing was calculated to be $d_{(002)}$=3.444 Å the other peak which was corresponding to (004) at 2θ= 54.692^0.The interplanar spacing was calculated to be $d_{(004)}$=3.1Å . Figure (3.26) refer to Full Width Half Maximum of main six peaks and table (3.4) informed all peaks were founded.

Table (3.5) Represent the value of (2θ) of the strong peaks 0f CNTs and its information's

2theta (Deg.)	d Exp.[Å]	FWHM (Deg.)	P.S (nm)	d Std. [Å]	Phase	hkl	Card No.
25.87	3.4446	2.027	3.8	3.3950	Hex.	(002)	96-120-0018
37.89	2.3747	0.188	42.1	2.3995	Ortho.	(021)	96-901-2232
42.70	2.1177	3.190	2.5	2.1391	Hex.	(100)	96-120-0018
44.15	2.0514	0.190	42.5	2.0402	Hex.	(101)	96-120-0018
53.83	1.7032	2.712	3.1	1.6975	Hex.	(004)	96-120-0018
64.42	1.4464	0.780	11.3	1.4517	Ortho.	(203)	96-901-2232
77.60	1.2303	0.213	45.1	1.2350	Hex.	(110)	96-120-0018

3.6.1.2 Fourier Transformation Infrared (FT-IR) spectra of Purchased CNTs

Over the process of FTIR, analysis of Purchased showed only one absorption peak due to its own formation characteristics. This peak appears at (1525.50) cm^{-1} as shown in Fig(3.27).

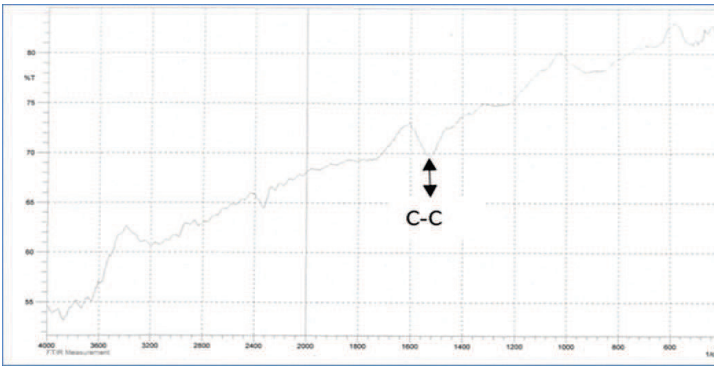

Fig (3.27)FT-IR of purchases MWNTs

3.6.1.3 Morphology of CNTs

Figure (3.28) refers to atypical AFM image of CNTs. The Carbon Nanotubes (CNTs) Normal disturbution are reported that the average outer diameter (OD)is about 28 nm as shown in table (3.6) and illustrated in figure(3.29)

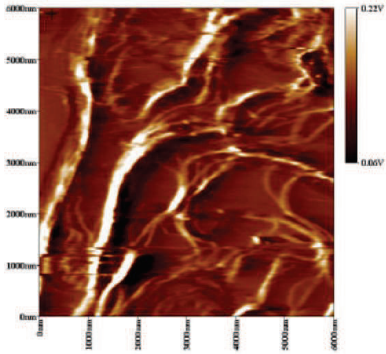

Fig(3.28)AFM image of CNTs

Table (3.6) Normal Distribution of CNTs

Diameter(nm)~	Volume(%)	Normal(%)	Diameter(nm)~	Volume(%)	Normal(%)	Diameter(nm)~	Volume(%)	Normal(%)
6.00	0.26	2.38	20.00	7.48	67.46	34.00	6.60	59.52
8.00	0.18	1.59	22.00	11.08	100.00	36.00	3.80	42.38
10.00	0.70	6.35	24.00	10.55	95.24	38.00	4.75	42.86
12.00	1.58	14.29	26.00	9.41	84.92	40.00	3.08	27.78
14.00	2.02	18.25	28.00	9.85	88.89	42.00	3.17	28.57
16.00	4.31	38.89	30.00	6.93	62.70			
18.00	5.72	51.59	32.00	6.51	58.73			

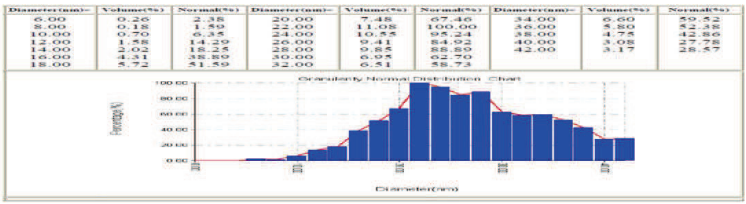

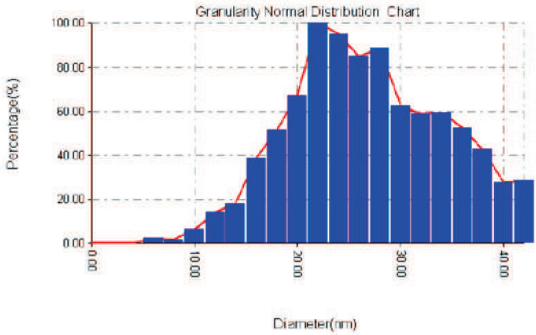

Fig(3.29) Normal distribution chart for CNTs

3.6.2 Cyclic voltammetry of PANI/CNTs composite

Figures (3.30),(3.31), and(3.32) show cyclic voltammogram with potential range (-100mV to 1500mV) and scan rate 30 mV/s for six repetition of PANI(0.1 aniline+0.3M H_2SO)/0.25 wt% CNTs ,PANI/0.5 wt% CNTs and PANI/1 wt% CNTs composite respectively on SUS(304) stainless steel electrodes.

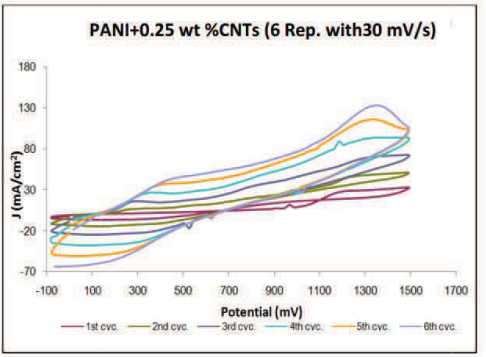

Fig (3.30)PANI+0.25 wt% CNTs composite fabricated at scan rate 30mV/s with six repetition

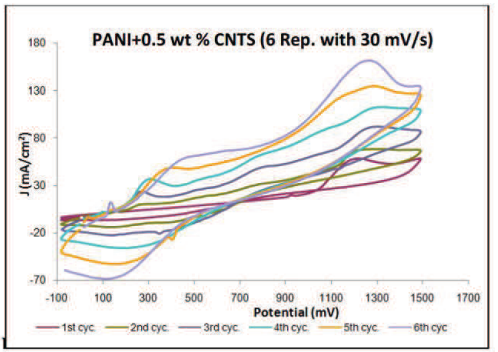

Fig (3.31)PANI+0.5 wt% CNTs composite fabricated at scan rate 30mV/s with six renetition

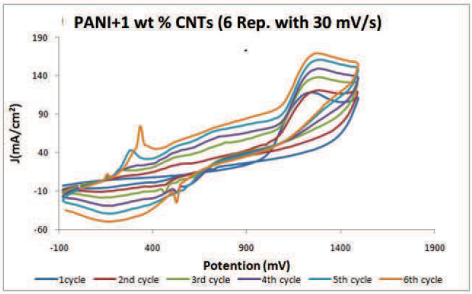

Fig (3.32)PANI+1 wt% CNTs composite fabricated at scan rate 30mV/s with six repetition

It was found that an addition of CNTs to the PANI for the formation of PANI composite, the deposition current density(J) was increased with increasing addition ratio. In other words the increase of addition ratio from 0.25 wt% to 1wt% CNTs resulted in an enhancement in (J) as in figures (3.30, 3.31,and 3.32).

3.6.3 Characterization Of PANI/CNTs Composite

The crystallographic, FT-IR, morphology, and I-V characteristics of PANI/CNTs composite were explained in following paragraphs:

3.6.3.1 Crystallographic Structure of PANI/CNTs Composite

Figure (3.33) shows XRD of PANI/1wt% CNTs composite . The XRD pattern for the MWNT doped PANI composite exhibits the crystalline peaks around $2\theta=27.74^0,32.17^0,43.75^0,50.92^0$, and 74.70^0, table(3.7).

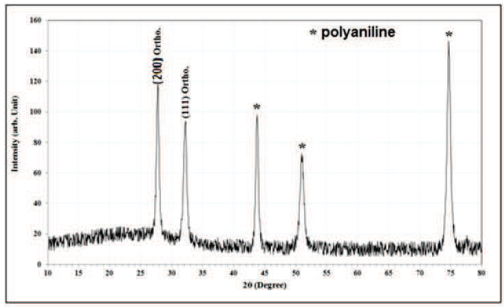

Fig(3.33)XRD of PANI/1wt% CNTs composite

peaks are observed which clearly reveals that form a structural point view ,no additional order has been introduced. The high intensity of peaks may be attribute to the occurrence of MWNT in PANI matrix hence increase in the extension of microcrystalline domains in the MWNT doped PANI composite[219].

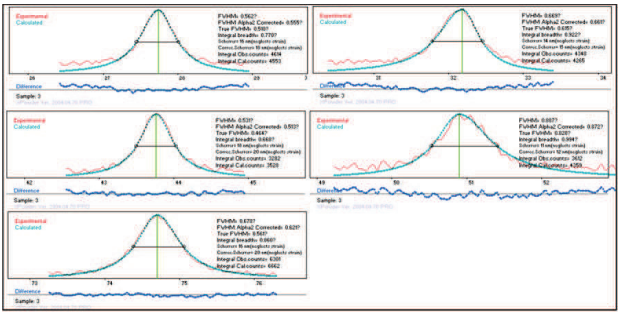

Fig(3.34) Full Width of Half Maximum of five main peaks in

Table (3.7) Represent the value of (2θ) of the strong peaks of PANI/CNTs composite and its information's

2theta (Deg.)	d Exp.[Å]	FWHM (Deg.)	P.S (nm)	d Std. [Å]	Phase	hkl	Card No.
27.74	3.2164	0.510	15.1	3.2475	Ortho.	(200)	96-901-2235
32.17	2.7822	0.615	12.7	2.8101	Ortho.	(111)	96-901-2235
43.75	2.0692	0.464	17.4	Polyaniline			
50.92	1.7935	0.820	10.1	Polyaniline			
74.70	1.2707	0.561	16.8	Polyaniline			

3.6.3.2 Fourier Transformation Infrared spectra of PANI/CNTs Composite synthesis

Figure (3.35) gives a typical Infrared spectra of the PANI/1wt%CNTs composite product where the main absorption peaks shows 3448 cm^{-1} it is possible assign asymmetric stretching vibration of NH_2. The N-H stretching in benzoid-NH-benzoid(B-NH-B) ,the broad band at 3232 cm^{-1} to hydrogen stretching bonded NH and 3163 cm^{-1} to terminal quinoid =NH (Q=NH). The 2954 cm^{-1} represented C-H stretching region.

The absorption peak observed at 1643.35 cm^{-1} were attributed to C=C stretching in aromatic nuclei Absorption bands .the bonds situated 1482.04 cm^{-1}

and 1585.49 cm^{-1} are attributed to benzoid and quinoid ring vibration respectively[162].its commonly observed for PANI that the quinoid band at 1585 cm^{-1} is less intense than that benzenoid band at 1482 cm^{-1} .As shown in spectrum of PANI/CNTs composite, an inverse 1585/1482 cm^{-1} intensity ratios was exhibited .These data reveal that PANI in composite is richer in quinoid units than the pure PANI. This fact may suggest that PANI-CNTS. The polymer shows a interaction promote and stabilize the quinoid ring structure .this interaction between PANI and CNTs may result in "charge transfer"[165]. The π- bonded surface of carbon Nanotubes might interact strongly with conjugated structure of poly aniline, especially through the quinoid ring figure (1.30)[166].The strong band at 1149 cm^{-1} is considered to be a measure of the degree of delocalization of electrons and thus it is characteristics peak of PANI conductivity [162].The increase of the signal at 1149 cm^{-1} is in good agreement with conductivity measurements result given by S. Quillard et al. [162]. It appears that the interaction between PANI and CNTs increase the effective degree of electron delocalization, and thus enhances the conductivity of polymer chains.

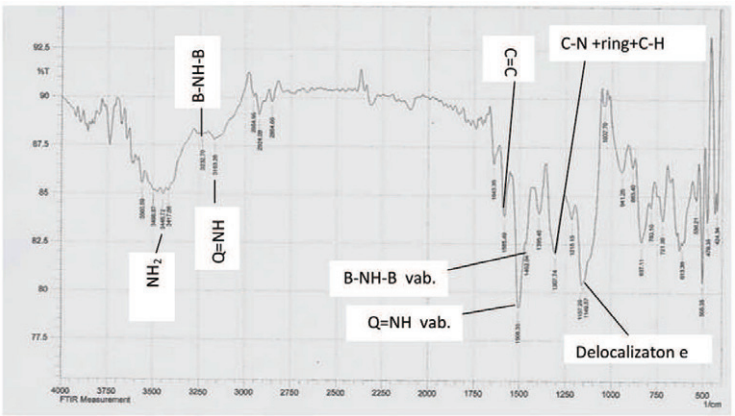

Fig(3.35) FT-IR spectra for PANI/ 1wt% CNTs

3.6.3.3 Morphology of PANI/CNTS composite

Figures 3.36 , 3.67, 3.68 showed SEM images of PANI(0.1 M aniline+0.3 M H_2SO_4)/0.25wt% CNTs , PANI/0.5 wt % CNTs, and PANI/1wt% CNTs respectively. This all images appears that the well –formed CNT inside

PANI. This result can be consider that agreement with the schematic of Chuizhou Meng et al figure (3.39)[220].SEM revealed a uniform deposition of PANI onto the CNTs ,whereby the diameter of the PANI-coated CNTs was estimated to be in the range (55-80)nm.

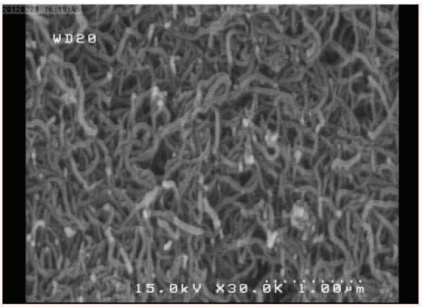

Fig(3.36) SEM image of PANI/0.25 wt% CNT composite magnified 30000 times

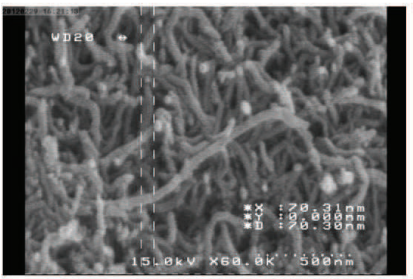

Fig(3.37) SEM image of PANI/0.5 wt% CNT composite magnified 60000 times

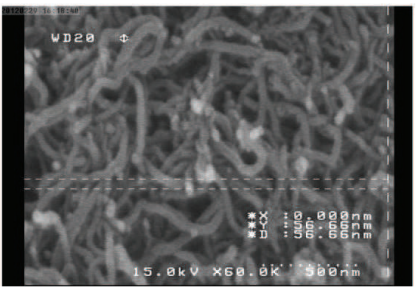

Fig(3.38) SEM image of PANI/1 wt% CNT composite magnified 60000 times

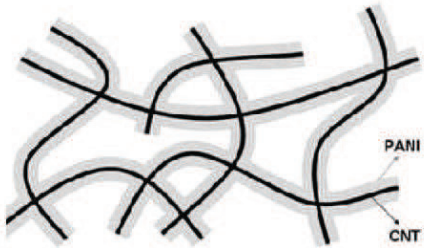

Fig.(3.39)schematic illustration the well-formed CNTs network inside PANI[220]

3.6.3.4 Current-voltage characteristics of PANI and PANI/CNTs composite

I-V characteristics of electrochemical deposition of PANI and PANI/CNTs composite film onto SUS (304) stainless steel substrate show symmetric behavior of the applied forward and reverse bias voltage.

Figure (3.40) noticed that the curves exhibit non-linear feature and this is an indication the prevalent conduction mechanism is non-Ohmic in nature and it may reveal for existence of different kinds of conduction mechanisms. The interaction of CNTs with nitrogen of PANI, leading to an expansion of compact PANI chains into more stretching conformations.

This in turn, is expected to increase to the crystallinity of the composite film and decrease its electric resistance this result also have been reported by Subodh et al. [221]. Figure (3.41a) show the electrical resistance of PANI, PANI/0.25 wt% CNTs, PANI/0.5 wt% CNTs, and PANI/1 wt% CNTs. Reduction of resistance was recorded for increased proportions of CNTs figure (3.41b) ,resulting in good contact(better conductivity) and the well-formed CNT network inside PANI .

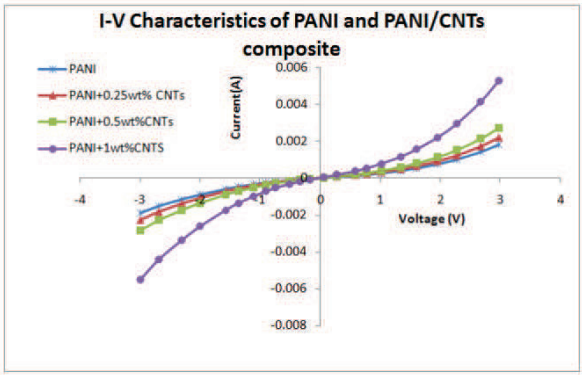

Fig(3.40)Current-Voltage characteristics of PANI and PANI/CNTs composite

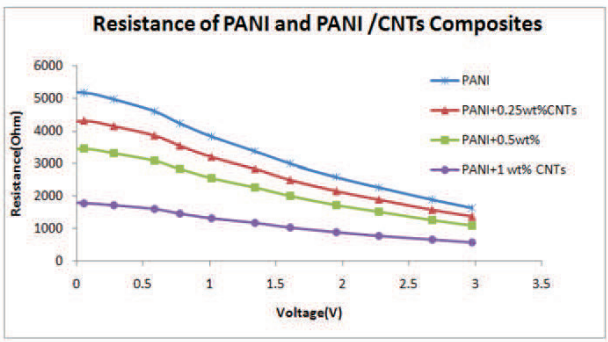

Fig(3.41) Resistance of PANI and PANI/CNTs composites

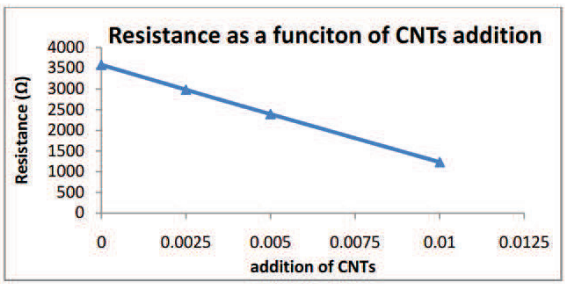

Fig(3.41 b)Resistance as a function of CNTs at applied voltage 1V

3.7 Liquid sensing measurements

In Voltammetric a time –depended potential is applied to an electrochemical cell, and the current flowing through the cell is measured as a function of that potential. The cyclic potential mode from -1000 mV to 1000 mV at scan rate 20mV/s was applied on the electrode surface of PANI and PANI/CNTs composite films (thickness about 204 nm).these films had been deposited on SUS304 stainless steel and dipped in to an aqueous of two types hydrochloric acid (HCl) and ammonia (NH_3). Figure (3.42) shows the applied potential as a function of time.

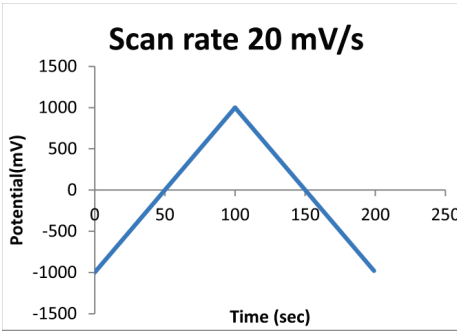

Fig(3.42)Scan rate of the applied cyclic potential

3.7.1 Sensors in aqueous solution of HCl

The surface electrode of PANI and PANI/(0.25, 0.5, and 1)wt %CNTs composite electrochemically deposited on SUS 304 stainless steel in aqueous solution of (1000, 2000, 3000, and 4000)ppm concentrations of HCl acid .

Figure (3.43) demonstrates a typical PANI sensor in aqueous of (1000, 2000, 3000, and 4000) ppm concentration of HCl. A high response is observed for 3000 and 4000 ppm and lower response at 1000 ppm and 2000 ppm can also be noticed. The maximum values of current density recorded at 3000 ppm and 4000 ppm were 25.9 mA/cm^2 and 38.1 mA/cm^2 respectively .No considerable variation in current density at 1000 ppm and 2000 ppm HCl is featurized.

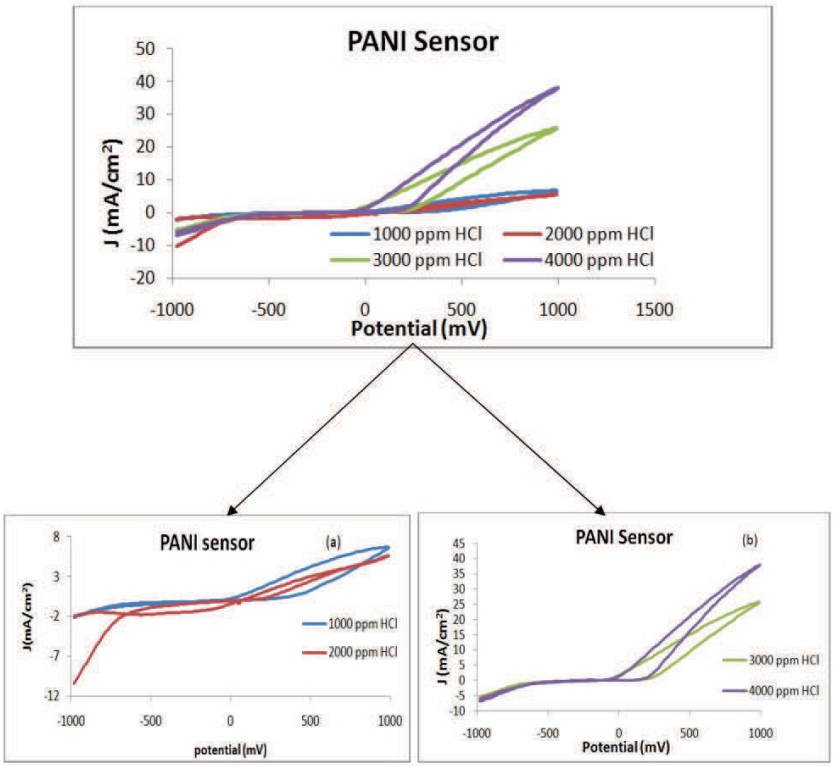

Fig(3.43)Cycle Voltammetry of PANI sensor in aqueous a)(1000 and 2000)ppm b)(3000 and 4000)ppm concentrations of HCl at scan rate 20mV/s at room temperature

Figure (3.44) shows a PANI/0.25 wt %CNTs sensor in aqueous of (1000, 2000, 3000, and 4000) ppm concentration of HCl. In comparison with figure (3.43), undetectable changes in current density were observed.

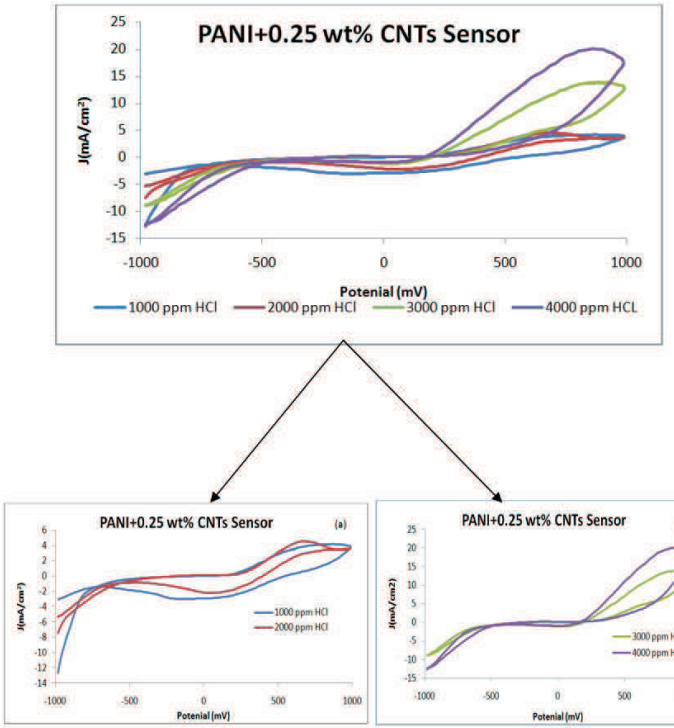

Fig(3.44)Cycle Voltammetry of PANI/0.25 wt% CNTs sensor in aqueous a)(1000 and 2000)ppm b)(3000 and 4000)ppm concentrations of HCl at scan rate 20mV/s at room temperature

Figure (3.45) shows the PANI/0.5 wt% CNTs sensor in aqueous of (1000, 2000, 3000, and 4000) ppm concentration of HCl. When compared to the PANI sensor of figure 3.43, an increase in the current density was recorded specially with concentrations (3000 and 4000) ppm. The range of maximum values of current density are about 5 mA/cm^2 and 66 mA/cm^2 for (3000 and 4000) ppm HCl concentrations respectively. Similarly no substantial alteration in (J) at 1000 ppm and 2000 ppm HCl conc. was noticeable.

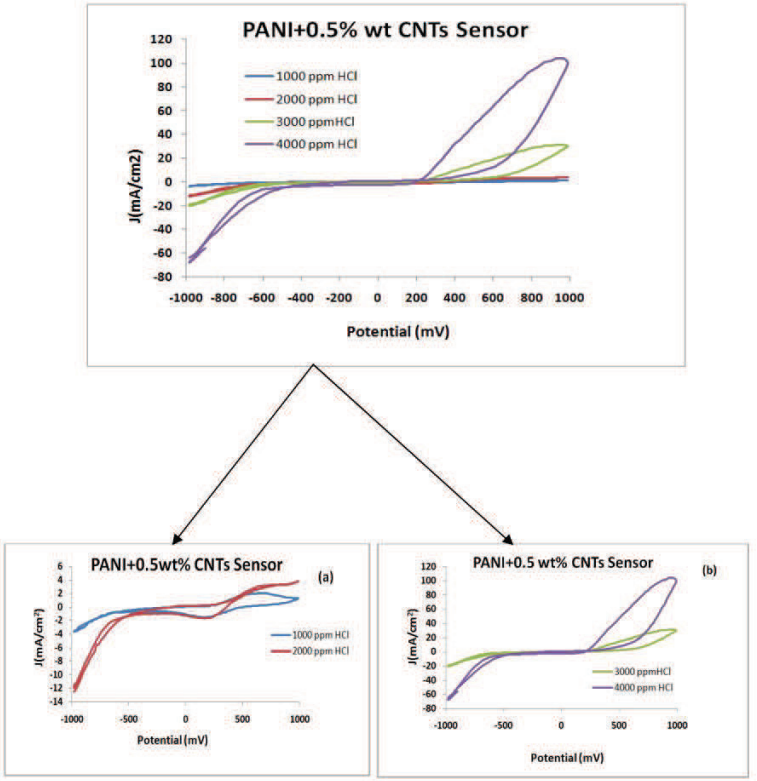

Fig(3.45)Cycle Voltammetry of PANI/0.5wt % CNTs sensor in aqueous a)(1000 and 2000)ppm b)(3000 and 4000)ppm concentrations of HCl at scan rate 20mV/s at room temperature

Figure (3.46) shows PANI/1wt% CNTs sensor in aqueous of (1000, 2000, 3000, and 4000) ppm concentration of HCl. It can be seen that a highest increase in the current density is recorded when compared with all other conditions discuss above. Table (3.8) lists all different values of maximum current densities for the all fabricated sensors.

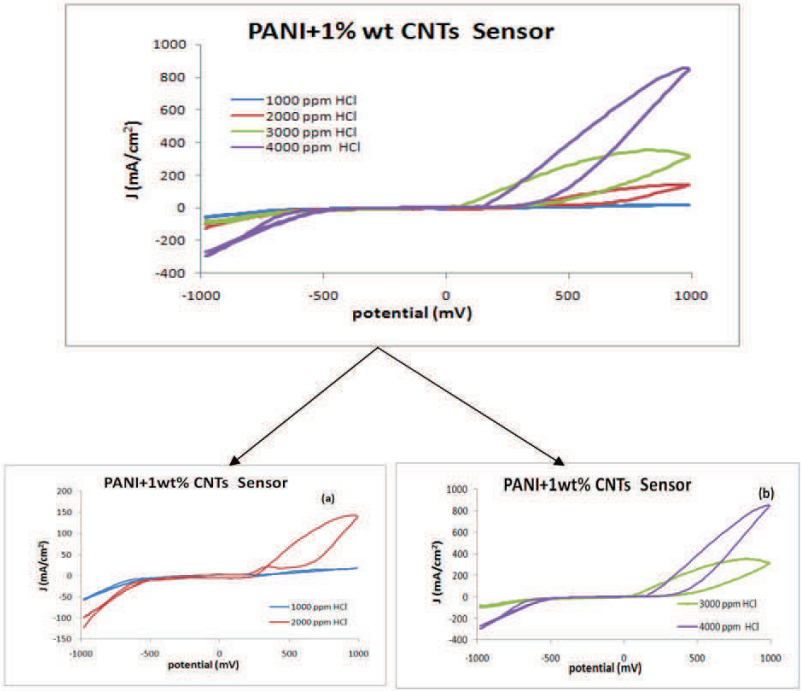

Fig(3.46)Cycle Voltammetry of PANI/1 wt% CNTs sensor in aqueous a)(1000 and 2000)ppm b)(3000 and 4000)ppm concentrations of HCl at scan rate 20mV/s at room temperature

Table (3.8)Maximum current density of the sensors obtained at the varying HCl concentrations

Sensor	**J_1**	J_2	**J_3**	**J_4**
PANI	6.67	5.65	25.9	38.1
PANI/0.25wt% CNTs	4.18	4.54	13.95	20
PANI/0.5 wt% CNTs	2.04	3.83	31.22	104
PANI/1 wt% CNTs	18.5	142.6	353.8	855

J_1:Max. Current Density J (mA/cm^2) 1000 ppm HCl conc. J_2:Max. Current Density J (mA/cm^2) 2000 ppm HCl conc. J_3:Max. Current Density J (mA/cm^2) 3000 ppm HCl conc. J_4:Max. Current Density J (mA/cm^2) 4000 ppm HCl conc.

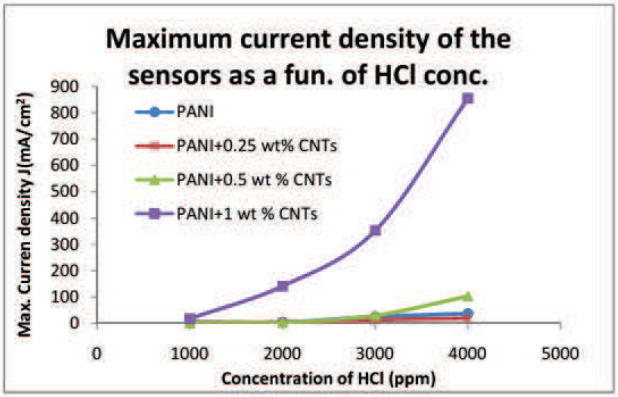

Fig. (3.47)Maximum current density of the sensors obtained at the varying HCl concentrations

Often, the desired redox reaction at the bare electrode involves slow electron transfer kinetics and therefore occurs at an appreciable rate only at potentials substantially higher than thermodynamic redox potential. such reaction can be catalyzed by attaching to the surface a suitable electron transfer mediator [222].Since this does not respond to the required reaction , a modifying material was added to the bare electrode (mediator) .the function of the mediator(PANI and PANI/CNTs composite) is to facilitate charge transfer between analyte (HCl) and electrode. In most cases the mediated reaction sequence (e.g., for an oxidation process) is described in equations (3.1) and (3.2) [223].

$$M_{red} \rightarrow M_{ox} + ne \ldots\ldots\ldots\ldots\ldots\ldots\ldots\ldots\ldots\ldots (3.1)$$
$$M_{ox} + A_{red} \rightarrow M_{red} + A_{ox} \ldots\ldots\ldots\ldots\ldots\ldots\ldots\ldots (3.2)$$

Where M represents the mediator (or modifier) on the electrode surface and A is analyte[223].Hence, the electron transfer takes place between the electrode and mediator and not directly between the electrode and analyte .the active process produced by a catalyst is being electrochemically regenerated .The net results of the electron shutting are a lowering of the overvoltage of analyte oxidation to be the formal of the mediator and increase in current density see figure (3.47) . The PANI/1 wt %CNTs have a high electron transfer rate constant because this modifier in the absence of HCl analyte exhibit a well-behaved redox reaction in cyclic voltammetry technique. But in the presence of analyte the anodic peak

current in cyclic voltammogram increased drastically and cathodic peak eliminated at suitable potential scan rate[222].

The attainable I-V characteristic curves supported the interpretation of the sensors behavior in acid concentrations. The less resistance was achieved for the PANI/1 wt% CNTs and hence the sensor may be consider as the most efficient one. As a common feature, it was found that the resistance of the sensor is degraded with increasing acid concentration. Particularly with that of PANI/1 wt% CNTS. As a medication, any increase in (J) implies a reduction in the resistance which may be arisen from electron transfer between modifying material and analyte.

3.7.2 Sensors in aqueous solution of NH_3

Ammonia is a toxic in liquid as a gas that is naturally present in the atmosphere in sub part per million (ppm) levels. However, much large concentrations can be detect near farms with domestic animals. A large amount of ammonia is produced by the chemical industry for production of fertilizers or for used in refrigeration system .Increase of amount of ammonia contained in exhaled air can be connected with certain disease, including kidney disorders [224].

In order to detecting ammonia ,the surface electrode of PANI and PANI/(0.25, 0.5, and 1)wt %CNTs composite films(sensors) deposition electrochemically on SUS 304 stainless steel in aqueous of (1000, 2000, 3000, and 4000)ppm concentration of ammonia (NH_3) .

Figure 3.48 shows the PANI sensor in aqueous solution s of (1000, 2000, 3000, and 4000) ppm concentration of NH_3, an increase of the current density results from a reduction in NH_3 concentrations.

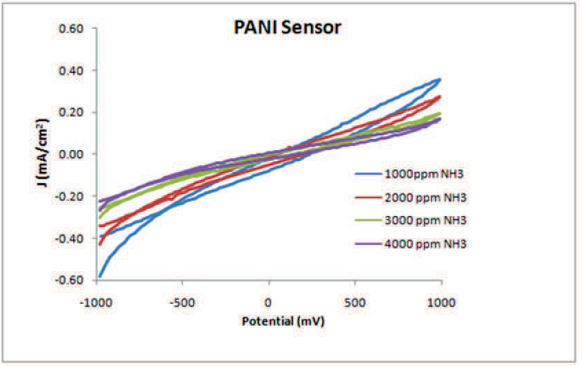

Fig(3.48)Cycle Voltammetry of PANI sensor in aqueous (1000, 2000, 3000 and 4000)ppm concentrations of NH_3 at scan rate 20mV/s at room temperature

Figure (3.49) shows the PANI/0.25 wt %CNTs sensor in aqueous solutions of (1000, 2000, 3000, and 4000) ppm concentration of NH_3. An almost unchanged (J) was attained except for that 1000ppm NH_3 .Although such increase is noticeable but it is still considerably low.

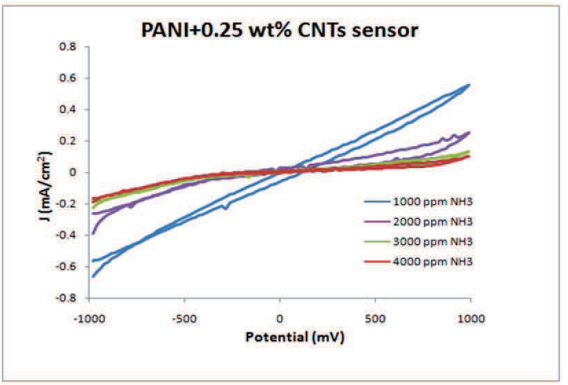

Fig(3.49)Cycle Voltammetry of PANI/0.25 wt %CNTs sensor in aqueous (1000 , 2000, 3000 and 4000)ppm concentrations of NH_3 at scan rate 20mV/s at room temperature

Figure (3.50) shows the PANI/0.5 wt %CNTs sensor in aqueous solutions of (1000, 2000, 3000, and 4000) ppm concentration of NH_3. Results demonstrated a pronounced increase of (J) with the use of two concentrations; 1000 and 2000 ppm only when PANI/0,5wt % CNTSs sensor was tested. Meanwhile, slight changes in J were recorded with other concentrations.

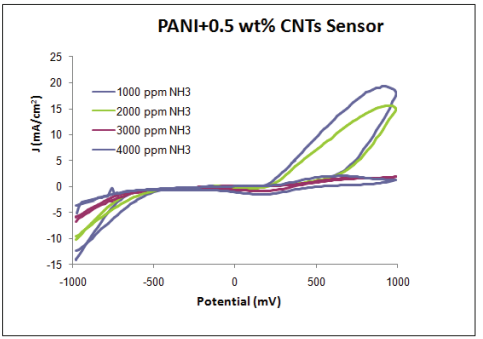

Fig(3.50)Cycle Voltammetry of PANI/0.5 wt %CNTs sensor in aqueous (1000 , 2000, 3000 and 4000)ppm concentrations of NH_3 at scan rate 20mV/s at room temperature

Figure (3.51) shows the PANI/1 wt %CNTs sensor in aqueous solutions of (1000, 2000, 3000, and 4000) ppm concentration of NH_3. From this figure, one can recognize substantial increase in the values of J corresponding to the concentrations of 1000,2000,3000 and 4000 ppm . In comparison with other sensors the increase in J is apparently higher with two concentrations of 1000 ppm and 2000ppm figure (3.52).

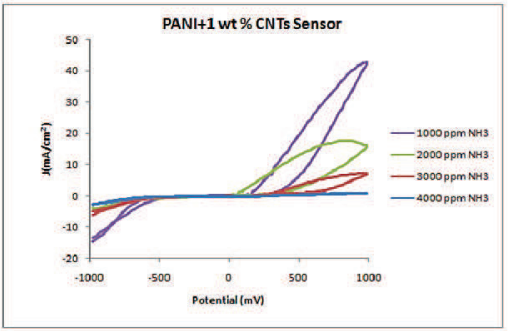

Fig(3.51)Cycle Voltammetry of PANI/1 wt %CNTs sensor in aqueous (1000 , 2000, 3000 and 4000)ppm concentrations of NH_3 at scan rate 20mV/s at room temperature

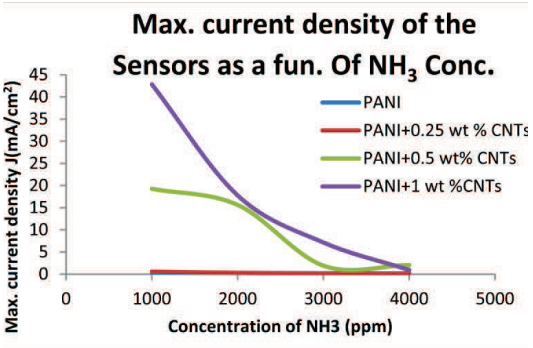

Fig. (3.52)Maximum current density of the sensors obtained at the varying NH_3 concentrations

Table (3.9)gives the maximum current density values at varying NH_3 concentration for sensors.In general, its concluded that when the concentrations of NH_3 is made less there is a corresponding reduction in the resistance of the sensors.

Table (3.9)Maximum current density of the sensor obtained at the varying NH_3 concentrations

Sensor	J_a	J_b	J_c	J_d
PANI	0.357	0.275	0.195	0.168
PANI/0.25wt% CNTs	0.555	0.257	0.132	0.1006
PANI/0.5 wt% CNTs	19.26	15.61	1.9	2.04
PANI/1 wt% CNTs	42.8	17.74	7.13	0.927

J_a: Max. Current Density J (mA/cm^2) 1000 ppm NH_3 conc. J_b: Max. Current Density J (mA/cm^2) 2000 ppm NH_3 conc. J_c: Max. Current Density J (mA/cm^2) 3000 ppm NH_3 conc. J_d: Max. Current Density J (mA/cm^2) 4000 ppm NH_3 conc.

In general, its concluded that as the concentrations of NH_3 is reduced there is a corresponding reduction in the resistance of the sensors. When exposed in ammonia, PANI undergo dedoping by deprotonation [225] figure (3.53) .

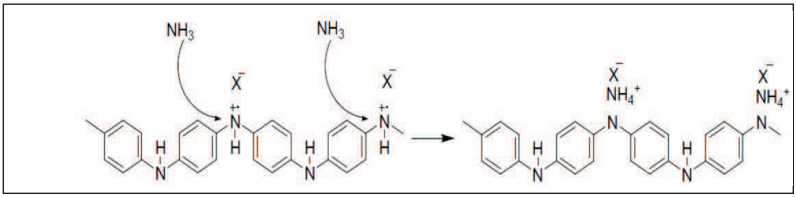

Fig(3.53) shown the protons on –NH- groups transferred to NH_3 molecules to form ammonium ions[226]

The protons on –NH– groups were transferred to NH_3 molecules to form ammonium ions while PANI itself turned into its base form. This process is reversible, and in fact, when ammonia atmosphere is removed, the ammonium ion can be decomposed to ammonia gas and proton[226].

The existence of CNTs contributes to the enhancement of electrons transfer .this may justify the reduction of the resistance at a concentration of 1000 ppm with increasing proportions of carbon nano tubes . Addition of CNTs in the process provides a subsequent explanation for the reasons behind the improvement of the response of PANI sensors. All above characteristic behavior of the sensors are provided by the nature of the I-V characteristics which are experienced by the operational sensor .

3.8 Hydrogen Gas sensing measurements

The primary physical hazards associated with hydrogen gas are its flammability and potential for explosions. This is because hydrogen forms flammable mixtures in air over a wide range of concentrations (4-75%) and very low energy is needed to ignite hydrogen-air mixtures. Hence sensors are required to detect hydrogen leaks to warn of explosion hazards[227].

The gas sensing characteristics of the PANI and PANI/CNTs composite films (deposited by spin coating method on IDE (Au) electrode) are carried out for H_2 gas: air at different mixing ratios and different operating temperature. As it's known that an amount of target gas is introduced after the Ohmic resistance of the sensor material gets stabilized. The recovery characteristics (when the target gas is withdrawn)are also monitored as a function of time. The temperatures

at which the test is carried out were 298K (room temperature) and 333 K.These selection of these two temperature values was arisen due to the nature of the Iraqi climate condition under which these sensor are operated.

3.8.1 Sensing Characteristics at Room Temperature

The response ($S=R_{air}/R_g$) of the sensors toward hydrogen gas of different mixing ratios has been explored. The successive tests were performed at a bias voltage of 5V with a room temperature (298 K).

3.8.1.1 Sensing characteristics of pure PANI toward Hydrogen gas

Figure (3.54) shows the switching behavior of the PANI gas sensor followed by a film surface with a baseline resistance of R_{air} =1.05 M Ω in atmospheric air (before gas exposure). Both response time (time interval over which resistance attains fixed percentage(usually 90%)of final value when the sensor is exposed to full-scale concentration of the gas) and recovery time(time interval , over sensor resistance reduces to 10 % of the saturation value when the sensor is exposed to full-scale concentration of gas) are experienced .

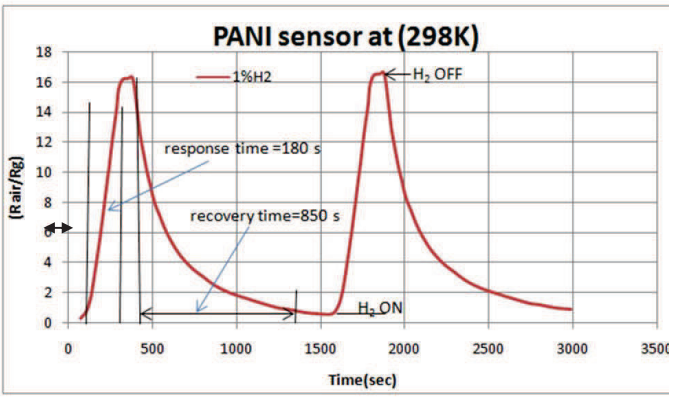

Fig(3.54)Switch behavior of PANI sensor sensitized to 1% hydrogen gas: air mixing ratio at 298K

Figure (3.55) demonstrates the response of pure PANI toward hydrogen gas of different mixing ratios .As it is apparent, the sensor sensitivity to hydrogen gas

increases linearly with H_2 test gas mixing ratio. A maximum sensitivity value of (S=29) has been registered when the sensor is exposed to 4% H_2 gas in air.

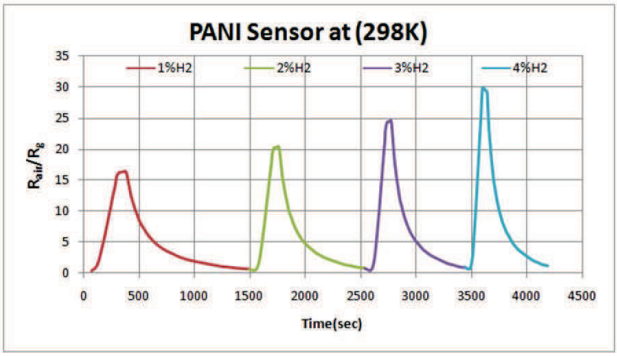

Fig(3.55)Sensitivity behavior of PANI sensor to different hydrogen gas: air mixing ratio at 298K

Figure (3.56) exhibits both response and recovery times. The shortest response and recovery times were about 85 s and 290 s respectively at 4%H_2: air gas mixing.

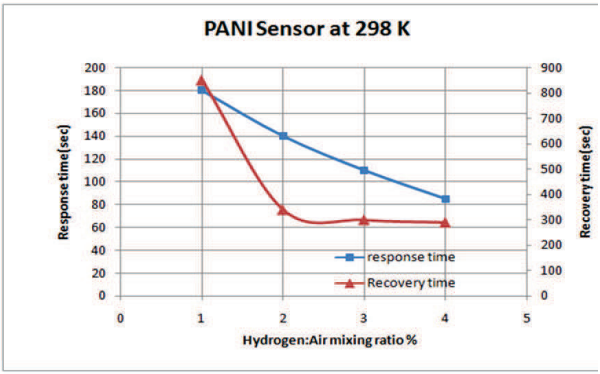

Fig(3.56)Response and Recovery times of PANI sensor As a function of testing gas mixing ratio at 298K

3.8.1.2 Sensing characteristics of PANI/0.25 wt% CNTs composite toward Hydrogen Gas

In order to enhance the sensing characteristics for improving PANI sensor, the MWNTs was doped into pure PANI .The PANI/0.25 wt %CNTs film gas sensing element (baseline resistance in atmospheric air was R_{air}=1.2 M Ω).

Figure (3.57) illustrates the response of PANI/0.25 wt %CNTs film sensor sensitivity to hydrogen gas of different mixing ratio. The minimum value of sensitivity was 17 at 1%H_2: air ratio and maximum value of sensitivity was 28 at 4%H_2. In spite of the change in S of PANI/0.25wt % CNTs when compare to that for pure PANI is slight, but it can be looked upon considerable ,it is possible to say that considerable because of the degradation of response and recovery times specially at 2%, 3% and 4% H_2 :air mixing ratio figure (3.58).

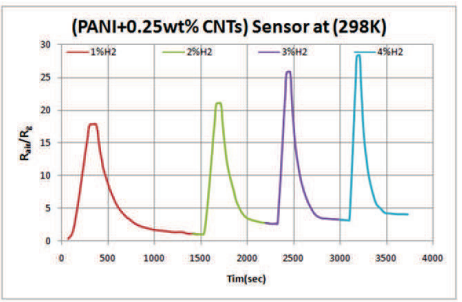

Fig(3.57)Sensitivity behavior of PANI/0.25 wt % CNTs sensor to different hydrogen gas: air mixing ratio at 298 K

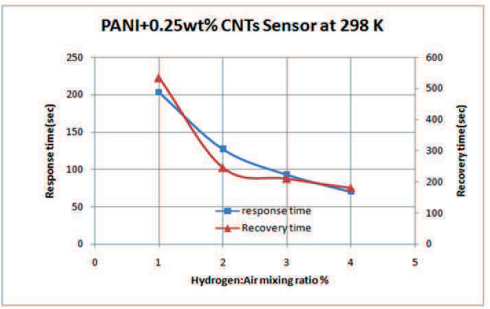

Fig(3.58)Response and Recovery times of PANI/0.25wt% CNTs sensor As a function of testing gas mixing ratio at room temperature

3.8.1.3 Sensing characteristics of PANI/0.5wt%CNTs Composite toward Hydrogen Gas

Figure (3.59) depicts the response of PANI/0.5 wt %CNTs film sensor sensitivity(baseline resistance was R_{air}=1.05 M Ω) to hydrogen gas of different mixing ratio. From this figure, one can recognize substantial increase in the values of S with increasing H2: air mixing ratio.

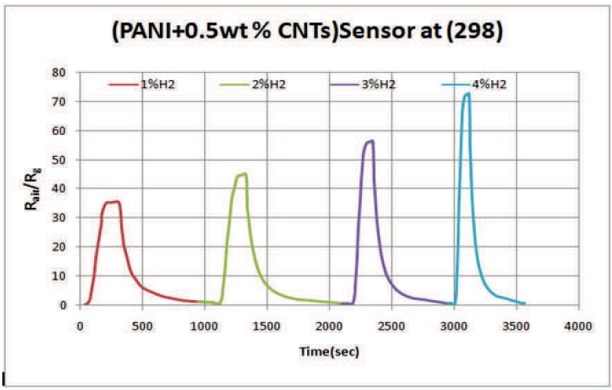

Fig(3.59)Sensitivity behavior of PANI/0.5wt % CNTs sensor to different hydrogen gas: air mixing ratio at room temperature

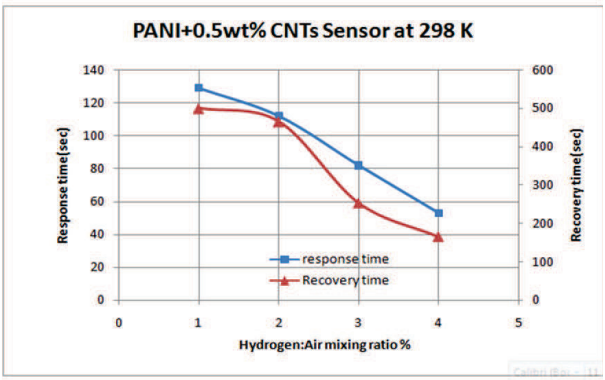

Fig(3.60)Response and Recovery times of PANI/0.5wt%CNTs sensor As a function of testing gas mixing ratio at room temperature

A maximum sensitivity of about 72 at 4% H_2: air mixing ratio and minimum sensitivity of 35 at 1% H_2: air mixing ratio are recorded. Also, the shortest response and recovery times of about 53 s, and 165 s respectively is observed at 4% H_2 figure (3.60).

3.8.1.4 Sensing Characteristics of PANI/1wt% CNTs composite toward Hydrogen Gas

As it's apparent from figure (3.61), the response of PANI/1 wt %CNTs film sensor sensitivity (baseline resistance was R_{air}= 1.3 M Ω) to hydrogen gas of different mixing ratio .It is obvious the sensor sensitivity to hydrogen gas increases gradually with raising of H_2: air mixing ratio.

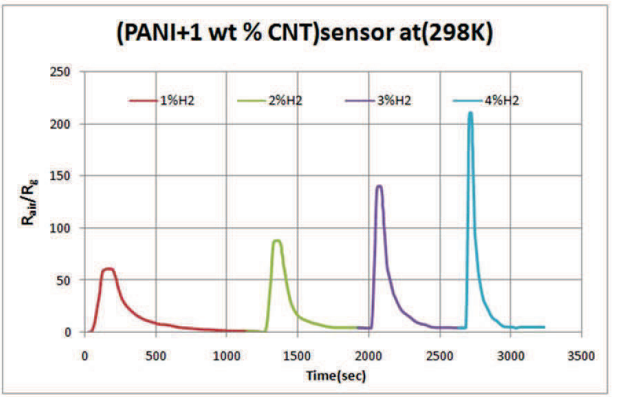

Fig(3.61)Sensitivity behavior of PANI/1wt% CNTs sensor to different hydrogen gas: air mixing ratio at room temperature

The highest response was about 209 at 4% H_2: air mixing ratio and the shortest response and recovery times are about 22 s and 137s respectively at the same above H_2 concentration figure (3.62).

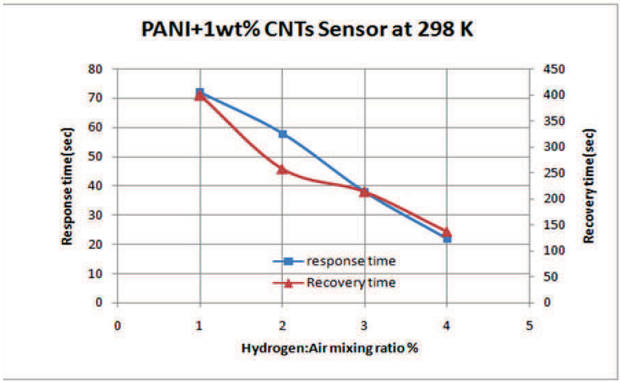

Fig(3.62)Response and Recovery time of PANI/1wt% CNTs sensor As a function of testing gas mixing ratio at room temperature

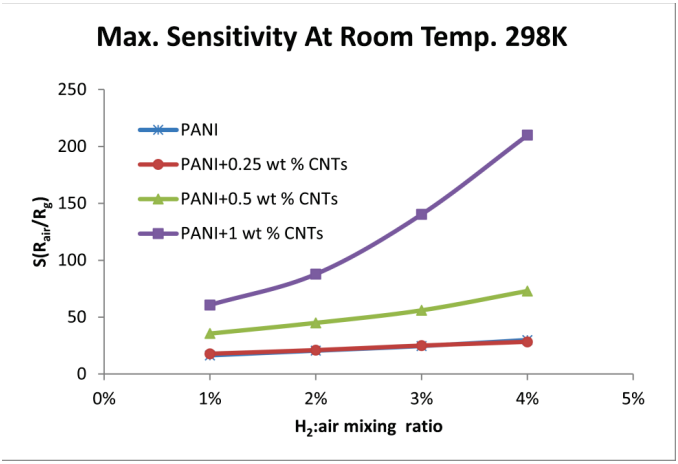

Fig(3.63)Maximum Sensitivity of the sensors to different hydrogen gas: air mixing ratio at 298K

Table (3.10) Response and Recovery time of the H_2 sensors at 298K

	Response time (sec)				Recovery time(sec)			
H_2Conc.	PANI	PANI+0.25 wt%CNTs	PANI+0.5 wt%CNTs	PANI+1 wt %CNTs	PANI	PANI+0.25 wt%CNTs	PANI+0.5 wt%CNTs	PANI+1 wt %CNTs
1%	180	203	129	72	850	534	500	400
2%	140	127	112	58	340	245	465	258
3%	110	93	82	38	300	210	253	214
4%	85	70	53	22	290	180	165	137

3.8.2 Sensing characteristics at 333K

The response, ($S=R_{air}/R_g$) of the sensors toward hydrogen gas of different mixing ratios has been explored. The successive tests were performed at a bias voltage of 5V with a 333K.

3.8.2.1 Sensing characteristics of Pure PANI toward Hydrogen gas

Figure (3.64) depicts the response of PANI film sensor sensitivity (baseline resistance was R_{air}= 1.6 M Ω) to hydrogen gas of different mixing ratio at 333K. One can recognize substantial increase in the values of S with increasing H_2 :air mixing ratio. Upon exposure to 1% mixture of hydrogen in air, polyaniline film shows a 1.25 times increase in sensitivity at 333k in comparison with the same sensor at room temperature[figure (3.53)].

A maximum sensitivity of 37 was recorded by the PANI sensor at 4% H_2. Figure (3.64) exhibits an increase in the response and recovery times in comparison with PANI Sensor at room temperature.

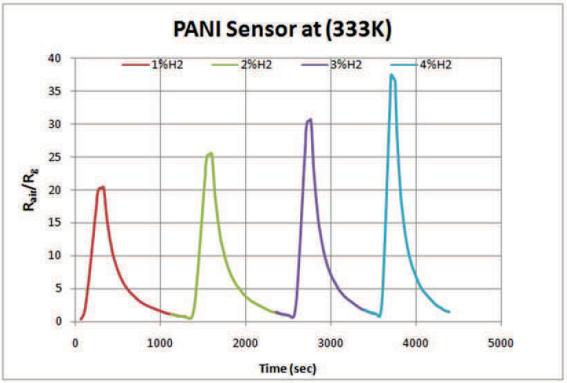

Fig(3.64)Sensitivity behavior of PANI sensor to different hydrogen gas: air mixing ratio at 333K

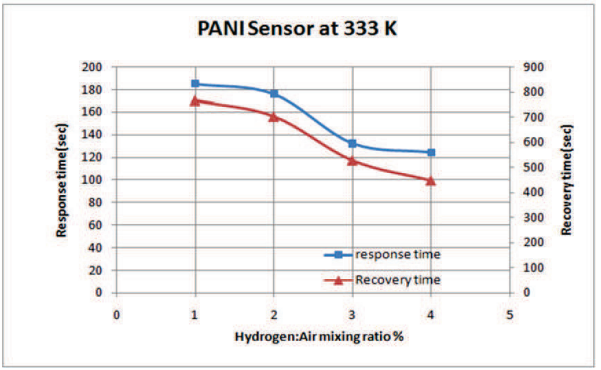

Fig(3.65)Response and Recovery times of PANI/1wt% CNTs sensor As a function of testing gas mixing ratio at 333K

3.8.2.2 Sensing characteristics of PANI/0.25wt%CNTs composite toward Hydrogen gas

Figure (3.66) demonstrates the response of PANI/0.25 wt %CNTs (baseline resistance was R_{air}=1.7 M Ω) toward hydrogen gas of different mixing ratios. No alteration of sensors sensitivity was observed at both room temperature and at 333K. This proportion did not result any improvement in the response of the same sensor at room temperature

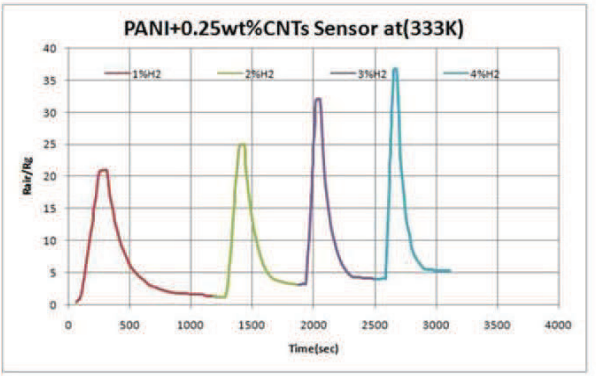

Fig(3.66)Sensitivity behavior of PANI/0.25wt% CNTs sensor to different hydrogen gas: air mixing ratio at 333K

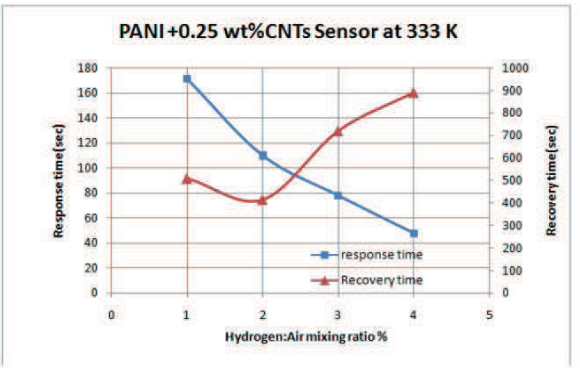

Fig(3.67)Response and Recovery time of PANI/0.25wt% CNTs sensor As a function of testing gas mixing ratio a at 333K

The recovery time experienced a different behavior by decreasing first at 2% H_2 followed by an increase beyond this concentration figure (3.65). The reason behind the variation of recovery time may be due to the change in relative humidity under which these experiments were accomplished.

3.8.2.3 Sensing characteristics of PANI/0.5wt%CNTs composite toward Hydrogen gas

The response of PANI/0.5 wt %CNTs (baseline resistance was R_{air}= 1.7 M Ω) toward hydrogen gas of different mixing ratios at temperature 333K illustrated in figure(3.68).In this figure, a large increase in sensitivity was recorded for all concentrations when compared to that at room temperature.

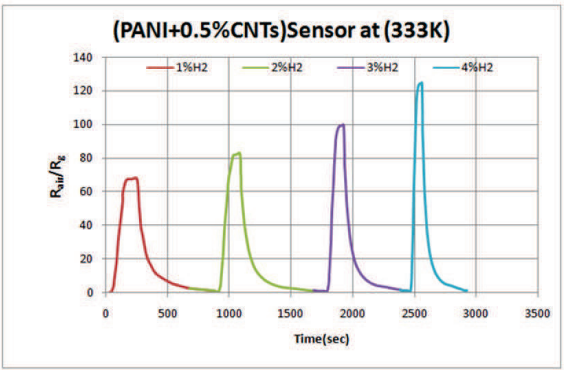

Fig(3.68)Sensitivity behavior of PANI/0.5wt% CNTs sensor to different hydrogen gas: air mixing ratio at 333K

The response and recovery times are versus H_2 concentrations at 333K figure (3.69).both response and recovery times at all same H_2 concentrations are shorter than those sensor at room temperature [figure (3.60)].

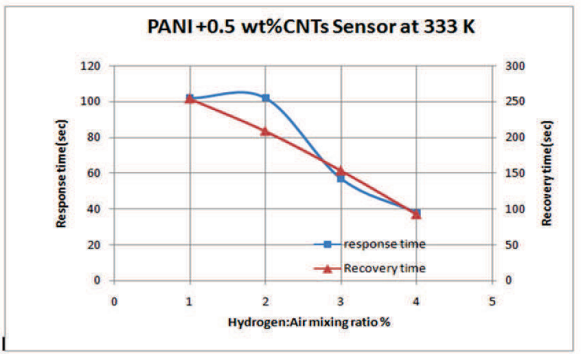

Fig(3.69)Response and Recovery time of PANI/0.5wt% CNTs sensor As a function of testing gas mixing ratio at 333K

3.8.2.4 Sensing Characteristics of PANI/1wt%CNTs composite toward Hydrogen gas

As its apparent from figure (3.70), the response of PANI/1 wt %CNTs film sensor sensitivity (baseline resistance was R_{air}= 1.9M Ω) to hydrogen gas of different mixing ratio.

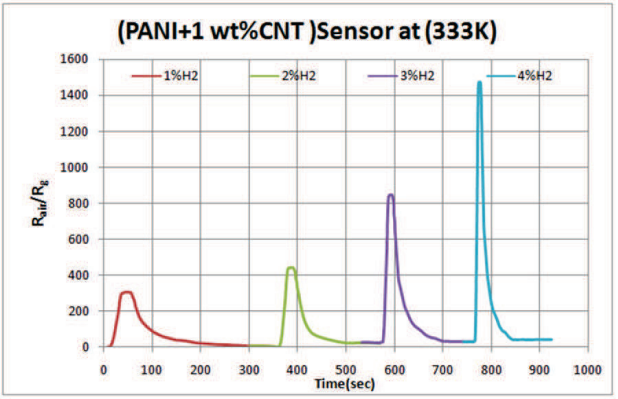

Fig(3.70)Sensitivity behavior of PANI/1wt% CNTs sensor to different hydrogen gas: air mixing ratio at 333K

Figure (3.71) exhibits both response and recovery times toward the H_2 concentrations at 333K. Results show that the response and recovery times were the shortest (4 s and 45s at 4%H_2 conc.) for all sensors under two operating temperatures (298K and 333K) tables (3.10) and (3.11).

A maximum sensitivity of 1463 is recorded at 4%H_2 mixing ratio(figure(3.72) and its alteration is about 7 times of that concentration at room temperature .Other alterations of sensitivity are 4.8 times, 4.9 times, and 6 times at 1% H_2, 2% H_2 , and 3% H_2 concentrations of these concentrations at room temperature respectively [figure(3.63)].

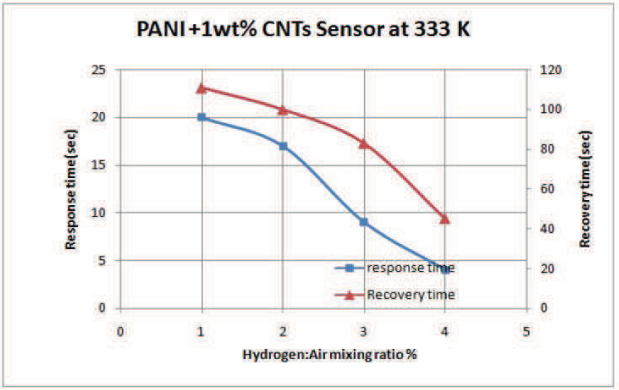

Fig(3.71)Response and Recovery time of PANI/1wt% CNTs sensor As a function of testing gas mixing ratio at 333K

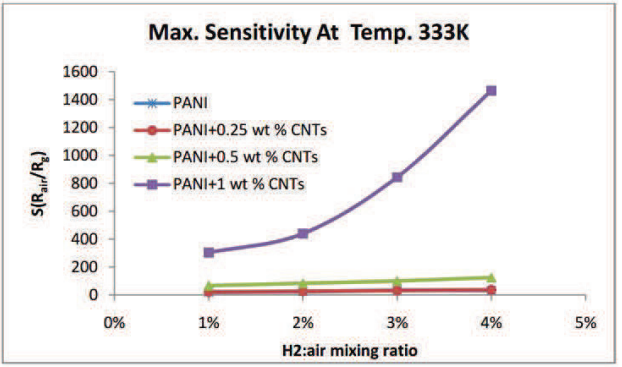

Fig(3.72)Maximum Sensitivity of the sensors to different hydrogen gas: air mixing ratio at 333K

Table (3.11)Response and Recovery time of the H_2 sensors at 333K

	Response time (sec)				Recovery time(sec)			
H_2Conc.	PANI	PANI+0.25 wt%CNTs	PANI+0.5 wt%CNTs	PANI+1 wt %CNTs	PANI	PANI+0.25 wt%CNTs	PANI+0.5 wt%CNTs	PANI+1 wt %CNTs
1%	160	217	98	20	550	502	305	111
2%	125	147	87	17	310	260	239	100
3%	100	87	55	9	270	242	174	83
4%	60	78	32	4	110	234	104	45

Under all circumstances, the hydrogen response from conventional polyaniline is much smaller than that for the nanofibers. Hydrogen causes a reversible decrease in the resistance of film sensors (PANI nanofibers and PANI/CNTs composite).The core issue of whole results is polyaniline and the additive CNTs is the reason of increasing of charge transfer. Moreover, the I-V characteristics may be consider as another evidence for increasing charge transfer.

A possible mechanism for interaction of hydrogen with PANI was presented by MacDiarmid [227], and is reproduced in figure (3.73). In this figure A^- denotes any dopant anion. Hydrogen interacts with doped polyaniline at charged amine nitrogen sites. H_2 bond dissociation follows with formation of new N-H bonds to the amine nitrogen of the polyaniline chain[208]. Subsequent charge transfer between adjacent amine nitrogens returns the polyaniline back to its polaronic, doped, emeraldine salt state with a release of hydrogen, making this reaction fully reversible[208].

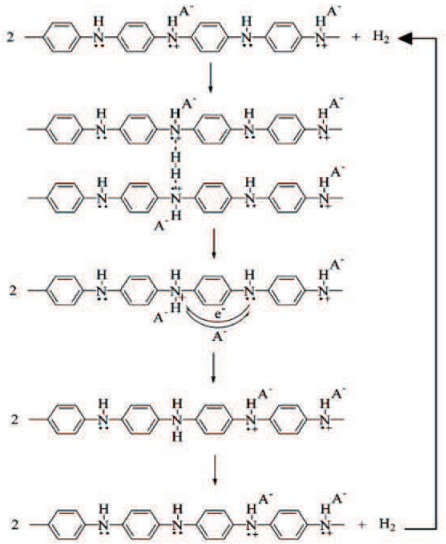

Fig(3.73) A Mechanism of H_2 Adsorption/Desorption via interaction with free-spins on adjacent polyaniline chains to form N-H bonds in metastable species[227]

As seen from the proposed mechanism in figure (3.73), the first step is hydrogen bonding with polyaniline at the nitrogen atoms of the polyaniline chain. Our observation of complete suppression of the hydrogen response in a humid atmosphere is consistent with this mechanism. The sensitivity raises to a higher value with heat accumulation up to a certain level where it goes down afterward .the increase in temperature allows an addition energy which contributes in increasing charge transfer. The hydrogen response is completely suppressed in the presence of humidity[208]. This may justify the increase of recovery time which leads to an irreversible process.

Chapter Four

The Inference and Final Outcome

4.1 The inference and final outcome

To carry out both liquid and gas sensing nanomaterials have been fabricated via a specially –proposed procedure. With starting materials of various concentrations, nanostructures were prepared and characterized to meet the testing requirements. The procedure involved the preparation of PANI by an electrochemical method using 0.1 M aniline with HCl(0.1M, 0.2 M and 0.3 M) and H2SO4 (0.1 M, 0.2 M, and 0.3 M) separately. Arc discharge technique was used for the fabrication of carbon nanopowder and then PANI CNpowder composite using electrochemical method.. Experiments also necessitated the use of a ready- made CNTs for fabricating more PANI/CNTs composite. By doing so, one can conclude the following:

1. more homogeneous PANI nanofibers with optimum deposition current density of 121.6 mA/cm2 were prepared by 0.1 M aniline and 0.3 M H2SO4 under six repetition of cyclic potential from -100 mV to 1500 mV and scan rate of 30 mV/s.
2. Increase of CNpowder proportion to PANI provides lower electrical conductivity than pure PANI due to the existence of CNpowder at certain intersection points. The tangible evidence for such behavior is the reduction of current density (J) values due to bad contacts at these intersection points.
3. Addition of CNTs to PANI for the formation of PANI/CNTs composite resulted in an upgrade in the electrical conductivity indicated by an increase in J. This reveals a well formed CNTs network inside PANI.
4. In the liquid type sensing, it was found that with the increase of HCl concentrations, the value of J could be raised and found pronounced at 3000 ppm and 4000ppm concentration along with PANI/0.5 wt %CNTs and PANI/1 wt% CNTs sensors. The reason behind that may be the enhancement of more efficient transfer of charges.
5. **5.** Upon using different concentrations of NH3, results showed a reduction in J with increasing concentration and found apparent with 1000 ppm and 2000 ppm concentrations along with PANI/0.5wt % CNTs and PANI/1wt % CNTs sensors. The enhancement of the deprotonation process could have been the governing factor in this process.
6. In H2 -gas sensing tests , the present result showed that the PANI/1 wt% CNTs sensor was the best among all other sensors at a temperature 333K with all concentrations. The characteristic features of this sensor were better sensitivity and shorter both response and recovery times. Such sensor characteristics are justified by the interaction of H2 with PANI/1 wt % CNTs sensor at charged amine

nitrogen sites. Hydrogen bonds dissociation follows a formation of new N-H bonds to the amine nitrogen of the polyaniline chain. This process could lead to an adsorption when interaction of H2 with the sensor took place and desorption after the gas had left the sensor.

4.2 Advanced future projects

1. The fabricated sensor may be capable for sensing a number of gases such as H2S, CO, and NH3.
2. Different dimensions of IDE can be used with the same fabricated materials discuses above.
3. Other concentrations of aniline may be significant for nanofiber synthesis to perform similar procedures.
4. Fabrication of wavelength sensor from the PANI-CNTs nanofiber.

References

References

[1] K. Hirao, "*Nanotechnology and Materials Technology Development Department*", National Institute of Advanced Industrial Science and Technology, Kyoto University, (2005).

[2] B. Bhushan, "*Hand Book of Nanotechnology*", Springer, (2007).

[3] R. P. Feynman, "*There is Plenty of Room at the Bottom*", Engineering and Science 36, 23 (1960).

[4] D. Minoli, "*Nanotechnology Application to Telecommunications and Networking*", John Wiley and Sons, Inc., Hoboken, New Jersey, (2006).

[5] M. Di Ventra, S. Evoy, James R. and J. Heflin, "*Introduction to Nanoscale Science and Technology*", Springer Science and Business Media, Inc, (2004).

[6] J. M. Martínez-Duart, R. J. Martín-Palma and F. Agulló-Rueda, "*Nanotechnology for Microelectronics and Optoelectronic*", Elsevier USA, Oxford and London, (2006).

[7] J. H. Davies "*The Physics of Low-Dimensional Semiconductors*" (University Press, Cambridge). (1998).

[8] T. Pradeep, " *Nano*", Tata McGraw-Hill NEW DELHI, (2007).

[9] M. S. Ahmad, Y. Ramadin, S. A. Jawad and A. M. Zihlif. ,"*Analysis of The ac Current Properties of PANI- Based Carbon-Fiber Polycarbonate Composite*", Journal of Thermoplastic Composite Materials, 6,pp. 108-118, (1993).

[10] L. Ding, J. Sw, C. Yang and S. Dong, "*Ionic Conductivity of Solid Polymer Electrolytes*", Polymer Journal, 29 (5), pp.410-416, (1997).

[11] O. Bohnke, G. Frand, M. Rrzrazi, C. Rousselot and C. Truche, "*Fast Ion Transport in New Lithium Electrolytes Gelled with PMMA Influence of Lithium Salt Concentration*" Solid State Ionic, 66, pp.105-112, (1993).

[12] L. dai., "*Intelligent Macromolecules of Smart Devices from Materials Synthesis to Device Application*", 291, (2004).

[13] A. J. Heeger, "*Noble Lecture: Semi Conducting and Metallic Polymer: the fourth Generation of Polymeric Materials*", Reviews of Modern physics, 73(3),pp. 681-699, (2001).

[14] I. Jacghelin , Kroschwitz, *"Electrical and Electronic Properties of Polymers"*, John Wiley and Sons, New York, (1988).

[15] L. Dai, B. Winkler, L. Dong, L. Tong and A. H. Mau, *"Conjugated Polymers for Light- Emitting Applications"*, Advanced Materials, 13, (12-13), pp. 915-925, (2001).

[16] J. R. Renolds, "*Conjugated Polymer for Organic Photovoltaic Device*" Department of Chemistry at the University of Florida, (2001).

[17] G. A. Rimbu, I. Stamatin, C. L. Jackson and K. Sott, "*The Morphology Control of Polyaniline as Conducting Polymer in Fuel Cell Technology*", Journal of Optoelectronics and Advanced Materials", 8, (2), pp. 670-674, (2006).

[18] M. F. Rubner, J. H. Cheung, "*Molecular self- Assembly of Electrically Conductive Polymers*", United states Patent, No.5, 518, 767, (1996).

[19] A. N. Samukhin, "*Metallic State of Conducting Polymers*", Physical Review Letters, 78, pp. 3915-3918, (1997).

[20] J. Kim, "*Assemblies of Conjugated Polymers Intermolecular and Intermolecular Effect on The Photo physical Properties of Conjugated Polymers"*, Pure Applied Chemistry,74, (11), pp. 2031-2044, (2002).

[21] A. J. Breeze, Z. Schlesinger, S. A. Carter and H. Tillmsnn, "*Improving Power Efficiencies in Polymer-Polymer Blend Photovoltaic*", Solar Energy Materials and Solar Cells, 83, pp. 263-271, (2004).

[22] S. A. Carter, M. Angelopoulos, S. Karg, P. J. Brock and J. C. scott ,"*Polymeric Anodes for Improved Polymer Light–Emitting Diode Performance*" Applied Physics Letter, 70(16), pp. 2067-2069, (1997).

[23] D. A. Fungaro, "*Sulfonated Polyaniline Coated Mercury Film Electrodes for Voltametric Analysis of Metals in Water*", Sensors, 1, pp. 206-214, (2001).

[24] V. Sholin, E. J. Lopez and S. A. Carter, "*Photoluminescence Enhancement in MEH-PPV Polymer Thin Films by Surfactant Addition*", Macromolecules, 39, pp. 5830-5835, (2006).

[25] M. S. Freund and B. A. Deore, "*Self-Doped Conducting Polymers*", John Wily and Sons, New York, (2007).

[26] B. R. Mattes, "*Synthesis of Polyaniline*", United States Patent Application Publication, N0 us. 2249803, (2007).

[27] S. Venora, S. Khasim, M. Anasiddappa, M. A. Prasad and Abkulkarni "*Synthesis Characterization and Low Frequency a.c Conduction of Polyaniline Fly ash Composite"*, Bull. Mater. Sci. 26 (7), pp. 733-739, (2003).

[28] Z. Opilski, T. Pustelny, E. Maclak, M. Bednorz, A. Stolarczyk and M. Jadamiec, "*Investigation of Optical Interferometric Structures Applied in Toxic Gas Sensors*", Bulletin of the Polish Academy of Sciences, 53(2), pp. 151-156, (2005).

[29] H. Vanhoang, "*Electrochemical Synthesis of Novl Polyaniline-Montmarillonite Nanocomposites and Corrosion Protection"*, M.Sc. Thesis, Vietnam, (2006).

[30] V. Mottaghtalab, "*Development and Characterization of polyanilin - Carboon Nanotube Conducting Composite Fiber*", Ph.D. Thesis, University of Wollongong, (2006).

[31] D. A. Savall, K. P. Knkakde and M. D. Shirssat, "*Potentiometric Study of Polyaniline Synthesize With Various Dopants and Composite–Dopant*" Bull. Mater. Sci., 29(4), (2006).

[32] D. H. Lee, H. J. Hwang, C. W. Lee and S. H. Lee, "*Synthesis and Properties of Photo Acid Generators from Conducting polyaniline*", Polymer Preprints, 45(1), 273, (2004).

[33] R. V. Gregory and R. J. Samules, "*Effect of Molecular Structure on the Mechanical Optical and Electrical Properties of High Technology Fibers*", National Textile Center Annual Report, (1996).

[34] J. Choi, M. Chipara, B. Xu, C. S. Yang, B. Doudiu and P. A. Dowben "*Comparison of π- Conjugated Ring Orientations in Polyaniline and Polypyrrol*", Chemical Physics Letter, 343, pp. 193-200, (2001).

[35] J. B. Veluru, K.K Saheesh, D.C Trivedi., "*Electrical Properties of Electrospun Fibers of PANI PMMA Composites*", Journal of Engineered Fibers and Fabrics, 2 Issue 2, (2007).

[36] A. Baba, R. C. Advincule and W. Knoll, "*Insitu Investigations on the Electrochemical Polymerization and Properties of Polyaniline Thin Films by Surface Plasmon Optical Tecniques*", Journal Physics Chemistry B, 106, 1581-1567, (2002).

[37] A. Bozkyrt, U. Akbulut and L. Toppare, "*Conducting Polymers Composites of Polypyrrole and Polyaniline*", Synthetic Metals, 82, pp. 41-46, (1996).

[38] W. K. Maser, A. M. Benito, M. A. Callejas and T. Seeger, "*Synthesis and Characterization of New Polyaniline/ Nanotube Composites*", Material Science and Engineering C, 33, 87, (2003).

[39] A. Macdiarmid, J. Chiang; A. Richter and A. Epstein, "*Polyaniline: a New Concept in Conducting Polymers*", Synthetic Metals, Vol. 18, N. 1-3, pp. 285-290, (1987).

[40] A. Pron and P. Rannou, "*Processible Conjugated Polymers: from Organic Semiconductors to Organic Metals and Superconductors*", Progress in Polymer Science, Vol. 27, No. 1, pp. 135-190, February (2002).

[41] P. Fedorko; M. Trznadel; A. Pron; D. Djurado; J. Planès and J.Travers, "*New Analytical Approach to the Insulator–Metal Transition in Conductive Polyaniline*", Synthetic Metals, Vol. 160, No. 15-16, pp. 1668-1671, August (2010).

[42] N. Gospodinova and L. Terlemezyan "*Conducting Polymers Prepared by Oxidative Polymerization: Polyaniline*", Progress in Polymer Science, Vol. 23, No. 8, pp. 1443-1484, December (1998).

[43] J.Stejskal; P. Kratochvil and A.Jenkins, "*The Formation of Polyaniline and Nature of its Structures*", Polymer, Vol. 37, No. 2, pp. 367-369, February (1996).

[44] J. Stejskal, I. Sapurina and M. Trchova,"*Polyaniline Nanostructures and the Role Of aniline Oligomers in their Formation*", Progress in Polymer Science, Vol. 35, No. 12, pp. 1420-1481, December (2010).

[45] G.Wallace; G.Spinks; L.Kane-Maguire and P.Teasdale "*Conductive Electroactive Polymers",* CRC Press, Taylor and Francis Group, ISBN 978-1-4200-6709-5, (2009).

[46] K.Tanaka; S. Wang and T.Yamabe, "*Will Bipolarons be Formed in Heavily Oxidized Polyaniline*", Synthetic Metals, Vol. 36, No.1, pp. 129-135, ISSN0379-6779, May (1990).

[47] S. Mu and H. Xue " *Bioelectrochemical characteristics of glucose oxidase immobilized in a polyaniline Film*", Sensors and Actuators B: Chemical", Vol. 31, No. 3, pp. 155-160 ISSN0925-4005, March (1996).

[48] R. Patil; Y. Harima; K. Yamashita; K. Komaguchi; Y. Itagaki and M. Shiotani, "*Charge Carriers in Polyaniline Film: a Correlation Between Mobility and in-situ ESR Meausurements*", Journal of Electroanalytical Chemistry, Vol. 518, No. 1, pp. 13-19, January (2002).

[49] J. Tanaka; N. Mashita; K. Mizoguchi and K. Kume, "*Molecular and Electronic Structures of Doped Polyaniline*", Synthetic Metals, Vol. 29, No. 1, pp. 175-184, March (1989).

[50] G. Inzelt "*Conducting Polymers-A New Era in Electrochemistr*", Springer-Verlag, Berlin, Heidelberg, (2008).

[51] P.Kahol; A. Dyakonov; B. and McCormick "*An Electron-Spin-Resonance Study of Polymer Interactions with Moisture in Polyaniline and its Derivatives*" Synthetic Metals, Vol. 89, No. 1, pp. 17-28, July (1997).

[52] S. Zhou; T. Wu; J.Kan, "*Effect of Methanol on Morphology of Polyaniline*", European, Polymer Journal, Vol. 43, No. 2, pp. 395-402, February (2007).

[53] M. Probst and R. Holze, "*Time- and Temperature-Dependent Changes of the in Situ conductivity of Polyaniline and Polyindoline*", Electrochimica Acta, Vol. 40, No. 2, (1995).

[54] A. J. Heeger, "*Noble Lecture: Semi Conducting and Metallic Polymer: the Fourth Generation of Polymeric Materials*", Reviews of Modern physics,73(3), pp. 681-699, (2001).

[55] M. S. Freund and B. A. Deore, "*Self-Doped Conducting Polymers*", John Wily and Sons, New York, (2007).

[56] J. Vivekanandan , V. Ponnusamy , A. Mahudeswaran and P. S. Vijayanand, *"Synthesis, Characterization and Conductivity Study of Polyaniline Prepared by Chemical Oxidative and Electrochemical Methods",* Arch. Appl. Sci. Res., 3(6): pp. 147-153, (2011).

[57] N. Toshima, K. Eguch , M. Inokuchi, M. Ueda and Huyan , "*Self Forming Microtubes of Polypyrrole Reaction Condition and Physical Properties*", Synthetic Metals, pp. 152-168, (2005).

[58] K. Tanaka, S. Wang and T. Yamabe, "*Will Bibolarins be Formed in Heavily Oxidized Polyaniline*", Synthetic Metals, 36, 129-135, (1990).

[59] G. Inzelt, M. Pineri, J. Schultze and M.Vorotyntsev "*Electron and proton conducting polymers:recent developments and prospects*", Electrochimica Acta, Vol. 45, No. 15-16, pp. 2403-2421, ISSN0013-4686, May (2000).

[60] J. Heinze, B.Frontana-Uribe and S. Ludwigs, "*Electrochemistry of Conducting Polymers-Persistent Models and New Concepts*", Chemical Reviews, Vol.110, No. 8, pp. 4724-4771, June (2010).

[61] J.Kankare, "*Electronically Conducting Polymers: Basic Methods of Synthesis and Characterization, In: Electrical and Optical Polymer Systems: Fundamentals: Methods, and Applications*", Ed. by: Wise D.; Wnek G.; Trantolo D.; Cooper J. and Gresser D. , pp.167-199, Marcel Dekker, New York, (1998).

[62] G. Andrade; M. Aguirre and S. Biaggi "*Influence of the First Potential Scan on the Morphology and Electrical Properties of Potentiodynamically Grown Polyaniline Films*", Electrochimica Acta, Vol. 44, No. 4, pp. 633-642, September (1998).

[63] Lj. Arsov, W. Plieth and Kobmehl. "*Electrochemical and Raman Spectroscopic Study of Polyaniline; Influence of the Potential on the Degradation of Polyaniline*", Journal of Solid State Electrochemistry, Vol. 2, No. 5, pp. 355-361, August (1998).

[64] A. Hussain and A. Kumar, "*Electrochemical Synthesis and Characterization of Chloride Doped Polyaniline*", Bulletin of Material Science, Vol. 26, No. 3, pp. 329-334, April (2003).

[65] K. Bade, V.Tsakova and J. Schultze "*Nucleation Growth and Branching of Polyaniline from Microelectrode Experiments*", Electrochimica Acta, Vol. 37, No. 12, pp. 2255-2261, September (1992).

[66] M. Lapkowski "*Electrochemical Synthesis of Linear Polyaniline in Aqouos Solutions*", Synthetic Metals, Vol. 35, No. 1-2, pp. 169-182, March (1990).

[67] Z. Mandić, Lj Duić. and F. Kovačiček, "*The Influence of Counter-Ions on Nucleation and Growth of Electrochemically Synthetized Polyaniline Film*" Electrochimica Acta, Vol. 42, No. 9, pp. 1389-1402, (1997).

[68] S. Mu; C. Chen and J.Wan, "*The Kinetic Behavior for the Electrochemical Polymerization of Aniline in Aqueous Solution*", Synthetic Metals, Vol.88, pp. 249-254, April (1997).

[69] G. Zotti, S. Cattarin and N. Comiss, "*Electrodeposition of Polythiophene, Polypyrrole and Polyaniline by the Cyclic Potential Sweep Method*", Journal of Electroanalytical Chemistry and Interfacial Electrochemistry, Vol. 235, No. 1-2, pp. 259-273, October (1987).

[70] G. Zotti, S. Cattarin and N. Comiss, "*Cyclic Potential Sweep Electropolymerization of Aniline: The Role of Anions in the Polymerization Mechanism*", Journal of Electroanalytical Chemistry and Interfacial Electrochemistry, Vol. 239, No. 1-2, pp. 387-396, January (1988).

[71] Park S. and Joong H., "*Recent Advances in Electrochemical Studies of π-Conjugated Polymers*", Buillten of the Korean Chemical Society, Vol. 26, No. 5, pp. 697-706, May (2005).

[72] S. Mu and J. Kan, "*Evidence for the autocatalitic polymerization of aniline*", Electrochimica Acta, Vol.4, No.10, pp. 1593-1599, ISSN0013-4686, November (1996).

[73] R. Córdova, M.del Valle; A. Arratia; H. R. Gómez Schrelber, "*Effects of Anions on the Nucleation and Growth Mechanism of Polyaniline*", Journal of Electroanalytical Chemistry, Vol. 377, No. 1-2, pp. 75-83, October (1994).

[74] C. Cruz and E. Ticianelli, "*Electrochemical and Ellipsometric Studies of Polyaniline Films Grown Under Cycling Conditions*", Journal of Electroanalytical Chemistry, Vol. 428, No.1-2, pp. 185-192, May (1997).

[75] J. Yano, Y.Ota and A. Kitani, "*Electrochemical Preparation of Conductive Poly (Nalkylaniline) with Long N-alkyl Chains Using Appropriate Dopant Anions and Organic Solvents*", Materials Letters, Vol. 58, No. 12-13, pp. 1934-1937, May (2004).

[76] S. Mu, "*Pronounced Effect of the Ionic Liquid on the Electrochromic Property of the Polyaniline Film: Color Changes in the Wide Wavelength Range*", Electrochimica Acta,Vol. 52, No. 28, pp. 7827-7834, November (2007).

[77] S. Zhou; T. Wu, J. Kan, "*Effect of Methanol on Morphology of Polyaniline*", European Polymer Journal, Vol. 43, No. 2, pp. 395-402, (2007).

[78] S.Biallozor and A.Kupniewska, "*Conducting Polymers Electrodeposited on Active Metals*", Synthetic Metals, Vol. 155, No. 3, pp. 443-449, December (2005).

[79] N. Martyak, P. McAndrew, J. McCaskie and J.Dijon "*Electrochemical Polymerization of Aniline From an Oxalic Acid Medium*", Progress in Organic Coatings, Vol. 45, No. 1, pp. 23-32, September (2002).

[80] A. A. Sayed and M. K. Dinesan, "*Polyaniline-A Novel Polymeric Material*", Talanta , 38 (8), pp. 815–837, (1991).
[81] A. Malinauskas, "*Chemical Deposition of Conducting Polymers*", *Polymer* 42, pp. 3957–3972, (2001).

[82] G.W Lu, L.T.Qu, G.Q.Shi , "*Electrochemical Fabrication of Neuron-Type Networks Based Oncrystalline Oligopyrene Nanosheets*", Electrochim. Acta, 51, pp. 340-346, (2005).

[83] J. Reemts, J. Parisi, D. Schlettwein, "*Electrochemical Growth of Gas-Sensitive Polyaniline Thin Films across an Insulating Gap*", Thin Solid Films, 466, pp. 320-325, (2004).

[84] S.T. McGovern, G.M. Spinks, G.G. Wallace, "*Micro-Humidity Sensors Based on a Processable Polyaniline Blend*", Sens. Actuators B, 107, pp. 657-665, (2005).
[85] J.H. Cho, J.B. Yu, J.S. Kim, S.O.Sohn, D.D. Lee, J.S. Huh, "*Sensing Behaviors of Polypyrrole Sensor under Humidity Condition*", Sens. Actuators B, *108*, pp. 389-392, (2005).

[86] S. Brady, K.T. Lau, W. Megill,; G.G. Wallace, D. Diamond, "*The Development and Characterisation of Conducting Polymeric-Based Sensing Devices*", Synth. Met., *154*, pp. 25-28, (2005).

[87] M.S. Silverstein, H.W. Tai, A. Sergienko, Y.L. Lumelsky, S.Pavlovsky, , PolyHIPE: IPNs, "*Hybrids Nanoscale Porosity Silica Monoliths and ICP-Based Sensors*", Polymer, 46, pp. 6682-6694, (2005).

[88] G.K.Prasad, T.P. Radhakrishnan, D.S. Kumar, M.G. Krishna, "*Ammonia Sensing Characteristics of Thin Film Based on Polyelectrolyte Templated Polyaniline*", Sens. Actuators B, 106, pp. 626-631, (2005).

[89] R.Tongpool,; S.Yoriya, , "*Kinetics of Nitrogen Dioxide Exposure in Lead Phthalocyanine Sensors*", Thin Solid Films, 477, pp. 148-152, (2005).

[90] Dan Xie ,Yadong Jiang ,Wei Pan, Dan Li, Ziming Wu, Yanrong Li, "*Fabrication and Characterization of Polyaniline–Based Gas Sensor by Ultra-Thin Film Technology*", Sensor and actuators B81 , pp. 158-164, (2002).

[91] M.K. Ram, O. Yavuz, V. Lahsangah, M. CO Aldissi, , "*Gas Sensing From Uultrathin Nano-Composite Conducting Polymer Film*", Sens. Actuators B, 106, pp. 750-757, (2005).

[92] R. Nohria, R.K. Khillan, Y. Su, R. Dikshit, Y. Lvov, K. Varahramyan, , "*Humidity Sensor Based on Ultrathin Polyaniline Film Deposited Using Layer-by-Layer Nano-Assembly*", Sens. Actuators B, 114, pp. 218-222, (2006).

[93] N.E. Agbor,; M.C. Petty,; A.P. Monkman, , "*Polyaniline Thin-Films for Gas-Sensing*", Sens. Actuators B, 28, pp. 173-179, (1995).

[94] E. Stussi, S. Cella, G. Serra,; G.S. Venier, "*Fabrication of Conducting Polymer Patterns for Gas Sensing by a Dry Technique*", Mater. Sci. Eng. C-Biomimetic Mater. Sens. Syst. 4, pp. 27-33, (1996).

[95]L. Ruangchuay, A. Sirivat, J. Schwank, , "*Selective Conductivity Response of Polypyrrole-Based Sensor on Flammable Chemicals*", React. Funct. Polym., 61, 11-22, (2004).

[96]H.G.O. Sandberg, T.G. Backlund, R. Osterbacka, S. Jussila, T.Makela, H. Stubb, "*Applications of an All-Polymer Solution-Processed High-Performance, Transistor*", Synth. Met., 155, pp. 662-665, (2005).

[97] M. Su, L. Fu, N.Q. Wu, M. Aslam, V.P.Dravid, "*Individually Addressed Large-Scale Patterning of Conducting Polymers by Localized Electric Fields*", Appl. Phys. Lett., 84, pp. 828-830, (2004).

[98] G.F. Li, C. Martinez, S. Semancik, "*Controlled Electrophoretic Patterning of Polyaniline From a Colloidal Suspension*", J. Am. Chem. Soc., 127, pp. 4903-4909, (2005).

[99] . M.F. Mabrook,; C. Pearson,; M.C. Petty, , "*Inkjet-Printed Polypyrrole Thin Films For Vapour Sensing*", Sens. Actuators B, 115, 547-551, (2006).

[100] A.A. Athawale, M.V. Kulkarni, "*Polyaniline and Its Substituted Derivatives as Sensor for Aliphatic Alcohols*", Sens. Actuators B, 67, pp. 173-177, (2000).

[101] A.A. Athawale,; S.V. Bhagwat,; P.P. Katre, , "*Nanocomposite of Pd-Polyaniline as a Selective Methanol Sensor*", Sens. Actuators B, 114, pp. 263-267, (2006).

[102] H.S.Cho, and Y.H. Park, , "*Preparation and Characterization of Conducting Poly(Vinyl Chloride)-G-Poly(Aniline) Copolymer"*, Synthetic Metals, 145(2-3): pp. 141-146, (2004).

[103] G.M. Spinks, P.C. Innis, T.W. Kane, L.A.P. Maguire and G.G.Wallace, "*Current state and Future Directions of Research and Development in Conducting Polymer*", Materials Forum, 24: pp. 125-166, (2000).

[104] W.J. Feast, J. Tsibouklis, K.L. Pouwer, L. Groenendaal, and E.W.Meijer, "*Synthesis, Processing and Material Properties of Conjugated Polymers*", Polymer. 37(22): pp. 5017-5047, (1996).

[105] W. Shenglong, W. Fosong, and G.Xiaohui, "*Polymerization of substitutedaniline and characterization of the polymers obtained*", Synthetic Metals. 16 (1): pp. 99-104, (1986).

[106] R. Bacon, "Growth*, Structure, and Properties of Graphite Whiskers*", Journal of Applied Physics Vol.31, pp. 283-290, (1960).

[107] Endo, A. Oberlin, and T. Koyama. "*Filamentous Growth of Carbon through Benzene Decomposition*", Journal of Crystal Growth, Vol. 32, pp. 335-349, (1976).

[108] H. W. Kroto, J. R. Heath, S. C. Obrien, R. F. Curl, and R. E. Smalley ,"*C-60-Buckminsterfullerene*", Nature, Vol. 318, pp. 162-163, (1985).

[109] M. S. Dresselhaus, G. Dresselhaus, and R. Saito. "*Physics of Carbon Nanotubes"*, Carbon, Vol. 33, 883-91, (1995).

[110] S. Iijima, "*Helical Microtubules of Graphitic Carbon"*, Nature Vol. 354, pp. 56-58, (1991).

[111] S. Iijima and T. Ichihashi, "*Single-Shell Carbon Nanotubes of 1-nm Diamete"*", Nature,Vol. 363, pp. 603-605, (1993).

[112] D. S. Bethune, C. H. Klang, M. S. de Vries, G. Gorman, R. Savoy, J. Vazquez and R. Beyers, "*Cobalt-Catalysed Growth of Carbon Nanotubes with Single- Atomic-Layer Walls"*, Nature, Vol. 363, pp. 605-607, (1993).

[113] M. Terrones, "*Science and Technology of the Twenty-First Century: Synthesis, Properties and Applications of Carbon Nanotubes"*, Annual Review of Materials Research, Vol. 33, pp. 419-509, (2003).

[114] J.O Michael· Connell, "*Carbon Nanotubes Properties and Application"*, Taylor and Francis Group London, New York, (2006).

[115] A. E. Agboola, "*Development and Model Formation of Scalable Carbon Nanotube Processes HiPCO and CoMoCAT Process Models*", M.Sc. of Science in Chemical Engineering, Louisiana State University and Mechanical College, (2005).

[116] M. S. Dresselhaus, G. Dresselhaus and P. C. Eklund, "*Science of Fullerenes and Carbon Nanotubes*", Academic Press, San Diego, 2C, (1996).

[117] P.M. Ajayan and T.W. Ebbesen, "*Nanometer-Size Tubes of Carbon"* Rep. Prog. Phys., Vol. 60, pp. 1025-1062, (1997).

[118] T. W. Ebbesen, P. M. Ajayan, "*Large Scale Synthesis of Carbon Nanotubes"*, Nature, Vol. 358, pp. 220-222, (1992).

[119] M. Meyyappan, "*Carbon Nanotubes Science and Applications"*; CRC Press: Boca Raton, FL, (2005).

[120] R. Saito, "*Physical Properties of Carbon Nanotubes*", Imperial College Press, (1998).

[121] P. M. Ajayan, "*Carbon Nanotubes",* Handbook of Nanostructure Materials and Nanotechnology, Vol. 5, pp. 375-403, (2000).

[122] F. Li, H. M. Cheng, S. Bai, G. Su, M. S. Dresselhaus, "*Tensile Strength of Single-Walled Carbon Nanotubes Directly Measured from Their Macroscopic Ropes*", Applied Physics Letters, 77 (20), pp. 3161- 3163, (2000).

[123] Y. J. Kim, T. S. Shin, H. D. Choi, J. H. Kwon, Y. C. Chung and H. G. Yoon, "*Electrical Conductivity of Chemically Modified Multiwalled Carbon Nanotube/Epoxy Composites"*, Carbon, 43 (1), pp. 23-30, (2005).

[124] T. W. Odom, J. L. Huang, Kim, C. M. P. Lieber, "*Atomic Structure and Electronic Properties of Single-Walled Carbon Nanotubes*", Nature, Vol. 391 (6662), pp. 62-64, (1998).

[125] M. Daenen, R. D. de Fouw, B. Hamers, P. G. A. Janssen, K. Schouteden and M. A. J. Veld, "*The Wondrous Word of Carbon Nanotubes"*, Eindhoven University of Technology, (2003).

[126] M. D. Ventra, S. Evoy and J. R. Heflin, "*Introduction to Nanoscale Science and Technology*", Springer Science and Business Media, Inc, (2004).

[127] Porter, Alexandra, "*Direct Imaging of Single-Walled Carbon Nanotubes in Cells*", Nature Nanotechnology, Vol. 2, No. 11, pp. 713-717, (2007).

[128] R. E. Smalley, A. Thess, R. Lee, P. Nikolaev, H. Dai, P. Petit, J. Robert, C. Xu, Y. H. Lee, S. G. Kim, A. G. Rinzler, D. T. Colbert, G. E. Scuseria, "Crystalline ropes of metallic carbon Nanotubes Science , Vol.273 No. 5274, p.483 (1996).

[129] J. O' Michael Connell, "*Carbon Nanotubes properties and Application*" Taylor and Francis Group, (2006).

[130] J. Furer, "*Growth of Single-Wall Carbon Nanotubes by Chemical Vapor Deposition for Electrical Devices*", Ph.D. thesis, Basel University, (2006).

[131] R. Yeetsorn, "*Carbon Nanotubes: A New Advanced Material Rapidly Interested Scientists*", the Journal of KMITNB, Vol. 14, No. 4, pp. 60-64, (2004).

[132] M. Daenen, R. D. de Fouw, B. Hamers, P. G. A. Janssen, K. Schouteden and M. A. J. Veld, "*The Wondrous Word of Crbon Nanotubes*", Eindhoven University of Technology, (2003).

[133] M. Endo, K. Takeuchi, S. Igarashi, K. Kobori, M. Shiraishi, and H. W. Kroto, "*The Production and Structure of Pyrolytic Carbon Nanotubes (PCNTs*) ", Journal of the Physics and Chemistry of Solids, Vol. 54, pp. 1841-1848, (1993).

[134] M. Li, Z. Hu, X. Wang, Q. Wu, Y. Chen, Y. Tian, "*Low Temperature Synthesis of Carbon Nanotubes Using Corona Discharge Plasma at Atmospheric Pressure"*, Diamond and Related Materials, Vo. 13, pp. 111-115, (2004).

[135] W. K Hsu, M. Terrones, J. P. Hare, H. Terrones, H. W. Kroto, D. R. Walton, "*Electrolytic Formation of Carbon Nanostructures"*, Chemical Physics Letters, Vol. 262, pp. 161-166, (1996).

[136] T. Guillard, S. Cetout, G. Flamant, D. Laplaze, "*Solar Production of Carbon Nanotubes, Structure, Evolution with Experimental Conditions*", Journal of Materials Science, Vol. 35, pp. 419-425, (2000).

[136] R. E. Smalley, S. Bandow, A. M. Rao, K. A. Williams, A. Thess, P. C. Eklund, *"Purification of Single–Wall Carbon Nanotubes by Microfiltration"*, Journal of Physical Chemistry B, 101, pp. 8839-8842, (1997).

[137] L. Thien-Nga, K. Hernadi, E. Ljubovic, S. Garaj, L. Forro, "*Mechanical Purification of Single-Walled Carbon Nanotube Bundles from Catalytic Particles"*, Nano Letters, 2(12), pp. 1349-1352, (2002).

[138] H. Shirakawa, E. J. Louis, A. G. MacDiarmid, C. K. Chiang, A. J. Heeger., "*Synthesis of Electrically Conducting Organic Polymers: Halogen Derivatives of Polyacetylene, $(CH)_x$*", J. Chem. Soc. Chem.Commun. 578, (1977).

[139] T. A. Skotheim, R. L. Elsenbaumer, J. R. Reynolds, "*Handbook of Conducting Polymers*", 2nd ed., Marcel Dekker, New York (1998).

[140] P. Chandrasekhar, *"Conducting Polymers, Fundamentals and Applications*: *A Practical Approach"*, Kluwer Academic, Boston (1999).

[141] E. M. Geniés, A. Boyle, M. Lapkowski, and C.Tsintavis, "*Polyaniline-A Historical Survey*", Synth. Met., 36, 2, pp. 139-182, 0379-6779, (1990).

[142] A. A.Syed, and M. K. Dineson "*Polyaniline-A Novel Polymeric Material-Rreview*", Talanta, 38, 8, pp. 815-837, 0039-9140, (1991).

[143]. D. C. Trivedi, "In *Handbook of Organic Conducting Molecules and Polymers*", H. S. Nalwa (Ed.), 2, Chap. 12, John Wiley, New York (1997).

[144] E. T. Kang, K. G. Neoh, K. L. Tan, "*Polyaniline: a Polymer with Many Interesting Intrinsic Redox States*", Prog. Polym. Sci. 23, 277, (1998).

[145] R. Gangopadhyay, "In *Encyclopaedia of Nanoscience and Nanotechnology*", H. S. Nalwa (Ed.), 2, pp.105-131, American Scientific Publishers, (2004).

[146] S. Neves, W. A. Gazotti , M. A. D. Paoli, "In *Encyclopaedia of Nanoscience and Nanotechnology*", H. S. Nalwa (Ed.), 2, pp. 133-152, American Scientific Publishers, (2004).

[147] M. Wan, "In *Encyclopaedia of Nanoscience and Nanotechnology*", H. S. Nalwa, (Ed.), 2, pp. 153-169, American Scientific Publishers, (2004).

[148]G. Kickelbick, "*Hybrid Materials: Synthesis, Characterization and Applications*", Wiley-VCH, Darmstadt, (2007).

[149] J. Anand, S. Palaniappan, D. N. Sathyanarayana, "*Conducting Polyaniline Blends and Composites*", Prog. Polym. Sci. 23, 993, (1998).

[150]A. Pud, N. Ogurtsov, A. Korzhenko, G. Shapoval Prog, "*Some Aspects of Preparation Methods and Properties of Polyaniline Blends and Composites with Organic Polymers*", Polym. Sci. 28, 1701, (2003).

[151] L. Dai. *Aust. J. Chem*., "*Electrochemical Sensors Based on Architectural Diversity of the P-Conjugated Structure: Recent Advancements from Conducting Polymers to Carbon Nanotubes*", 60, 472, (2007).

[152] C. Downs, J. Nugent, P. M. Ajayan, D. J. Duquette and K. S. Santhanam, "*Efficient Polymerization of Aniline at Carbon Nanotube Electrodes*", Adv. Mater. 11, 1028, (1999).

[153] I. A. Tchmutin, A. T. Ponomarenko, E. P. Krinichnaya, G. I. Kozub and O. N. Efinov, "*Electrical Properties of Composites Based on Conjugated Polymers and Conductive Fillers*", Carbon 41,1391 (2003).

[154] M. Baibarac, I. Batlog, S. Lefrant, J. Y. Mavellec, O. Chauvet, "*Polyaniline and Carbon Nanotubes Based Composites Containing Whole Units and Fragments of Nanotubes*", Chem. Mater. 15, 4149, (2003).

[155] X. Bi, Z. J. Han, Y. Yang, B. K. Tay, "*Fabrication of Carbon Nanotube-Polyaniline Composites via Electrostatic Adsorption in Aqueous Colloids*", J. Phys. Chem. C 111, 4125, (2007).

[156] M. Cochet, W. K. Maser, A. M. Benito, M. A. Callejas, M. T. Martinez, J. M. Benoit, J. Schreiber and O. Chauvet. "*Synthesis of a new Polyaniline/Nanotube Composite: "*in-situ*" Polymerisation and Charge Transfer through Site-Selective Interaction*", Chem. Commun. 1450 (2001).

[157] M. R. Karim, C. J. Lee, Y. Y. Park and M. S. Lee, "*SWNTs Coated by Conducting Polyaniline: Synthesis and Modified Properties*", Synth. Met. 151, 131, (2005).

[158] P. Gajendran and R. Saraswathi, "*Enhanced Electrochemical Growth and Redox Characteristics of Poly (o-phenylenediamine) on a Carbon Nanotube Modified Glassy Carbon Electrode and Its Application in the Electrocatalytic Reduction of Oxygen*", J. Phys. Chem. C 111, 11320, (2007).

[159] R. Sainz, A. M. Benito, M. T. Martinez, J. F. Galindo, J. Stores, A. M. Baro, B. Corraze,O. Chauvet and W. K. Maser, "*soluble Self-Aligned Carbon Nanotube/Polyaniline Composites*" Adv. Mater. Vol. 17, 278, (2005).

[160]S. E. Kooi, U. Schlecht, M. Burghard and K. Kern, "*Electrochemical Modification of Single Carbon Nanotubes*", Angew. Chem., Int. Ed. Vol. 41, pp. 1353-1355, (2002).

[161] J. Shi, Z. Wang and Hu-lin Li, "*Electrochemical Fabrication of Polyaniline/Multi-Walled Carbon Nanotube Composite Films for Electrooxidation of Methanol*", J Mater Sci., Vol. 42, pp. 539-544, (2007).

[162]S. Quillard, G. Louarn, S. Lefrant, A.G. MacDiarmid ,*"Vibrational analysis of polyaniline. A comparative study of leucoemeraldine ,emeraldine, and pernigraniline bases*", Phys Rev B 50:12496(1994).

[163] Y. Furukawa, F. Ueda, Y. Hyodo, I. Harada, T. Nakajima, T. Kawagoe (1988)Macromolecules 21:1297 sit in "Jin Shi , Zhe Wang , Hu-lin Li" ;" *Electrochemical fabrication of polyaniline/multi-walled carbon nanotube composite films for electrooxidation of methanol*";J Mater Sci 42 pp539–544;(2007).

[164] H. Zengin, W. Zhou, JY. Jin, R. Czerw, D.W. Smith, L.Echegoyen, DL. Carroll, SH. Foulger, J. Battato(2002) Adv Mater 14:1480 sit in "Jin Shi , Zhe Wang , Hu-lin Li" ;" *Electrochemical fabrication of polyaniline/multi-walled carbon nanotube composite films for electrooxidation of methanol*";J Mater Sci 42 pp539–544;(2007).

[165] M. Baibarac , I. Baltog , S. Lefrant , J. Y. Mevellec and O. Chauvet *"Polyaniline and Carbon Nanotubes Based Composites Containing Whole Units and Fragments of Nanotubes"*; Chem. Mater. 15, 4149 (2003).

[166] M. Trchova, J. Stejskal, J. Prokes sit in "Jin Shi , Zhe Wang , Hu-lin Li" " *Electrochemical fabrication of polyaniline/multi-walled carbon nanotube composite films for electrooxidation of methanol*";J Mater Sci 42 pp539–544;(2007).

[167] O'Connell MJ, Boul P, Ericson LM, Hauffman C, Wang Y,Kuper C, Tour J, Ausman KD, Smalley RE (2001) sit in "Jin Shi , Zhe Wang , Hu-lin Li" " *Electrochemical fabrication of polyaniline/multi-walled carbon nanotube composite films for electrooxidation of methanol*";J Mater Sci 42 pp539–544;(2007).

[168] V.C. Nguyen,; K. Potje-Kamloth, , "*Electrical and Chemical Sensing Properties of Doped Polypyrrole/Gold Schottky Barrier Diodes*", Thin Solid Films, 338, pp. 142-148, (1999).

[169]C.N.Van, K. Potje-Kamloth, "*Electrical and NOx Gas Sensing Properties of Metallophthalocyanine-Doped Polypyrrole/Silicon Heterojunctions*", Thin Solid Films, 392, pp. 113-121, (2001).

[170] D. Xie, Y.D. Jiang, W. Pan, D. Li, Z.M. Wu, Y.R. Li, "*Fabrication and Characterization of Polyaniline-Based Gas Sensor by Ultra-Thin Film Technology*", Sens. Actuators B, 81, pp. 158-164, (2002).

[171] S.V. Mello, P. Dynarowicz-Latka, A. Dhanabalan, R.F. Bianchi, Onmori, R., R.A.J. Janssen, O.N.Oliveira, "*Langmuir and Langmuir-Blodgett Films from the N-Hexyl-Pyrrole-Thiophene (AB) Semi-Amphiphilic Copolymer*", Colloid Surf. A-Physicochem. Eng. Asp., 198, pp. 45-51, (2002).

[172] N.V. Bhat, A.P. Gadre, V.A. Bambole, "*Investigation of Electropolymerized Polypyrrole Composite Film: Characterization and Application to Gas Sensors*", *J. Appl. Polym. Sci.*, *88*, pp. 22-29, (2003).

[173] K.H. An, S.Y. Jeong, H.R. Hwang, Y.H. Lee, "*Enhanced Sensitivity of a Gas Sensor Incorporating Single-Walled Carbon Nanotube-Polypyrrole Nanocomposites*", Adv. Mater., 16, pp. 1005-1009, (2004).

[174] G.F. Li, M. Josowicz, J.Janata, S. Semancik, "*Effect of Thermal Excitation on Intermolecular Charge Transfer Efficiency in Conducting Polyaniline*", Appl. Phys. Lett., 85, pp. 1187-1189, (2004).

[175] J. Elizalde-Torres, H.L. Hu, A. Garcia-Valenzuela, "*NO2-Induced Optical Absorbance Changes in Semiconductor Polyaniline Thin Films*", Sens. Actuators B, 98, pp. 218-226, (2004).

[176] M.K.Ram, O. Yavuz, M. Aldissi, "*NO_2 Gas Sensing Based on Ordered Ultrathin Films of Conducting Polymer and its Nanocomposite*", Synth. Met., 151, pp. 77-84, (2005).

[177] N.V. Bhat, A.P. Gadre, V.A.Bambole, "*Structural, Mechanical, and Electrical Properties of Electropolymerized Polypyrrole Composite Films*". J. Appl. Polym. Sci.,Vol. 80, pp.2511-2517, (2001).

[178] H. Yoon, M. Chang, J. Jang, "*Sensing behaviors of Polypyrrole Panotubes Prepared in Reverse Microemulsions: Effects of Transducer Size and Transduction Mechanism*", J. Phys. Chem. B, Vol. 110, pp.14074-14077, (2006).

[179] H.Q. Liu, J. Kameoka, D.A. Czaplewski, H.G. Craighead, "*Polymeric nanowire chemical sensor*", Nano Lett., Vol.4,pp. 671-675(2004).

[180] E. Krivan, C. Visy, R. Dobay, G. Harsanyi, O. Berkesi, "*Irregular Response of the Polypyrrole Films to H_2S*", Electroanalysis, *12*, pp. 1195-1200, (2000).

[181] N.V. Lavrik, D. DeRossi, Z.I. Kazantseva, A.V. Nabok, B.A. Nesterenko, S.A.Piletsky, V.I. Kalchenko, A.N. Shivaniuk, L.N. Markovskiy, "*Composite Polyaniline/Calixarene Langmuir-Blodgett Films for Gas Sensing*", Nanotechnology, Vol. 7, pp. 315-319, (1996).

[182] J. Janata, M. Josowicz, "*Conducting Polymers in Electronic Chemical Sensors*", Nat. Mater ,Vol. 2, pp. 19-24, (2003).

[183] N.E. Agbor, M.C.Petty, A.P. Monkman, "*Polyaniline Thin-Films for Gas-Sensing*", Sens.Actuators *B*, Vol. 28, pp. 173-179, (1995).

[184] G.F. Li, C. Martinez, S. Semancik, *"Controlled Electrophoretic Patterning of Polyaniline from a Colloidal Suspension*", J. Am. Chem. Soc., Vol. 127, pp. 4903-909, (2005).

[185] H.Yoon, M.Chang, J. Jang, , "*Sensing Behaviors of Polypyrrole Nanotubes Prepared in Reverse Microemulsions: Effects of Transducer Size and Transduction Mechanism*", J. Phys. Chem. B, 110, pp. 14074-14077, (2006).

[186] J. Janata, "*Electrochemical Microsensors*". Proc. IEEE, Vol. 91, pp. 864-869 (2003).

[187] Q.L. Hao, V. Kulikov, V.A. Mirsky , "*Investigation of Contact and Bulk Resistance of Conducting Polymers by Simultaneous Two and Four-Point Technique*", Sens. Actuators B, Vol. 94, pp. 352-357, (2003).

[188] M. Krondak, G. Broncova, S. Anikin, A. Merz, V.M. Mirsky, "*Chemosensitive Properties of Poly-4,4'-Dialkoxy-2,2'-Bipyrroles*", J. Solid State Electrochem., Vol. 10, pp. 185-191, (2006).

[189] F. Musio, M. C. Ferrara, "*Low Frequency a.c. Response of Polypyrrole Gas Sensors*", Sens. Actuators B, Vol. 41, pp. 97-103, (1997).

[190] M.E.H. Amrani, K.C. Persaud,; P. A. Payne. "*High-Frequency Measurements of Conducting Polymers-Development of a New Technique for Sensing Volatile Chemicals*", Meas. Sci. Technol. Vol. 6, No.10, (2010).

[191] M.E.H. Amrani, P. A. Payne, "*Multi-Frequency Interrogation Technique Applied to Conducting Polymer Gas and Odour Sensors*", IEE Proc.-Sci. Meas. Technol. Vol. 146, pp. 95-101, (1999) .

[192] D.K. Aswal, S. K. Gupta, "*Science and Technology of Chemiresistor Gas Sensors*", Nova Science publishers. Inc., pp. 33-93, (2007).

[193] A. Pron, F. Genoud, C. Menardo,, and M. Nechtschein, , *"The Effect of the Oxidation Conditions on the Chemical Polymerization of Polyaniline*", Synthetic Metals., Vol. 24, No. 3, pp. 193-201, (1988).

[194] S. Bhadra, N. K. Singha, D. Khastgir, "*Electrochemical Synthesis of Polyaniline and Its Comparison with Chemically Synthesized Polyaniline*", Journal of Applied Polymer Science, Vol. 104, pp. 1900-1904, (2007).

[195] S. Mu and Y. Yang, "*Spectral Characteristics of Polyaniline Nanostructures Synthesized by Using Cyclic Voltammetry*". Journal of Physical Chemistry B. Vol. 112, No. 37, pp. 11558-11563, September (2008).

[196] M. Gvozdenović; B. Jugović; T. Trišović; J. Stevanović and B. Grgur, "*Electrochemical Characterization of Polyaniline Electrode in Ammonium Citrate Containing Electrolyte*", Materials Chemistry and Physics, Vol. 125, No. 3, pp. 601-605, (2011).

[197] C. Journet, , W. K. Maser, P. Bernier, A. Loiseau, M. Lamy de la Chapelle, S. Lefrant, P. Denlard, R. Lee, J. E Fischer, "*Large-Scale Production of Single-Walled Carbon Nanotubes by Electric-Arc Technique*", Nature, Vol. 388, pp. 756- 758, (1997).

[198] H. Kataura, Y. Kumazawa, Y. Maniwa, I. Umezu, S. Suzuki, Y. Ohtsuka and Y. Achiba, "*Optical Properties of Single Wall Carbon Nanotubes*", Synthetic Metals, Vol. 103, pp. 2555-2558, (1999).

[199] Y. S. Park, Y. C. Choi, K. S. Kim, D. C. Chung, D. J. Bae, K. H. An, S. C. Lim, X. Y. Zhu and Y. H. Lee, "*High Yield Purification of Multi–walled Carbon Nanotubes by Selective Oxidation during Thermal Annealing*", Carbon, Vol. 39, pp. 655-661, (2001).

[200] Y. Maniwa, R. Fujiwara, H. Kira, H. Tou, E. Nishibori, M. Takata, M. Sakata, A. Fujiwara, X. Zhao, S. Iijima and Y. Ando, "*Multi Walled Carbon Nanotubes Grown in Hydrogen Atmosphere: An X-Ray Diffraction Study*", Phy. Rev. B, Vol. 64, 073105, (2001) .

[201] S. H. Jung, M. R. Kim, S. H. Jeong, S. U. Kim, O. J. Lee, K. H. Lee, J. H. Suh and C. K. Park, "*High–Yield Synthesis of Multi–Walled Carbon Nanotubes by Arc Discharge in Liquid Nitrogen*", Applied Physics A 76, pp. 285-286, (2003).

[202] B. Debasis, C. Suresh, M. Matthem, K. Arnold, H. H. Meyyappan and S. Sudipta, "*In-Situ Synthesi of Palladium Nanoparticals-Filled Carbon Nanotubes Using Arc-Disharge in Souliousion*", Chemical Physics Letter , Vol. 4386, pp. 364-368, (2004).

[203] A. Ambrosio, M. Ambrosio G. Ambrosone, M. F. Bevilacqua, F. Bussolotti, V. Casuscelli, U. Oscia F. Gesuele, V. Grossi Lozzi, P. Maddalena, M. Passacantando and S. Santucci, "*Use of Carbon Nanotubes as Radiation Detectors*" Napoli, (2005).

[204] B. Hicks, S. Getty and D. Allred, "*Diode Properties of Nanotube Networks*" Materials Engineering, N283 ESC, Provo, UT 84602, Provo, UT, 84606, pp. 1-16, (2007).

[205] Y. Wanna, S. Pratontep, A. Wisistoraat, A. Tuantranont, "*Development of Nanofiber Composite Polyaniline/CNT Fabricated by Elevtro Spinning Technique for CO Gas Sensor*", IEEE sensors, pp. 342-345, October (2006).

[206]Shabnam Virji, B. Kaner, and H. Wweiller Bruce, "*Hydrogen sensors based on conductivity changes in polyaniline nanofibers*", J. phys.Chem B,110, pp.22266-22270;(2006).

[207] R. Emanalisabzil, K. Rezapour and N. Samadi, "*Polyaniline–Multi-Mall-Carbon Nanotube Nanocompositesas a Dopamine Sensor*", J. Serb. Chem. Soc., Vol. 75, No. 4, pp. 537-549, (2010).

[208] S. Srivastava, S. S. Sharma, S. Agrwal, S. Kumar, M. Singh, Y. k. Vijay, "*Study Chemeiresistor Type CNT Doped Polyaniline Gas Sensor "*, Synthetic Material, 160, pp. 529-534, (2010).

[209][210] I. Kim, K. Y. Dong, B. Ju and H. H. Choi, "*Gas Sensor for CO and NH_3 Using Polyaniline/CNTs Composite at Room Temperature*", Proceeding of 10th IEEE International Conference on Nanotechnology Joint Symposium wiyh Korea, pp. 466-469, August (2010).

[210] W. Li, D. Zhai, L. Pan, L. Pu, J. Xu and Y. Shi, "*Synthesis of Multishell Carbon Nanotube Composites via Template Method*"; Chin. J. Chem. Phys., Vol. 24, No. 2, pp. 206-210, (2011).

[211]Y. Liao, C. Zhang, Y. Zhang, V. Strong, J. Tang, X. Li, K. Kalantar-zadeh, E. M. Hoek, K. L. Wang and R. B. Kaner, "*Carbon Nanotube/Polyaniline Composite Nanofibers: Facile Synthesis and Chemosensors*", Nano Lett., Vol. 11, pp. 954-959, (2011).

[212] M.A.S. Ibrahem "*Study the Optical and Electrical Properties of Silicon Nanostructure*", M.Sc. Thesis, Applied Science Dept., University of Technology (2007).

[213] C. Kittle "*Introduction to Solid State Physics*" Eight Edition, John Wiley and Sons, p.416(2005).

[214] L.V. Azaroff, " *Elements of X- Ray Cryctallography*", McGraw-Hill, Inc (1968).

[215] A M Pharhad Hussain and A Kumar;"*Electrochemical synthesis and characterization of chloride doped polyaniline*" Mater.sci. Vol. 26,No. 3,pp.329-334 ,(2003).

[216] E.M. Genies and M. Lapkowski, "*polyaniline films ,electrochemical redox mechanisms*", synthetic Metals ,24:pp 61-68 (1988).

[217] J. Howe, C. Rawn , L.Jones, , Ow, H."*Improve crystallographic data for graphite*", Powder Diffraction **18**, 159; (2003).

[218] A.A. Thamir Hassan , M. Izzat Al-Essa , A.Al-Ajaj Ekram and M. Ali Abdul Kareem;"*Fabrication carbon nanopowder by arc discharge technique*", Iraqi Journal of physics ,vol. 10 ,No. 19, pp.41-46,(2012).

[219] W. Fing, F. Zhou, X. Wang, H. Liang, K. Yoshino, "*fabrication of composit films by controlling molecular doping processes between polyanilne and soluble multiwall Nanotubes on their optical characteristics*", Jpn J appl phys 42,pp.5726-5730;(2003).

[220] Chuizhou Meng. Changhong Liu ,Shoushan Fan,"*flexiblecarbon nanotube/polyaniline paper-like films and their enhanced electrochemical properties*", Electrochemistry communications 11,pp.186-189;(2009).

[221] Subodh srivastava, S.S. Sharma ,Sumit Kumar, Shweta Agrawal ,M.singh, Y.K.Vijay, "*charachterization of gas sensing behavior of nulti walled carbon nanotube polyaniline composite films*", International Journal of Hydrogen Energy 34,pp.8444-8450,(2009).

[222] M. Mazloum-Ardakani and M.A. Shiekh-Mohseni, "*Carbon Nanotubes in electrochemical sensors*", edited by Mohammed Naaghi, Intech,pp.395-411;(2011).

[223] A.J. Bard and L.R. Faulkner , "*Electrochemical methods fundamentals and applications*", John Wiley and Sons ,3rd edition New York;(2001).

[224] V. E. Bochenkove and G. B.sergeev, "*sensetivity ,selectivity ,stability of gas sensitive metal-oxide nanostructure*",Amirican scientific publishers,Edited by Ahmed Umer and Yoon Bong Hahn,Vol.3 pp.31-52;(2010).

[225] Z. Jin, Y.X Su, Y.X. Duan, "*Development of a polyaniline-based optical ammonia sensor*". Sens. Actuators B *72*, 75-79**;(2001)**.

[226] Hau Bai and Gaoquan Shi*,"gas sensors based on conducting polymers"*, sensors,7,pp.267-307;(2007).

[227] A.G. MacDiamid ,"*conducting polymers as a new materials for hydrogen storage* ", U.S. Department of Energy presentation, (2005)

Publications

1. A.A. Thamir Hassan , M. Izzat Al-Essa , A.Al-Ajaj Ekram and M. Ali Abdul Kareem;"*Fabrication carbon nanopowder by arc discharge technique*", Iraqi Journal of physics ,vol. 10 ,No. 19, pp.41-46,(2012).

2. A.A. Thamir Hassan , M. Izzat Al-Essa , A.Al-Ajaj Ekram and M. Ali Abdul Kareem;"*Current-Voltage Of Polyaniline Nanofibers And Polyaniline /MWNTs Nanofibers Fabricated By Electrochemical Polymerization*", IJIRST-ISSN2229-3116,Vol. 4 No.2(2013).